The Arctic winter stratosphere

Simulated with a 3-D Chemistry Transport Model

De stratosfeer tijdens de Arctische winter

Simulaties met een 3-D Chemie Transport Model

(met een samenvatting in het Nederlands)

Proefschrift ter verkrijging van de graad van doctor aan de Universiteit Utrecht op gezag van de Rector Magnificus, Prof. Dr. W.H. Gispen, ingevolge het besluit van het College voor Promoties in het openbaar te verdedigen op maandag 4 oktober 2004 des middags te 14:30 uur

door

Martina Maria Petronella van den Broek

geboren op 26 januari 1970, te Heeswijk-Dinther

Promotor: ..... Prof. Dr. Jos Lelieveld

Co-promotor:..... Dr. Ir. Bram Bregman

Instituut voor Marien en Atmosferisch onderzoek Utrecht (IMAU)
Faculteit Natuur- en Sterrenkunde
Universiteit Utrecht

Dit proefschrift is mede mogelijk gemaakt door financiële steun van het Nationaal Programma Gebruikersondersteuning (GO-2) van NWO, onder projectnummer eo-022.

ISBN 90-9018407-4

Index

Voorwoord

Het schrijven van een proefschrift is wel te vergelijken, en ik ben vast niet de eerste die het probeert, met een bepaald soort sportwedstrijd. De soort waarbij meedoen-en-uitlopen voor de meeste deelnemers daadwerkelijk belangrijker is dan winnen. Ik noem een elfstedentocht, vierdaagse, een marathon of een triatlon. Als het maar veel uithoudingsvermogen vraagt wordt er, gelukkig, nog maar weinig geïnformeerd naar de plek in het eindklassement. Zoals zo'n wedstrijd heeft ook dit proefschrift heel wat zweet, tranen en vooral tijd gekost.
Gelukkig heb ik niet alleen hoeven zwoegen en had ik een uitgebreid team van deskundigen om me heen, die me gecoacht, gesponsord, gesteund en soms zelfs een beetje geduwd hebben. Op deze paar pagina's wil ik jullie graag bedanken. Een deel van de overwinningsroes hebben jullie zeker verdiend.

De belangrijkste 'coach' noem ik hier als eerste: Bram Bregman. Ik ben je eerste promovenda en hopelijk nog lang niet de laatste, want ik gun vele anderen jouw enthousiaste en motiverende begeleiding. Een grote mate van betrokkenheid weet je toch te combineren met een relaxte houding en oog voor het stressniveau. Niet alleen zit je vol met kennis en ideeën, je bent ook altijd bereid die te delen en tijd vrij te maken, zowel voor discussie op hoog niveau als voor geniepige computerprobleempjes. Bedankt voor je begeleiding en gefeliciteerd met het behaalde resultaat. Je mag even trots zijn als ik op dit boekje.
Ook mijn promotor, Jos Lelieveld, heeft een belangrijke rol gespeeld. Vooral in de eerste jaren van deze onderneming, toen je nog professor was aan het IMAU (Instituut voor Marien en Atmosferisch onderzoek, Utrecht), gaf je richting aan het onderzoek. Soms sloeg ik desondanks (en dankzij mijn eigenwijsheid) een doodlopend paadje in. Achteraf bezien ben ik het met je eens dat dat een essentieel onderdeel is van het leerproces van een promovendus. Je bent heel open en helder in je begeleiding, wat het voor mij altijd erg prettig heeft gemaakt om met je samen te werken. Ook al werk je sinds een paar jaar in Mainz en zien we elkaar sindsdien wat minder, je bent toch al die tijd gemakkelijk benaderbaar gebleven en ik heb altijd veel gehad aan je adviezen. Veel dank daarvoor.
Bij de start van dit promotietraject ben ik als O.I.O. aangenomen bij de Stichting Ruimteonderzoek Nederland (SRON). In eerste instantie werkte ik daar in de EOS (Earth Oriented Science) groep, onder Albert Goede. In deze hoedanigheid van "eerste sponsor" wil ik je hartelijk danken, Albert. Vooral in het begin heb jij je ook inhoudelijk beziggehouden met dit proefschrift en mij wegwijs gemaakt in de wereld van internationale wetenschappelijke projecten. In een later stadium hebben Avri Selig en Ilse Aben het stokje overgenomen namens SRON. Ook hen wil ik hartelijk danken voor hun steun en vertrouwen. Jullie hadden nog vertrouwen in mij, toen het vertrouwen in mijzelf tot op een dieptepunt gezakt was. Zonder de daaruit voortvloeiende contractverlengingen was dit boekje niet tot stand gekomen.

De nodige pecunia werden al die tijd door SRON en NWO verzorgd, maar ook het IMAU en het KNMI hebben een bijdrage geleverd door mij de afgelopen jaren gastvrij onderdak te verlenen. De collega's van EOS, IMAU en KS-AS (de KNMI-afdeling Atmosferische Samenstelling van Henny Kelder) voorzagen me van een gezellige werkomgeving, inclusief zwemclubjes. Alleen daarvoor al wil ik hen allemaal bedanken, speciaal degenen met wie ik voor kortere of langere tijd een kamer gedeeld heb.

Een aantal collega's heeft rechtstreeks aan dit proefschrift bijgedragen. Zo zijn daar natuurlijk de medeauteurs van de artikelen, waar dit proefschrift uit opgebouwd is. Hoofdstuk 3 is tot stand gekomen door goede en intensieve samenwerking met Maarten van Aalst. We hebben ieder een artikel kunnen destilleren uit dit deelonderzoek. Bedankt en veel succes met je eigen promotie over een paar maanden. Ook Maarten Krol is medeauteur van dit hoofdstuk. Door je werk aan de ontwikkeling van de TM3 en TM5 modellen is je bijdrage echter veel groter dan dit ene hoofdstuk. Niet alleen sta je aan de basis van het TM5-model, ook aan je wetenschappelijke input heb ik veel gehad. Jason Williams was the second author and a great help in the writing of Chapter IV on NAT particles. For you, it was the umpteenth atmospheric topic that you mastered, which you did very well.
Ken Carslaw was very helpful in getting me started in the world of modeling Polar Stratospheric Clouds. Besides that, you also read and approved of the manuscript, as well as Henny Kelder, Ilse Aben and Theo Opsteegh, for which I thank them.
Many other researchers contributed to Chapters 2-4 by providing me with their data, sharing their model routines or calculations and discussing the scientific results. I'd like to thank each of these colleagues. Their individual contributions are acknowledged at the end of each chapter.
Dan zijn er nog een aantal collega's die het om de een of andere reden (nog) niet tot medeauteur geschopt hebben, maar die wel degelijk op de achtergrond hun bijdragen geleverd hebben. Daarmee doel ik bijvoorbeeld op Wouter Peters en Frank Dentener, die veel gedaan hebben voor de ontwikkeling van de TM3 en TM5 modellen. Aan het begin van mijn promotie heeft Geert-Jan Roelofs mij goed op gang geholpen met de EBI-routine. Vanuit het KNMI heb ik veel gehad aan discussies met de twee Peters: Peter Siegmund en Peter van Velthoven. Arjo Segers heeft me vaak geholpen met modelbugs. Je had ook een belangrijke functie als bliksemafleider, wanneer Bram er niet was. In het begin, toen ik bij SRON werkte op het ASUR-project, heb ik veel gehad aan de hulp van Hans Schrijver en Quintus Kleipool. Ik beschouw dit als een goede gelegenheid om ook de computer- en secretariële steun vanuit het IMAU, EOS en KS-AS te vermelden: Melinda, Marion, Inge, Ellen, Yvonne, Louise, Jennifer, Marcel, Marc, Hans, Piet en wie ik per ongeluk vergeet: Bedankt.

De voorgaande collega's hebben zich min of meer direct met het voor u liggende proefschrift bezig gehouden. Ze hebben materiaal, geld, en coaching aangeleverd om mij over de eindstreep te krijgen. Dat was hen (en mij) natuurlijk nooit gelukt zonder een enthousiast publiek. En ik had een fijn publiek, wat me heeft aangemoedigd en geprezen, maar ook bij tijd en wijle afgeleid van de "zware inspanning", vooral door gezellig te zijn.
Mutsen, Scene (eindelijk in een proefschrift beland), Franje en Gorgo: een paar cryptische namen, maar jullie weten wel wie ik hiermee wil bedanken. Geestelijke steun heb ik ook gekregen van Mirjam van den Heuvel en Desiree Tijdink, als vertegenwoordigers van een grotere groep van behulpzame mensen.
Mijn zus en broers vormen samen met mijn ouders een prettig thuis-thuisfront in Heeswijk-Dinther, Noord-Brabant. Patrick en Rene, mijn broers, fungeren tijdens de promotieplechtigheid ook als paranimf. Ik heb een speciale reden om jullie voor dit erebaantje te vragen. Volgens wetenschappers uit een heel ander vakgebied hebben jongens gemiddeld genomen meer ruimtelijk inzicht dan meisjes. Dit komt door hormoonverschillen die al bij de geboorte aanwezig zijn. Jongetjes hebben namelijk van nature een hogere testosteron-spiegel, die ervoor zorgt dat ze meer rondrennen. Nu zijn mijn broertjes slechts 1 en 2 jaar jonger dan ik. Het zou dus best kunnen dat

ik, door lekker met jullie mee te rennen, toch het nodige ruimtelijke inzicht opgedaan heb. In dat geval staan jullie aan de basis van dit proefschrift.

Speciale dank aan mijn ouders, van wie ik de belangrijkste eigenschappen meegekregen heb die nodig zijn voor het voltooien van een project als dit, en die me door dik en dun bijgestaan hebben. Nog een beetje specialere dank, als dat mogelijk is, aan Arjen. Niet alleen door dik en dun, maar ook altijd ben je er.
Stand by your woman! Ik ook bij jou.

Samenvatting

Op 12-15 km hoogte rondom de aarde, onder in de stratosfeer, bevindt zich de ozonlaag. Deze laag bevat, zoals de naam zegt, relatief grote concentraties ozon en beschermt daardoor de aarde tegen schadelijke UV-straling. De afgelopen twintig jaar is er elke Antarctische winter en lente een "gat" ontstaan in de ozonlaag boven de Zuidpool. Dezelfde processen die boven de Zuidpool voorafgaan aan ozonafbraak blijken ook boven de Noordpool op te treden. Het gaat hierbij om de katalytische omzetting van chloorhoudende stoffen op polaire stratosferische wolken (Polar Stratospheric Clouds of PSCs). Deze wolken kunnen alleen bestaan bij extreem lage temperaturen, onder 195 K. Boven deze temperatuur bevindt het chloor zich voornamelijk in stabiele componenten, die ozon niet af kunnen breken. Als gevolg van deze zogenaamde chlooractivatie op PSCs meet men ook boven de Noordpool substantiële ozonafbraak in koude winters, al is dat over het algemeen minder dan aan de Zuidpool.
De belangrijkste brongassen van deze chloor-(en broom-)componenten zijn de door de mens geproduceerde CFKs, en halonen. Sinds 1987 zijn politieke maatregelen van kracht die de productie en het gebruik van deze stoffen aan banden leggen en binnenkort wereldwijd verbieden. Echter, door de lange levensduur van deze stoffen in de atmosfeer, zal het nog enkele tientallen jaren duren voor het effect op de ozonlaag teniet is gedaan. Een extra complicerende factor hierbij is de potentiële afkoeling van de stratosfeer. Deze afkoeling wordt veroorzaakt door de afname van ozon, wat ook een broeikasgas is, en door de uitstoot van broeikasgassen in de onderste luchtlaag, de troposfeer. Lagere temperaturen kunnen leiden tot meer PSCs en daarmee voor een toename van chlooractivatie en ozonafbraak.
Per Arctische winter verschilt de hoeveelheid chlooractivering, ozonafbraak en gerelateerde processen sterk. Ook binnen één winter kunnen perioden van sterke en matige ozonafbraak elkaar afwisselen, afhankelijk van de temperatuur en de stabiliteit van de polaire vortex. De polaire vortex is het gebied in de stratosfeer wat in de winter min of meer geïsoleerd wordt van lagere breedtegraden, door de heersende, sterke, circumpolaire, wind. Vanwege de non-symmetrische aard van de Arctische polaire vortex, is een driedimensionale benadering nodig bij het simuleren van de processen die tot ozonafbraak leiden aan de Noordpool.
Dit proefschrift beschrijft een aantal van zulke simulatiestudies van de Arctische winter stratosfeer, uitgevoerd met een Chemie Transport Model (CTM). Dit is een zogenaamd "off-line" 3D model. Het maakt gebruik van 3D wind- en temperatuur-velden gegenereerd door het ECMWF, een weerverwachtingsmodel.
In hoofdstuk 2 is het CTM toegerust met een stratosferisch chemie-schema. Dit schema bevat een uitgebreide set van heterogene reacties op vloeibare aerosolen en ijsdeeltjes en gebruikt de Euler Backward Iterative benadering als numerieke oplosmethode. Deze methode is met succes getest aan de hand van een nauwkeurige oplosmethode. Deze stratosferische versie van het CTM is vervolgens gebruikt om chlooractivatie en ozonafbraak boven de Noorpool te berekenen voor de winter van 1996/1997.
Ozonkolommen en ClO concentraties, berekend door het model, zijn vergeleken met satellietmetingen voor februari en maart 1997. Ook zijn gemodelleerde ozonafbraaksnelheden vergeleken met geobserveerde waarden. De concentratie van ClO, een vorm van actief chloor, en de afbraak van ozon worden enigszins onderschat door het model.

Om de oorzaak van deze onderschatting te vinden zijn enkele sleutelparameters in het model gevarieerd. Een belangrijke modelonzekerheid is de temperatuur. Een gemiddelde temperatuurverhoging van 1.3 K, bij temperaturen waarbij PSCs kunnen ontstaan, op het 50 hPa modelniveau, geeft een reductie in ozonafbraak tussen februari en maart van ~35%.
Ook het vormingsmechanisme van vaste en/of vloeibare PSC-deeltjes is een belangrijke onzekerheid in het model. Het blijkt dat het model de grootste ClO-productie en ozonafbraak berekent wanneer vaste NAT-deeltjes (Nitric Acid Trihydrate) gevormd worden op het moment van verzadiging, terwijl vloeibare STS-deeltjes (Supercooled Ternary Solution) tegelijkertijd in het model aanwezig zijn.
Een derde parameter met een grote invloed op de berekende ClO en ozonafbraak is de hoeveelheid anorganisch chloor (Cly). Een verbetering in de representatie van transport van tracers in het CTM zou zowel de gemodelleerde hoeveelheid Cly als de absolute ozonconcentraties ten goede kunnen komen. Echter, zelfs de aanname van een maximale hoeveelheid Cly in het model, kan de onderschatting van ozonafbraak door het model niet volledig verklaren.
In hoofdstuk 3 wordt het CTM gebruikt om het stratosferische transport te evalueren, door de langlevende stoffen HF en CH_4 te simuleren tijdens de Arctische winter van 1999/2000. Verschillende modelsimulaties zijn uitgevoerd met gebruikmaking van een "zoom"-algoritme. Hiermee kunnen berekeningen voor een deelgebied met een hogere horizontale resolutie gedaan worden. Het effect van verschillende horizontale modelresoluties op de berekende concentraties is op deze manier onderzocht. Ballon- en satellietmetingen van HF en CH_4 zijn vergeleken met de modelresultaten. Daarnaast zijn modelberekeningen van het neerwaartse transport van stoffen in de polaire vortex vergeleken met soortgelijke berekeningen uit observaties. Buiten de vortex komen de modelresultaten goed overeen met de metingen. Daarbinnen onderschat het model de gemeten verticale gradiënt in HF en CH_4, zelfs wanneer de hoogste horizontale resolutie (1ºx1º) gebruikt wordt. Slechts boven een potentiële temperatuurniveau van 450 K (~ ter hoogte van het ozonmaximum) komen de berekeningen voor neerwaarts transport goed overeen met observaties. Deze modelresultaten suggereren dat een overschatting van menging door de rand van de vortex een oorzaak zou kunnen zijn voor de verschillen met de metingen. Dit zou veroorzaakt kunnen worden door onnauwkeurigheden in de uit het ECMWF berekende massafluxen. Andere mogelijke oorzaken worden ook besproken. Een recente studie heeft uitgewezen dat het gebruik van een gereduceerd grid rond de polen en het soort advectieschema een belangrijke rol spelen. Deze factoren kunnen de onderschatting van het neerwaartse transport grotendeels verklaren. Hiermee kan deze studie de onderschatting van ozonafbraak in hoofdstuk II gedeeltelijk verklaren. Door minder neerwaarts transport van Cly, dat toeneemt met de hoogte in de lagere stratosfeer, is minder chloor beschikbaar voor chlooractivatie en ozonafbraak.
Vanuit de modelstudies met verschillende resoluties kunnen we concluderen dat een globale resolutie van 6ºx9º te grof is om transport in/uit de polaire vortex te kunnen representeren. De hogere resoluties, 3ºx2º en 1ºx1º, geven identieke resultaten, zelfs als de resolutie 6ºx9º bedraagt in de tropen.
Zoals blijkt uit hoofdstuk II, kan ook de benadering van PSC-deeltjes in globale modellen een groot effect hebben op de berekende ozonafbraak. In hoofdstuk IV wordt een nieuw algoritme geïntroduceerd in het CTM, dat PSCs realistischer simuleert door de groei en sedimentatie van NAT-deeltjes mee te nemen. Na vorming worden de NAT-deeltjes in het model getransporteerd, onderverdeeld naar grootte. Hiervoor zijn twee verschillende benaderingen gekozen. De eerste benadering neemt

aan dat de deeltjes altijd met dezelfde deeltjesdichtheid bestaan. De andere methode gaat er van uit dat elke getransporteerde NAT-tracer een vaste deeltjesdiameter heeft. De simulaties zijn uitgevoerd voor drie 10-daagse perioden tijdens de 1999-2000 winter. Voor beide methodes komt de berekende maximale deeltjesgrootte op het 96 hPa modelniveau goed overeen met berekeningen van een Lagrangiaans model, en met *in-situ* metingen van grote NAT-deeltjes. Daarnaast zijn de berekeningen vergeleken met een zogenaamd 'evenwichts'-model, waarbij NAT niet getransporteerd wordt en dus niet kan groeien. De verschillen in herverdeling van HNO_3 zijn zeer groot. Een dergelijke 'evenwichts'-routine wordt over het algemeen gebruikt in CTM-studies, zoals de studie in hoofdstuk II. Introductie van het nieuw ontwikkelde algoritme zou de hoeveelheid denitrificatie doen toenemen, waardoor meer ozonafbraak berekend zou worden. Dit zou de eerder genoemde onderschatting van geobserveerde ozonafbraak uit hoofdstuk 2 kunnen verbeteren.
Voor beide benaderingen geldt dat het algoritme vrij ongevoelig is voor het aantal gebruikte deeltjesgroottes en voor de vorm van de grootteverdeling. Echter, de deeltjesdichtheid die gebruikt wordt voor iedere deeltjesgrootte, heeft een aanzienlijk effect op de hoeveelheid HNO_3 die opgenomen wordt in NAT, voor beide methodes. Uit hoofdstuk III en IV blijkt dus dat modelonnauwkeurigheden in het stratosferische transport en de vorming van PSC-deeltjes de onderschatte hoeveelheid ozonafbraak uit hoofdstuk II (gedeeltelijk) kunnen verklaren. Samengevat heeft dit proefschrift daarmee geleid tot een verbeterde modelrepresentatie van de processen die leiden tot ozonafbraak in de Arctische stratosfeer. Integratie van deze resultaten in het chemie-transport model en verdere analyse van de stratosfeer in de Arctische winters van de afgelopen decennia kan in de toekomst bijdragen aan een nog beter begrip en voorspelbaarheid van stratosferische ozonconcentraties.

Summary

During the past two decades, the ozone layer has developed a “hole” each winter and spring above the Antarctic continent. Also in cold Arctic winters substantial stratospheric ozone depletion has been measured, although less than in the Antarctic stratosphere. There is observational evidence of the processes that precede ozone depletion, i.e. chlorine activation on/in polar stratospheric clouds (PSCs). Since the late 1980’s, policy measures have been taken to reduce the halogen source gases that cause the ozone hole. However, because of the long lifetimes of these gases, recovery of the ozone layer is not expected before the next few decades. A further delay is introduced by a cooling of the stratosphere, caused by decreasing ozone and increasing carbon dioxide. These lower temperatures favour the formation of PSCs and thus increase polar stratospheric ozone depletion.

In the Arctic winter stratosphere, the amount of chlorine conversion, denitrification and ozone depletion vary interannually and within one winter, depending on vortex stability and temperature. The simulation of these processes and their variation requires a three-dimensional (3D) chemistry transport model (CTM), because of the non-symmetric behaviour of the Arctic polar vortex. This thesis reports on several studies of the Arctic winter stratosphere carried out with a CTM, being an off-line model that uses meteorological fields from the ECMWF model output.

In Chapter II, chlorine activation and ozone depletion in the Arctic winter stratosphere of 1996-1997 are studied using the newly developed stratospheric version of our CTM. The chemistry scheme, using a Euler Backward Iterative approximation method, includes a comprehensive set of heterogeneous reactions on aerosols and ice particles, which has been tested successfully against a numerically exact solver. Comparisons have been made with total O_3 columns and ClO concentrations observed by satellites, and with ozone loss rates derived from observations during February and March 1997. ClO concentrations and ozone depletion are somewhat underestimated by the model. Key model parameters have been varied to explain this underestimation. Next to temperature, the formation mechanism of solid and/or liquid PSC particles constitutes the main model uncertainty. The largest ClO production and ozone depletion are calculated when solid NAT (Nitric Acid Trihydrate) particles are formed at supersaturation and liquid STS (Supercooled Ternary Solution) particles are present simultaneously. A similar effect is obtained when correcting for an ECMWF temperature warm bias. An average warm bias of 1.3 K at PSC temperatures on the 50 hPa model level reduces the calculated ozone depletion rates over February and March by as much as 35%. A third parameter that influences ClO and ozone depletion is the abundance of inorganic chlorine (Cly). However, assuming maximum Cly alone cannot account for the underestimation of ozone depletion. Both the modelled Cly and ozone concentrations would benefit from a correct representation of tracer transport with the model.

In Chapter III, we have used the CTM to evaluate this stratospheric transport by simulating the long-lived tracers HF and CH_4 during the Arctic winter of 1999/2000. Several model simulations were carried out with the use of a zoom algorithm to investigate the effect of different horizontal resolutions. Balloon-borne and satellite-borne observations of HF and CH_4 were used to test the model. In addition, air mass descent rates within the polar vortex were calculated and compared to observations. Outside the vortex the model results agree well with the observations, but inside the vortex the model underestimates the observed vertical gradient in HF and CH_4, even when the highest available resolution ($1^\circ \times 1°$) is applied. The calculated diabatic

descent rates of the air masses agree with observations above potential temperature levels of 450 K. These model results suggest that too strong mixing through the vortex edge could be a plausible cause for the model discrepancies, associated with the calculated mass fluxes, although other possible reasons are also discussed. As later studies point out, the type of advection scheme and the use of a reduced grid around the poles also play an important role. The model underestimation of the net downward flux partly explain the underestimation of chemical ozone loss rates in Chapter II; less downward transport of Cly means less chlorine available for chemical ozone loss.
From the model simulations with different horizontal resolutions, we conclude that a global 6°x9° resolution is too coarse to represent the polar vortex, whereas the higher resolutions, 3°×2° and 1°×1°, yield similar results, even with a 6°×9° resolution in the tropical region.
Also based on the results in Chapter II, the treatment of PSC particles in global models can have a large effect on calculated ozone depletion. In Chapter IV a new algorithm is implemented in the CTM, which describes PSCs more realistically by mimicking the growth and sedimentation of nitric acid trihydrate (NAT) particles. Once formed, the NAT particles are transported in the model as tracers in the form of size-segregated quantities. Two different approaches were adopted for this purpose: one assuming a fixed particle number density and the other assuming a discrete set of particle diameter values. Simulations were performed for three separate 10-day periods during the 1999-2000 Arctic winter. The resulting maximum particle sizes for both our approaches compare favourably at 96hPa with those obtained from a previous Lagrangian model study, and also with *in-situ* observations related to the size of large NAT particles. Moreover, comparisons were made with a standard equilibrium approach and the differences in the redistribution of HNO_3 were found to be substantial. Such an equilibrium approach has been used in previous model studies, e.g. the model study presented in Chapter II. By implementing this new routine the calculated denitrification increased, which would lead to more chemical ozone depletion. For both approaches the performance of the algorithm is rather insensitive to both the number of size bins and the shape of the size distribution. However, the percentage of HNO_3 sequestered into NAT is critically dependent on the total number density prescribed for each size bin.
Overall, this thesis has led to an improved model representation of the processes leading to ozone depletion in the Arctic stratosphere. Integrating these results in a full chemistry transport model and further analysis of the past cold winters in the Arctic winter stratosphere will help increase our understanding and predictive capability of Arctic stratospheric ozone.

CHAPTER I

Introduction

Chapter I

About 20 years ago, extremely low ozone values in the Antarctic lower stratosphere, between ~14-20 km altitude, were discovered from ground based total ozone column observations [Farman et al., 1985]. This ozone "hole" quickly raised the general awareness towards the importance of the ozone layer, which protects mankind and its environment against harmful UV-B radiation. The man made substances from which this ozone hole arises are the chlorofluorocarbons (CFCs) and halons. These names will still ring a negative bell to many people, even though these substances have been banned from Western society since 1996, as a result of the international agreements laid down in the Montreal Protocol and its Amendments. The production of these substances will have stopped throughout the world in the near future, provided that governments and industry adhere to these agreements. The rapid political agreement following the discovery of the ozone hole is an ideal example of decisive and informed global legislation based upon the findings of atmospheric scientists.
Despite these measures, the ozone layer still suffers from these anthropogenic substances to this day, because of their long atmospheric lifetimes. The Antarctic ozone hole persistently returns each October, ozone depletion has also been observed over the more densely populated Arctic region and the trend in stratospheric ozone for most of the remaining globe is negative [WMO, 2003]. Stratospheric cooling caused by ozone decreases and increases of tropospheric greenhouse gases may cause further delay in the recovery of ozone, since low temperatures increase polar ozone depletion [Shindell, 1998]. Conversely, a decrease in some CFCs has already been reported in the lower part of the atmosphere, the troposphere [Montzka, 1999]. In the stratosphere, CFC growth rates are declining [Engel et al., 1998]. Also, a number of 2-D (latitude-altitude) model studies calculating future stratospheric ozone concentrations predict that the ozone hole will have recovered (i.e. returned to pre-1980 values) around 2050 [WMO, 2003]. Measurements indicate that the stratosphere has cooled with approximately ~0.6 K per decade [WMO, 2003]. Numerical predictions suggest ongoing cooling as a result of climate change, possibly slowing down ozone layer recovery.
The computer models used for these multi-year scenario studies include atmospheric dynamical and chemical processes, and the interaction between those processes, in more or less detail. However, the agreement between such models and observations varies. During some Arctic winters, for instance, ozone depletion in the Arctic winter is underestimated [Becker et al., 2000, Kopp et al., 2002]. A detailed quantitative understanding of the processes determining the concentration of stratospheric ozone is thus still lacking. On the other hand, this knowledge is needed to increase the predictive capabilities of the large-scale climate models. Other key model parameters, such as model resolution, are currently subject of discussion.
The principal aim of this thesis is to enhance the understanding of the chemical and physical processes determining the composition of the ozone layer, and their relative importance. More specifically, we will focus on the processes that lead to or affect ozone depletion during the Arctic winter. This region is crucial, because the climatological variability of this region complicates analysis and predictions of ozone columns, making it an ideal test case. An additional aim is to gain insight in the underlying model characteristics, such as meteorology, grid resolution and the representation of atmospheric chemistry and transport.

1 Background on ozone depletion

The physical history of the ozone layer began $7x10^8$ year ago, when the Earth's atmosphere started to fill up with oxygen (O_2), from which ozone (O_3) formed. The increasing levels of atmospheric O_2 and O_3 protected the Earth's surface from harmful UV-radiation. Eventually, this shielding permitted enhanced biological evolution on land [Graedel and Crutzen, 1993].
The scientific understanding of the ozone layer started less than a century ago, when Chapman et al. [1930] reported the atmospheric working of the chemical cycle combining oxygen, ozone and UV radiation. Through the photo dissociation of molecular oxygen by high-energy solar radiation (reaction 1), and the subsequent reaction of the excited O radical with O_2, ozone is able to form (reaction 2). O_3 then again forms O_2 while absorbing UV-B radiation (reaction 3).

$O_2 + h\nu$	$\rightarrow$	$O + O$	$h\nu < 240$ nm	(1)
$2\ (O + O_2 + M$	$\rightarrow$	$O_3 + M)$		(2)
$O_3 + h\nu$	$\rightarrow$	$O_2 + O$	$h\nu < 1180$ nm	(3)
$O_3 + O$	$\rightarrow$	$2\ O_2$		(4)

Reaction 4 from the Chapman-cycle is able to regenerate O_2 from the active $O+O_3$ ($=O_x$ or odd oxygen). Compared to observations of ozone however, this last reaction appeared too slow to predict an adequate rate of ozone depletion. Bates and Nicolet [1950] found that another chemical cycle, involving HO_2/OH radicals, was also able to catalytically decrease the ozone concentration. Two decades later, several other possibilities for ozone depletion through catalytic cycles were proposed, including cycles with NO/NO_2 [Crutzen, 1970] and ClO/Cl [Stolarski and Cicerone, 1974]. The first link to man-made substances was made in the early seventies, when Crutzen [1971] pointed out that NO/NO_2 exhausted by a fleet of supersonic aircraft would significantly decrease stratospheric ozone. A few years later, Molina and Rowland [1974] opted that CFCs could be a significant source for stratospheric Cl and ClO. Now that the impact of CFCs on the Earth's ozone layer is recognized, it is somewhat ironic that the first CFC, CFC-12 or 'Freon', was synthesized in 1928 by Thomas Midgley at General Motors, a few years before Chapman posed his theory on the working of the ozone layer.
In 1985 extremely low ozone over the Antarctic was found [Farman, 1985] by means of ozone soundings. Later on, satellite observations were able to confirm these observations [Stolarski et al., 1992]. Measurements of the TOMS satellite instruments (Total Ozone Monitoring Spectrometer) show a distinct ozone minimum that has increased over the past decades, inside the Antarctic polar vortex (Figure 1). The polar vortex is the region in the winter polar stratosphere isolated by circumpolar winds that is formed by wave-driven large-scale transport and radiative cooling. Even though the observed low ozone could not immediately be explained, Farman et al. [1985] suggested a connection between the extensive ozone depletion and the presence of chlorine from CFCs. However, the chemical cycles known thus far [Stolarski and Cicerone, 1974] included both the Cl and O radicals, whose production rate and lifetime are small during polar winter and spring, when no UV radiation is present.
In the laboratory, Molina and Molina [1987] discovered that the ClO radical could reaction with itself to form a dimer. The resulting reaction cycle reforms ClO radicals and destroys ozone following reactions (5)-(8):

$ClO + ClO + M$	$\leftrightarrow$	$Cl_2O_2 + M$	(5)
$Cl_2O_2 + h\nu$	$\rightarrow$	$Cl + ClOO$	(6)
$ClOO + h\nu$	$\rightarrow$	$Cl + O_2$	(7)
$2\ (Cl + O_3$	$\rightarrow$	$ClO + O_2)$	(8)

During polar winter, chlorine is bound within the reservoir species HCl and $ClONO_2$, which have relatively long lifetimes. Solomon et al. [1986] suggested that these species could be rapidly converted to the more active chlorine compounds Cl_2 and HOCl on the surface of polar stratospheric clouds (PSCs) by reactions (9)-(13):

$ClONO_2 + HCl$	$\rightarrow$	$Cl_2 + HNO_3$	(9)
$HCl + H_2O$	$\rightarrow$	$HOCl + H_2$	(10)
$ClONO_2 + H_2O$	$\rightarrow$	$HOCl + HNO_3$	(11)
$HCl + HOCl$	$\rightarrow$	$Cl_2 + H_2O$	(12)
$N_2O_5 + H_2O$	$\rightarrow$	$2\ HNO_3$	(13)

In contrast to the chlorine reservoir species, Cl_2 and HOCl are easily photolyzed at sunrise, forming Cl radicals, which destroy ozone catalytically through reactions (5)-(8). Additionally, the uptake of H_2O and HNO_3 by PSCs and subsequent sedimentation may lead to both dehydration and denitrification of the atmosphere. Denitrification, or removal of HNO_3 from the stratosphere, delays the recovery of ozone in springtime since the deactivation of ClO by NO_2 (reaction 14) is inhibited.

$ClO + NO_2 + M$	$\rightarrow$	$ClONO_2 + M$	(14)

When HNO_3 lacks due to denitrification, the NO_2 needed for this reaction is not able to form from HNO_3 photolysis or reaction with O radicals. Evidence of this vertical redistribution of HNO_3 was found soon after the discovery of the ozone hole [Toon et al, 1986; Arnold and Crutzen, 1986]. Shortly after the discovery of the ozone hole, several ground-based and airborne observations of chlorine containing species confirmed the relation between enhanced chlorine radicals and ozone depletion [de Zafra et al., 1987; Solomon et al., 1987; Anderson et al, 1989].
In addition to chlorine, bromine plays a significant role in ozone depletion, especially in combination with chlorine. Wofsy et al. [1975] found that halons, e.g. used in fire extinguishers, form a source of stratospheric bromine. Reactions (15)-(18) show the catalytic bromine and chlorine cycle [McElroy et al., 1986]:

$BrO + ClO$	$\rightarrow$	$Br + Cl + O_2$	(15)
$Br + O_3$	$\rightarrow$	$BrO + O_2$	(16)
$Cl + O_3$	$\rightarrow$	$ClO + O_2$	(17)

The relative contribution of reactions (15)-(17) to chemical ozone loss is higher in the Arctic region than in the Antarctic, where temperatures are higher and less chlorine activation takes place.
Politicians rapidly reacted on these findings and in 1987 the United Nations stated their agreement upon a gradual halting of CFC and halon production in the Montreal Protocol. Amendments and extensions to this agreement were made several times, of which the Copenhagen amendments in 1992 were the most extensive, providing for a total and world-wide ban of CFCs and halons.

Figure 1 TOMS measurements of total ozone in Dobson Units [DU] above the Antarctic region on 4th October of the years 1980 (before the ozone hole) and 1990, with TOMS mounted on the Nimbus-7 satellite, and 2000, when TOMS was mounted on the Earth Probe satellite.

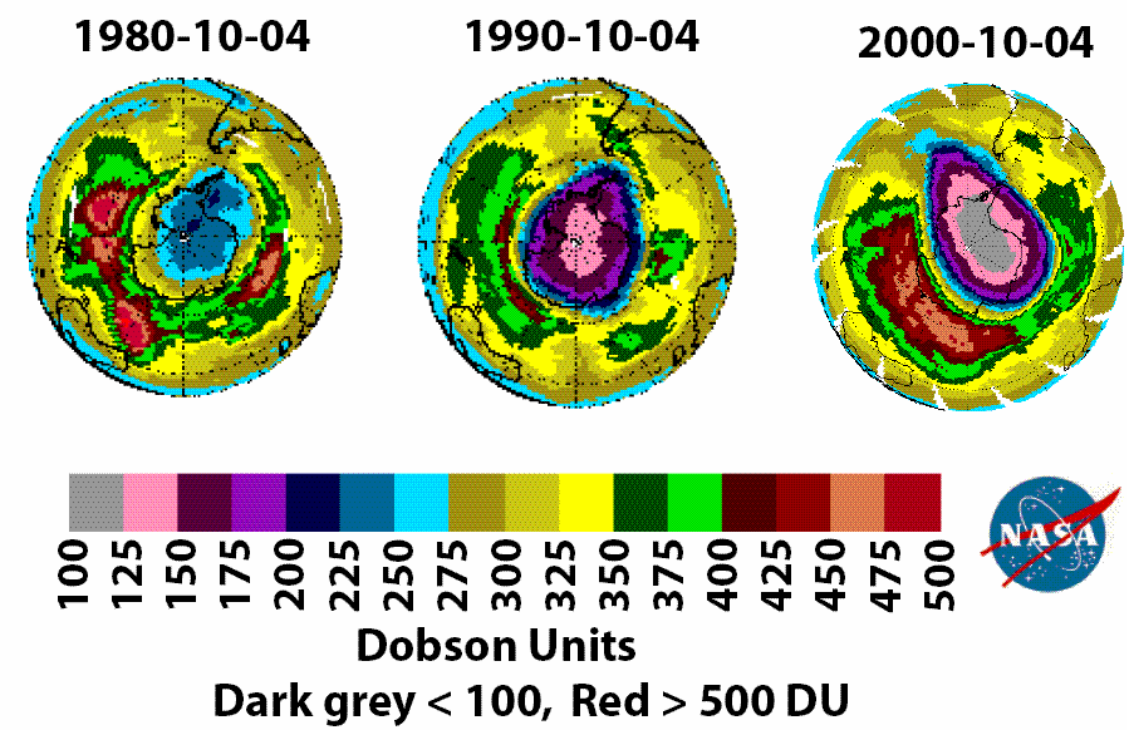

2 The Arctic winter stratosphere

Soon after the discovery of the ozone hole in the Antarctic, questions arose as to whether such low ozone values could occur in the Arctic stratosphere. Several field campaigns, satellite observations and model studies have been carried out in the past 15 years to answer this question [WMO, 2003]. Several important differences with the Antarctic region prevent the Arctic from experiencing a similar yearly ozone hole. First, there is a larger amount of wave activity in the Northern Hemisphere due to a more diverse distribution of land mass, which leads to a polar vortex that is more distorted, less isolated and less centred at the pole than the Antarctic vortex. Thus, mixing of low ozone air into mid latitudes takes place more readily in the Arctic, the vortex is more likely to break up early in winter and the vortex air does not experience darkness continuously throughout the winter. Second, the Arctic stratospheric winter is warmer, since the meridional Brewer-Dobson circulation is stronger in the Northern hemisphere. Whereas Antarctic stratospheric temperatures are below the PSC formation threshold throughout the winter, the Arctic polar vortex only experiences these low temperatures periodically and not in each winter. Third, the stronger Brewer-Dobson circulation causes stronger descent of trace gases during polar winter, resulting in naturally larger ozone column amounts in the Arctic region [WMO, 2003]. These differences between the Arctic and Antarctic stratospheric winter all imply higher ozone values in the Arctic winter/spring stratosphere and less chemical ozone loss.

Despite these less favourable conditions for ozone depletion, a number of Arctic winters during the 1990's, namely '93/'94, '94/'95,'95/'96, '96/'97 and '99/'00, experienced temperatures that were low enough for PSC formation [Manney and Sabutis, 2000; Pawson, Naujokat, 1999]. Subsequently, enhanced ClO was observed

by a number of research groups [e.g. Santee et al., 2000; Crewell et al., 1995; Raffalski et al., 1998; Klein et al., 2000], as well as ozone depletion [e.g. Rex et al., 1997; Müller et al., 1997a; Müller et al., 1997b; Rex, 2002]. Using the GOME instrument (Global Ozone Monitoring Experiment) observations of OClO, Wagner et al. [2001] showed that this active chlorine compound was present both in the Antarctic and Arctic winter stratospheres. However, the amount of OClO was higher in the Antarctic, whilst variability was higher in the Arctic region. These results all showed that similar processes as in the Antarctic could lead to chlorine activation and ozone depletion in the Arctic, but to a lesser extent and with larger interannual variability.

This variability requires a detailed analysis of the realization of stratospheric ozone columns and ozone depletion. Using a 3-D Chemistry Transport Model, Chipperfield and Jones [1999] underscored the dynamic behaviour of the Arctic polar vortex by showing that the total ozone column and the extent of ozone depletion in the Arctic are largely determined by vortex dynamics and the subsequent amount of tracer transport towards the poles. An accurate understanding of this pole ward transport, and mixing of ozone, is thus needed to comprehend and predict ozone concentrations accurately.

Regarding chemical ozone destruction, much of the interannual variability in the Arctic winter is reflected by temperature fluctuations, which often vary above and below the PSC formation threshold [Pawson and Naujokat, 1999]. It was known that PSCs and the heterogeneous reactions on them are a prerequisite to understand chemical ozone loss. Therefore, the influence of temperature and other atmospheric conditions on PSC formation, heterogeneous chlorine conversion and denitrification need to be known in detail to understand and predict ozone depletion. Within the Arctic stratosphere, temperatures are usually too high for ice clouds (PSC type II). Liquid PSCs (Type Ib) consisting of Super-cooled Ternary Solution (STS) have been predicted [Carslaw, 1995] and observed in the Arctic [Schreiner et al., 2000]. Since they can only grow to ~1 μm in size, their impact on denitrification is negligible, but they can contribute to heterogeneous chlorine activation significantly [Hanson et al., 1994]. Recently, during the winter of 1999/2000, a number of observations showed that clouds of solid Nitric Acid Trihydrate (NAT, PSC type Ia) were present [Voigt et al., 2000]. Number densities of ~1e-4 cm^{-3} and sizes up to 20 μm in diameter [Fahey et al., 2001; Northway et al., 2000] were observed. It cannot be ruled out that such large particles were present during earlier winters. The low number density may have been below observational limits at that time [e.g. Deshler and Oltmans, 1998] or it was not possible to determine the exact HNO_3:H_2O ratio [Dye et al., 1992]. Such large particles require a completely different treatment in global chemistry models than used so far, which may have a large impact on chemical ozone loss predictions.

3 Simulations with a 3-D chemistry transport model

Global analysis and prediction of the processes described above require the use of computer models with global coverage, including both tracer transport and chemistry. Several types of models have been used for this purpose. The earliest type of global stratospheric model is the 2-D latitude-altitude model, which uses a climatological description of the meridional circulation [e.g. Solomon et al, 1996; Grooβ et al., 1998; Portmann et al., 1999]. As shown before, the Arctic vortex does not behave in a symmetric way along longitudes, which points out the main disadvantage of this type

of model in this context. To account for the variation in exposure to sunlight of Arctic vortex air, a 3-D model is required.
Within the group of 3-D models, a distinction can be made between general circulation models (GCMs) or climate models, and chemistry transport models (CTMs). These models are also referred to as 'on-line' and 'off-line' models, respectively, since GCMs generate their own meteorological parameters, and CTMs use prescribed assimilated meteorology to calculate advective transport of atmospheric trace gases. These off-line meteorological parameters such as wind, pressure and temperature, are generally obtained from a weather forecast model. Whereas GCMs are mainly used for scenario calculations and calculations of the interactions between chemistry and climate [Shindell, 1998; Rosier and Shine, 2000; Steil et al., 2003], CTMs are more appropriate for detailed analysis of ozone chemistry and transport during a particular winter [Chipperfield, 1999; Lefèvre et al.1998]. The use of off-line meteorology allows for a direct comparison with observations and makes the model more efficient in a computational sense. This allows for more rigorous model sensitivity studies.
Another distinction can be made between Lagrangian and Eulerian models. A Lagrangian model calculates the change in chemical composition of separate air parcels, while an Eulerian model calculates these changes within gridded boxes. The latter assumption may initiate artificial mixing during transport. Generally, Eulerian models have been used for 3D model studies. 3-D Lagrangian simulations of polar ozone loss are being performed on a global scale [Reithmeier and Sausen, 2002; Konopka et al., 2004].
In this thesis, the Eulerian CTMs TM3 and its successor TM5 are used to simulate the Arctic winter stratosphere. These models originate from the tropospheric Transport Model developed by Heimann et al. [1998] and improved and used for the troposphere by Houweling et al. [1998], Dentener et al. [1999], Peters et al. [2002] and Krol et al. [2003; 2004]. The model transport is driven from the European Centre for Medium-range Weather Forecasting (ECMWF). These are either re-analysis data or 6-hour forecast fields, resulting in wind and temperature fields that are valid for the exact dates under study. The TM5 model has a higher altitude range and contains the option to 'zoom' in on a certain area by increasing the horizontal resolution locally. A more detailed description of these model versions is given at the start of each chapter and the model 'zoom' philosophy is presented by Krol et al. [2004]. Each chapter of this thesis discusses a key process that influences ozone concentrations in the Arctic winter stratosphere and the representation of this process in the model. The next section contains an outline of each of these chapters.

4 Outline of the thesis

The distribution of stratospheric ozone within the Arctic polar vortex is a combination of dynamical transport and chemistry. Both process have been investigated separately for two Arctic winters, 1996-1997 and 1999-2000.
In Chapter II, a full stratospheric chemistry scheme is added to the TM3 model to simulate chemical change in the 1996/1997 Arctic winter stratosphere. The model includes all relevant chemical processes. Resulting ClO, ozone columns and ozone depletion rates are compared to a number of observations. The sensitivity of the model to essential input parameters is tested. It was found that temperature, amount of PSC formation and the abundance of inorganic chlorine (Cly) are important model uncertainties, highly affecting the simulated amount of heterogeneous chlorine

conversion and ozone depletion. The inorganic chlorine abundance has a large vertical gradient in the lower stratosphere and its absolute quantity is therefore partly determined by meridional and vertical transport within the model.
In Chapter III, this tracer transport in the polar vortex is examined with the TM5 model by simulating the atmospheric tracers hydrogen fluoride (HF) and methane (CH_4) during the Arctic winter of 1999/2000. Since the chemical lifetimes of these species exceed a few months in the lower winter stratosphere, they provide a good way of testing model transport separately. It is investigated whether mixing across the vortex edge and downward diabatic transport are simulated accurately in TM5. The possibility of horizontal "zooming" that was implemented in TM5, is used to examine the influence of the horizontal model grid resolution inside and outside the polar vortex on the species transport.
Chapter IV addresses the other key uncertainty in chemical ozone loss, recognized in chapter II, namely the PSC particle representation. Recent observations [Fahey, 2003] show that NAT particles in the Arctic, which form a surface for heterogeneous chlorine conversion and lead to denitrification of the air, can get larger than previously thought. This finding may have an influence on the results of Chapter II, which only includes small NAT particles. This chapter isolates the process of NAT growth and denitrification in the Arctic vortex, by including an algorithm in TM5 that calculates the nonequilibrium growth and sedimentation of NAT in the 1999/2000 winter. Short simulations of 10 days are carried out, with using two different algorithms. A detailed description of these algorithms is given in Chapter IV. The resulting particle sizes and HNO_3 distribution are compared to observed values and values of a more detailed Lagrangian model. The difference between these nonequilibrium models and the equilibrium approach used in most models (see also Chapter II) is discussed.
In each chapter, partial conclusions are included. A summary of these, and general conclusions are given in Chapter V.

5 References

Anderson, J.G., W.H. Brune, and M.H. Proffitt, Ozone destruction by chlorine radicals within the Antarctic vortex: The spatial and temporal evolution of ClO-O3 anticorrelation based on *in situ* ER-2 data, *J. Geophys. Res., 94*, 11,465, 1989

Bates, D.R. and M. Nicolet, The photochemistry of atmospheric water vapour*, J. Geophys. Res., 55*, 301, 1950

Becker, G., R. Muller, D.S. McKenna, M. Rex, K.S. Carslaw, and H. Oelhaf, Ozone loss rates in the Arctic stratosphere in the winter 1994/1995: Model simulations underestimate result of the MATCH analysis, *J. Geophys. Res., 105*, 15,175-15,184, 2000

Carslaw, K.S., B.P. Luo, and Th. Peter, an Analytic Expression for the Composition of Aqueous HNO_3-H_2SO_4 stratospheric aerosol including gas phase removal of HNO_3, *Geophys. Res. Lett., 22*, 1877-1880, 1995.

Chapman, S., A theory of upper atmospheric ozone, *Mem. Roy. Soc., 3*, 103-125, 1930

Chipperfield, M.P., and R.L. Jones, Relative influences of atmospheric chemistry and transport on Arctic ozone trends, *Nature, 400*, 551-554, 1999

Chipperfield, M.P., Multiannual simulations with a three-dimensional chemical transport model, *J. Geophys. Res., 104*, 1781-1805, 1999

Crewell, S., R. Fabian, K. Künzi, and T. Wehr, Comparison of ClO measurements by airborne and spaceborne microwave radiometers in the Arctic winter stratosphere 1993, *Geophys. Res. Lett., 22*, 1489-1492, 1995

Crutzen, P.J., The influence of nitrogen oxides on the atmospheric ozone content, *Q.J.R. Meteorol. Soc., 96*, 320-325, 1970

Crutzen, P.J., Ozone production rates in an oxygen-hydrogen-nitrogen oxide atmosphere, *J. Geophys. Res., 76*, 7311-7327, 1971

Crutzen, P.J. and F. Arnold, Nitric acid cloud formation in the cold Antarctic stratosphere: a major cause for the springtime "ozone hole", *Nature, 324*, 651-655, 1986

Dentener, F.J., J. Feichter, and A. Jeuken, Simulation of the transport of Radon^{222} using on-line and off-line global models at different horizontal resolutions: a detailed comparison with measurements, *Tellus, 51B*, 573-602, 1999.

Deshler T., and S.J. Oltmans, Vertical profiles of volcanic aerosol and polar stratospheric clouds above Kiruna, Sweden: Winters 1993 and 1995, *J. Atmos. Chem., 30*, 11-23, 1998

De Zafra, R.L., M. Jaramillo, A. Parrish, P.W. Solomon, B. Connor, and J. Barrett, High concentration of chlorine monoxide at low altitudes in the Antarctic spring stratosphere, I. Diurnal variation, *Nature, 328*, 408-411, 1987

Dye, J.E., D. Baumgardner, B.W. Gandrud, S.R. Kawa, K.K. Kelly, M. Loewenstein, G.V. Ferry, K.R. Chan, and B.L. Gary, Particle size distributions in arctic polar stratospheric clouds, growth and freezing of sulfuric acid droplets and implications for cloud formation, *J. Geophys. Res., 97*, 8015-8034, 1992

Engel, A.E., U. Schmidt and D. McKenna, Stratospheric trends of CFC-12 over the past two decades: Recent observational evidence of declining growth rates, Geophys. Res. Lett., 25, 3319-3322, 1998

Eskes, H., P. van Velthoven, P. Valks, and H. Kelder, Assimilation of GOME total ozone satellite observations in a three-dimensional tracer transport model, *Q.J.R.Meteorol.Soc. 129*, 1663, 2003

Fahey, D.W., R.S. Gao, K.S. Carslaw, J. Kettleborough, P.J. Popp, M.J. Northway, J.C. Holecek, S.C. Ciciora, R.J. McLaughlin, T.L. Thompson, R.H. Winkler, D.G. Baumgardner, B. Gandrud, P.O. Wennberg, S. Dhaniyala, K. McKinney, Th. Peter, R.J. Salawitch, T.P. Bui, J.W. Elkins, C.R. Webster, E.L. Atlas, H. Jost, J.C. Wilson, R.L. Herman, A. Kleinböhl, M. von König, The detection of large HNO3-containing particles in the winter Arctic Stratosphere, *Science*, 1026-1031, 2001

Farman, J.C., B.G. Gardiner, and J.D. Shanklin, Large losses of total ozone in Antarctica reveal seasonal ClO_x/NO_x interaction, *Nature, 315*, 207-210, 1985

Grooβ, J.-U., C. Brühl, and T. Peter, Impact of aircraft emissions on tropospheric and stratospheric ozone, I, Chemistry and 2-D model results, *Atmos. Environ., 32*, 3173-3184, 1998

Grooβ, J.-U., G. Günther, P. Konopka, R. Müller, D.S. McKenna, F. Stroh, B. Vogel, A. Engel, M. Müller, K. Hoppel, R. Bevilacqua, E. Richard, C.R. Webster, J.W. Elkins, D.F. Hurst, P.A. Romashkin, and D.G. Baumgardner, Simulation of ozone depletion in spring 2000 with Chemical Lagrangian Model of the Stratosphere (ClaMS), *J. Geophys. Res., 107*, 8295, doi:10.1029/2001JD000456, 2002

Hanson, D.R., and K. Mauersberger, Vapor pressures of HNO_3/H_2O Solutions at Low Temperatures, *J. Phys. Chem., 92*, 6167-6170, 1988.

Hanson, D.R., A.R. Ravishankara and S. Solomon, Heterogeneous reactions in sulfuric acid aerosol: A framework for model calculations*, J. Geophys. Res., 99*, 3615, 1994

Heimann, M., P. Monfray and G. Polian, Long-range transport of ^{222}Rn – A test for 3D tracer models, *Chem. Geology, 70*, 98, 1988

Houweling, S., F.D. Dentener, and J. Lelieveld, The impact of nonmethane hydrocarbon compounds on tropospheric photochemistry, *J. Geophys. Res., 103*, 10,673-10,696, 1998.

Klein, U., K. Linder, I. Wohltmann, and K.F. Künzi, Winter and spring observations of stratospheric chlorine monoxide from Ny-Ålesund, Spitsbergen, in 1997/98 and 1998/99, *Geophys. Res. Lett., 27*, 4093-4096, 2000

Konopka, P., Steinhorst, H.-M., Grooß, J.-U., Günther, G., Müller, R., Elkins, J.W., Jost,H.-J., Richard, E., Schmidt, U., Toon, G., McKenna, D.S., Mixing and ozone loss in the 1999/2000 Arctic vortex: Simulations with the three-dimensional Chemical Lagrangian Model of the Stratosphere (CLaMS), *J. Geophys. Res., 109*, D02315, 10.1029 /2003JD003792, 2004

Kopp, G., H. Berg, T. Blumenstock, H. Fischer, F. Hase, G. Hochschild, M. Hoepfner, W. Kouker, I. Langbein, T. Reddmann, R. Ruhnke, U. Raffalski, and Y. Kondo, Evolution of ozone and ozone related species over Kiruna during the THESEO 2000-SOLVE campaign retrieved from groundbased millimeter wave and infrared observations*, J. Geophys. Res., 107*, 8308, doi:10.1029/2001JD001064, 2002

Krol, M.C., S. Houweling, B. Bregman, M. van den Broek, A. Segers, P. van Velthoven, W. Peters, F. Dentener, and P. Bergamaschi, The two-way nested global chemistry-transport zoom model TM5 : Algorithm and applications, *submitted to Atm. Chem. Phys. Disc.*, 2004

Krol, M.C., J. Lelieveld, D.E. Oram, G.A. Sturrock, S.A. Penkett, C.A.M. Brenninkmeier,V. Gros, J. Williams and H.A. Scheeren, Continuing emissions of methyl chloroform from Europe, *Nature, 421*, 131-135, 2003.

Lefèvre, F., F. Figarol, K.S. Carslaw and T. Peter, The 1997 Arctic ozone depletion quantified from three-dimensional model simulations, *Geophys. Res. Lett., 25*, 2425-2428, 1998

Manney, G.L. and J.L. Sabutis, Development of the polar vortex in the 1999-2000 Arctic winter stratosphere, *Geophys. Res. Lett., 27*, 2,589-2,592, 2000.

McElroy, M.B., R.J. Salawitch, S.C. Wofsy and J.A. Logan, Reductions of Antarctic ozone due to synergistic ingeractions of chlorine and bromine, *Nature, 321*, 759-762, 1986

Molina, M.J. and F.S. Rowland, Stratospheric sink of chlorofluoromethanes: Chlorine atom-catalized destruction of ozone, *Nature, 249*, 810-812, 1974

Molina, L.T. and M.J. Molina, Production of Cl_2O_2 from the self-reaction of the ClO radical, *J. Phys. Chem., 91*, 433, 1987

Montzka, S.A., J.H. Butler, J.W. Elkins, T.M. Thompson, A.D. Clarke and L.T. Lock, Present and future trends in the atmospheric burden of ozone-depleting halogens, *Nature, 398*, 690-694, 1999

Müller, R., P.J. Crutzen, J.-U. Grooβ, C. Brühl, J.M. Russell III, H. Gernandt, D.S. McKenna, and A. Tuck, Severe chemical ozone loss in the Arctic during the winter 1995-1996, *Nature, 389*, 709-712, 1997a.

Müller, R., J.-U. Grooβ, D.S. McKenna, P.J. Crutzen, C. Brühl, J.M. Russell II, and A.F. Tuck, HALOE observations of the vertical structure of chemical ozone depletion in the Arctic vortex during winter and early spring 1996-1997, *Geophys. Res. Lett., 24*, 2717-2720, 1997b

Northway, M.J., R.S. Gao, P.J. Popp, J.C. Holecek, D.W. Fahey, K.S. Carslaw, M.A. Tolbert, L.R. Lait, S. Dhaniyala, R.C. Flagan, P.O. Wennberg, M.J. Mahoney, R.L. Herman, G.C. Toon and T.P. Bui, An analysis of large HNO_3-containing particles sampled in the Arctic stratosphere during the winter of 1999/2000, *J. Geophys. Res., 107*, D20, 8298, doi:10.1029/2001JD001079, 2002

Pawson, S., and B. Naujokat, The cold winters of the middle 1990s in the Northern lower stratosphere, *J. Geophys. Res., 104*, 14,209-14,222, 1999

Peters, W., M.Krol, F. Dentener, A.M. Thompson, and J. Lelieveld, Chemistry-transport modeling of the satellite observed distribution of tropical tropospheric ozone, *Atmospheric Chemistry and Physics, 2*, 103-120, 2002.

Portmann, R.W., S.S. Brown, T. Gierczak, R.K. Talukdar, J.B. Burkholder, and A.R. Ravishankara, Role of nitrogen oxides in the stratosphere: A reevaluation based on laboratory data, *Geophys. Res. Lett., 26*, 2387-2390, 1999

Raffalski, U., U. Klein, B. Franke, J. Langer, B.-M. Sinnhuber, J. Trentmann, K.F. Künzi, and O. Schrems, Ground-based millimeter-wave observations of Arctic chlorine activation during winter and spring 1996/97, *Geophys. Res. Lett., 25*, 3331-3334, 1998

Reithmeier, C., and R. Sausen, ATTILA: atmospheric tracer transport in Lagrangian model, *Tellus, 54B*, 278-299, 2002

Rex, M., N.R.P. Harris, P. von der Gathen, R. Lehmann, G.O. Braathen, E. Reimer, A. Beck, M.P. Chipperfield, R. Alfier, M. Allaart, F. O'Connor, H. Dier, V. Dorokhov, H. Fast, M. Gil, E. Kyrö, Z. Litynska, I.S. Mikkelsen, M.G. Molyneux, H. Nakane, J. Notholt, M. Rummukainen, P. Viatte, and J. Wenger, Prolonged stratospheric ozone loss in the 1995-96 Arctic winter, *Nature, 389*, 835-838, 1997.

Rex, M., R.J. Salawitch, N.R.P. Harris, P. von der Gathen, G.O. Braathen, A. Schulz, H. Deckelmann, M. Chipperfield, B.-M. Sinnhuber, E. Reimer, R. Alfier, R. Bevilacqua, K. Hoppel, M. Fromm, J. Lumpe, H. Küllmann, A. Kleinböhl, H. Bremer, M. von König, K. Künzi, D. Toohey, H. Vömel, E. Richard, K. Aikin, H. Jost, J.B. Greenblatt, M. Loewenstein, J. R. Podolske, C.R. Webster, G.J. Flesch, D.C. Scott, R.L. Herman, J.W. Elkins, E.A. Ray, F.L. Moore, D.F. Hurst, P. Romashkin, G.C. Toon, B. Sen, J.J. Margitan, P. Wennberg, R. Neuber, M. Allaart, B.R. Bojkov, H. Claude, J. Davies, W. Davies, H. De Backer, H. Dier, V. Dorokhov, H. Fast, Y. Kondo, E. Kyrö, Z. Litynska, I.S. Mikkelsen, M.J. Molyneux, E. Moran, T. Nagai, H. Nakane, C. Parrondo, F. Ravegnani, P. Skrivankova, P. Viatte, V. Yushkov, Chemical depletion of Arctic ozone in winter 1999/2000, *J. Geophys. Res., 107*, D20, 8276, doi:10.1029/2001JD000533, 2002

Rosier, S.M. and K.P. Shine, The effect of two decaded of ozone change on stratospheric temperatures as indicated by a general circulation model, Geophys. Res. Lett., 27, 2617-2620, 2000

Schreiner, J., C. Voigt, A. Kohlmann, F. Arnold, K. Mauersberger, and N. Larsen, Chemical analysis of polar stratospheric cloud particles, *Science, 283*, 968-970, 1999

Shindell, D.T., D. Rind, and P. Lonergang, Increased polar stratospheric ozone losses and delayed eventual recovery owing to increasing greenhouse-gas concentrations, *Nature, 392*, 589-592, 1998

Solomon, S., R.W. Portmann, R.R. Garcia, L.W. Thomasson, L.R. Poole, and M.P. McCormick, The role aerosol variations in anthropogenic ozone depletion at northern mid-latitudes, J. Geophys. Res., 101, 6713-6727, 1996

Solomon, S., G.H. Mount, R.W. Sanders, and A.L. Schmeltekopf, Visible spectroscopy at McMurdo Station, Antarctica: Observations of OClO, *J. Geophys. Res., 92*, 8329-8338, 1987

Solomon, S. R.R. Garcia, F.S. Rowland, and D.J. Wuebbles, On the depletion of Antarctic ozone, *Nature, 321*, 755-758, 1986

Steil, B., C. Brühl, E. Manzini, P.J. Crutzen, J. Lelieveld, P.J. Rasch, E. Roeckner, K. Kruger, A new interactive chemistry-climate model: 1. Present-day climatology and interannual variability of the middle atmosphere using the model and 9 years of HALOE/UARS data, J. Geophys. Res., 108, 4290, doi: 10.1029/2002JD002971, 2003

Stolarski, R., R. Bojkov, L. Bishop, C. Zerefos, J. Staehelin, J. Zawodny, Measured trends in stratospheric ozone, *Science*, 256, 342-349, 1992

Stolarski, R.S. and R.J. Cicerone, Stratospheric chlorine: A possible sink for ozone, *Can. J. Chem., 52*, 1610, 1974

Toon, O.B., P. Hamill, R.P. Turco and J. Pinto, Condensation of HNO_3 and HCl in the winter polar stratosphere, *Geophys. Res. Lett., 13*, 1284-1287, 1986

Voigt, C., J. Schreiner, A. Kohlmann, P. Zink, K. Mauersberger, N. Larsen, T. Deshler, C. Kroger, J. Rosen, A. Adriani, F. Cairo, G. Di Donfrancesco, M. Viterbini, J. Ovarlez, H. Ovarlez, C. David, and A. Dörnbrack, Nitric acid trihydrate (NAT) in polar stratospheric clouds, *Science, 290,* 1756-1758, 2000

Wagner, C. Leue, K. Pfeilsticker, and U. Platt, Monitoring of the stratospheric chlorine activation by Global Ozone Monitoring Experiment (GOME) OClO measurements in the austral and boreal winter 1995 through 1999, *J. Geophys. Res., 106*, 4971-4986, 2001

Wofsy, S.C., M.B. McElroy and Y.L. Yung, The chemistry of atmospheric bromine, *Geophys. Res. Lett., 2*, 215-218, 1975

WMO (World Meteorological Organization), *Scientific assessment of ozone depletion: 2002*, Global Ozone Research and Monitoring Project-Report No. 47, 498 pp., Geneva, 2003

CHAPTER II

Model study of stratospheric chlorine activation and ozone loss during the 1996/97 winter

Published in the *Journal of Geophysical Research, 105*, 28,961-28,977 (2000) with A. Bregman[1] and J. Lelieveld[2] as co-authors

[1]The Royal Netherlands Meteorological Institute, De Bilt, the Netherlands
[2]Max-Panck Institute for Chemistry, Mainz, Germany

Abstract

Chlorine activation and ozone depletion in the Arctic winter stratosphere of 1996-97 have been studied with a newly developed stratospheric chemistry-transport model (CTM). The chemistry scheme, using a Euler Backward Iterative approximation method, includes a comprehensive set of reactions on ternary aerosol and ice particles, which has been tested against a numerically exact solver. Tracer transports in the CTM are calculated from ECMWF meteorological analyses. Comparisons have been made with O_3 and ClO measurements, and with ozone loss rates derived from observations during February and March, 1997. ClO production and ozone depletion are somewhat underestimated by the model. Furthermore, uncertainties regarding the aerosol phase are tested. Assuming Nitric Acid Trihydrate (NAT) particles to form at their melting point, while liquid aerosol is present simultaneously in the model, gives rise to the largest ClO production and the strongest ozone depletion. By correcting for an ECMWF temperature warm bias we obtain a similar large effect on calculated ClO production and ozone depletion for the 1996/97 Arctic winter, whereas uncertainties in the chlorine abundance seem less important. An average warm bias of 1.3 K at PSC temperatures on the 50 hPa model level reduces the calculated ozone depletion rates over February and March by 35%. Observations of ClO are reproduced when lower temperatures and maximum Cl_y abundance are assumed, but ozone depletion is slightly overestimated in that case.

1 Introduction

During the last decades, increasing ozone loss has been observed during springtime in the Antarctic lower stratosphere [Jones and Shanklin, 1995; WMO, 1999]. In the Arctic region, similar chemical ozone loss can occur during cold winters [Müller et al., 1997a; Rex et al., 1997]. The important contribution of heterogeneous chlorine conversion to these severe ozone losses was recognized shortly after the discovery of the Antarctic ozone hole [Farman et al., 1985; Crutzen and Arnold, 1986; Solomon et al., 1986]. On the surface of Polar Stratospheric Cloud (PSC) particles, the chlorine reservoir species HCl and $ClONO_2$ can be converted to HOCl and Cl_2, which are rapidly photodissociated into Cl radicals at sunrise, causing ozone destruction through several catalytic cycles.

Although research efforts on these heterogeneous processes have yielded significant progress, uncertainties remain, for instance regarding the freezing properties of PSC particles between the ice frost point (~188 K at 50 hPa) and the melting temperature of Nitric Acid Trihydrate (NAT, ~195.5 K at 50 hPa) [Peter, 1997]. Observations suggest that both solid and liquid PSC particles are present in this temperature range [Dye et al., 1992].

In global gridded chemistry-transport models either NAT formation below its melting temperature is assumed [M. Chipperfield, personal communication], or the aerosol is assumed to stay liquid down to the ice frost point [F. Lefèvre, personal communication]. In a box model study by Carslaw et al. [1997] it is shown that stronger ozone depletion is calculated when the aerosol is assumed to remain liquid until the temperature drops below the ice frost point, as compared to the assumption that only solid particles form. It is yet unclear what the differences are for calculation of chlorine activation and ozone depletion on a large scale, e.g. calculated by a 3-D chemistry-transport model (CTM). Previous 2-D and 3-D model studies [Portmann et al., 1996, Brasseur et al., 1997] show only a small difference in ozone depletion between these two assumptions in the Antarctic spring. In the Arctic winter, however, temperatures are usually higher and chlorine is not completely activated throughout the winter. Therefore the phase of the aerosol might be more important in the activation of chlorine and ozone depletion. Besides the uncertainties in aerosol phase, uncertainties regarding the reaction probabilities, temperature, total chlorine, water vapor, HNO_3 concentrations and aerosol abundance are known to influence the rate of heterogeneous conversion [Bregman et al., 1997]. The question arises how important these uncertainties are in the global assessment of chlorine activation and ozone depletion with models.

We present a new stratospheric chemistry model that describes heterogeneous chlorine and bromine reactions on NAT, ice and liquid particles. The results of the chemistry scheme have been evaluated by comparing the results with those obtained with a numerically exact solver [Müller et al., 1994]. The effects of uncertainties in the state of the aerosol on important trace species such as ClO and O_3 has been investigated for different temperatures and assumptions regarding the aerosol phase in the temperature regime between the ice frost point and the NAT melting point. In all cases either NAT, supercooled liquid aerosol or a combination of the two was assumed.

The newly developed chemistry scheme has been implemented in the 3-D global transport model TM3. Ozone, ClO production and ozone depletion, as calculated by the model, have been analyzed and compared to observations for the 1996-97 Arctic winter stratosphere. The uncertainties influencing heterogeneous chemistry have been

investigated by performing sensitivity calculations to assess whether these may explain discrepancies between the model results and measurements. The results are discussed in the light of other model uncertainties determining heterogeneous chemistry, such as temperature and chlorine abundance.

2 Description of the TM3-Stratosphere Model

A global three-dimensional CTM, version 3 (TM3), is used, being an extension to the stratosphere of the model described previously by Houweling et al. [1998]. The spatial resolution is 5˚ in longitude by 3.75˚ in latitude, with 19 vertical layers extending from ground level up to 10 hPa. Near the surface these levels are defined as terrain following sigma coordinates whereas the stratospheric layers are defined at pressure surfaces. A hybrid of the two is used between the lower levels and the stratosphere.

Six-hourly mean fields of temperature, surface pressure, wind and humidity from the European Centre for Medium-Range Weather Forecasting (ECMWF) analyses are used to drive the transport of trace species. The reanalyzed ECMWF data have been preprocessed by the Royal Dutch Meteorological Institute (KNMI) to fit the TM3-grid and maintain mass conservation. Every 3 hours the change in concentration through transport is calculated for 25 species and families of species. A second moment advection scheme [Prather, 1986] is used to calculate advective transport. For meridional and vertical transport a timestep of 45 minutes is applied, whereas the calculation of zonal transport uses an 18 minute timestep, which is further reduced near the poles. Convection is calculated with the Tiedtke [1989] mass flux parameterization for cumulus clouds, including entrainment and detrainment in updrafts and downdrafts. Tracer transport in TM3 has been tested by comparing Radon-222 observations at different locations to model simulations [Dentener et al., 1999]. High correlations of model results and measurements were obtained, ranging from $r = 0.5 - 0.8$.

Both anthropogenic (aircraft, industry) and biogenic (lightning, soil) sources of NO_x are included, as well as anthropogenic CO emissions at the surface. A detailed overview of these emissions is given by Houweling et al. [1998]. Methane, CFC-11, CFC-12 and N_2O are constrained at ground level according to the values listed in the 1994 Scientific Assessment of Ozone Depletion [WMO, 1995]. Dry deposition of reaction products at the surface is calculated using a resistance analogy-based parameterization [Ganzeveld et al., 1998]. Wet deposition of soluble trace species is calculated from precipitation rates and Henry's law coefficients [Houweling et al., 1998].

At the top level, boundary conditions are maintained for the long-lived trace gases methane, N_2O, CFC-11 and CFC-12, using monthly averaged data of 1992 from the CLAES instrument on the UARS satellite [Roche et al., 1996; Nightingale et al., 1996], and O_3, using climatological data [Fortuin and Kelder, 1998]. Total inorganic bromine, chlorine and odd nitrogen are prescribed in the top three model layers, using observed correlations with N_2O [Br_y: Daniel et al. 1996; Cl_y:Woodbridge et al. 1995; NO_y: Keim et al. 1997] . The stratospheric growth rates of these species are based on measurements presented in WMO [1999]. The model concentrations are adjusted towards the measurements with a relaxation time of 3 days. H_2O in the stratosphere is prescribed by seasonally and zonally averaged data of HALOE (HALogen Occultation Experiment) over the 5 year period from 1991 to 1996. These data have been validated by Harries et al. [1996].

The chemistry routine contains 46 species and 167 reactions relevant to the stratosphere and troposphere. The reaction scheme is listed in Table 1. Thirty heterogeneous chlorine and bromine reactions are included, of which 11 on ice and on NAT, and 8 on liquid particles. A Euler Backward Iterative (EBI) scheme is used to solve the photochemical differential equations [Hertel et al., 1993].
The reaction scheme is based on a photochemical box model [Müller et al., 1994]. Reaction constants of gas phase binary and ternary reactions are taken from DeMore et al. [1997]. Photolysis rates are calculated from an updated radiation code, originally developed by Lary and Pyle [1991]. Calculations of the absorption cross sections have been updated according to DeMore et al.[1997] and extended with additional species [G. Becker, personal communication]. The oxygen and nitric oxide absorption cross sections in the Schumann Runge wavelength band are calculated using the parameterization of Allen and Frederick [1982]. The temperature dependent cross sections are calculated at each chemistry time step. A matrix that lists precalculated values of incoming actinic fluxes, depending on zenith angle, pressure and latitude, is used to update the diurnal cycle of photolysis rates every 5 days. Every month a new table of actinic fluxes is calculated, using latitudinally varying ozone profiles from the ozone climatology of Fortuin and Kelder [1998].
Heterogeneous reaction rates are calculated at each chemistry timestep. Zonal mean H_2SO_4 concentrations are taken each month from the results of a two-dimensional microphysical model [Bekki and Pyle, 1994]. Effective radius, aerosol surface and volume are calculated in the model. A log-normal size distribution with a σ-value of 1.8, and a constant total aerosol number density of 10 particles cm^{-3} are assumed throughout the stratosphere. The input H_2SO_4 concentrations have been scaled to impose agreement of the modelled aerosol surface density with observations by SAGE (Stratospheric Aerosol and Gas phase Experiment) [Thomason et al., 1997]. The physical state of the particles is determined at each time step by comparing the equilibrium vapor pressures of ice and NAT to the H_2O and HNO_3 partial pressures, respectively, using the formulation of Hanson and Mauersberger [1988]. In the standard configuration, ice forms 3 K below its equilibrium vapor pressure, with a number density of 0.01 particles cm^{-3}. NAT formation yields a number density of 1 particle cm^{-3} at a supersaturation of 10. This latter assumption implies that an undercooling of 3 K is needed for formation of NAT at 50 mbar. Ice, NAT and supercooled ternary solution droplets are allowed to be present simultaneously. When the temperature is low enough, ice is formed before NAT, which is formed before liquid droplets. The aerosol composition is thus calculated from the remaining gas phase H_2O and HNO_3 concentrations. This order in which PSC particles are formed in the model is rather arbitrary. However, a box model study showed no difference in resulting chlorine distribution and ozone concentrations when the order was reversed, since only small differences in the surface area of NAT and liquid particles occurred. First-order reaction constants on solid PSCs are taken from DeMore et al. [1997] when available. The reaction probabilities of $ClONO_2$ with HCl and H_2O and of HOCl with HCl on NAT, are changing with the HCl partial pressure [Hanson and Ravishankara, 1993; Carslaw et al., 1997]. A correction is made for gas phase diffusion. The abundance, size and composition of liquid aerosol are calculated from the gas phase H_2O, HNO_3 and H_2SO_4 partial pressures and temperature, using an analytical expression developed by Carslaw et al. [1995]. The reaction probabilities of the reactions of $ClONO_2$ with H_2O and HCl, and the reaction of HOCl with HCl in liquid droplets are calculated with the parameterizations from Hanson and Ravishankara [1994] and Hanson et al. [1994], respectively. The reaction probability

of the $BrONO_2$ hydrolysis is taken from Hanson et al. [1996]. Solubilities of HOCl and HOBr are calculated as in Huthwelker et al. [1995], assuming a HOBr solubility of 18 times that of HOCl, in line with laboratory results of Hanson and Ravishankara [1995]. The parameterization of Luo et al. [1995] is used for calculation of the HCl and HBr solubility.
Sedimentation of solid particles and subsequent (de)nitrification and (de)hydration have been taken into account, by assuming constant fall velocities for NAT and ice particles [M. Chipperfield, personal communication].

3 Evaluation of the chemistry scheme

3.1 Validation of the numerical solver

The EBI approximation method [Hertel et al., 1993] was applied to solve the set of differential equations in the stratospheric chemistry scheme that has been included in the TM3 chemistry transport model. This scheme was tested against the chemical box model by Müller et al. [1994], which uses the solver FACSIMILE [Curtis and Sweetenham, 1987]. The latter is based on a Gear method with a variable time step. This solver is known to be very accurate but computationally expensive.
Meteorological input for the box model was provided by an idealized 90-day trajectory for a typical polar stratospheric winter from January to March [Lefèvre, personal communication]. The trajectory includes two periods with temperatures below the threshold of polar stratospheric cloud formation (I and II), see Figure 1a. In period I the temperature decreases to 187 K, ~1 K below the ice frost point at 50 hPa, and to 192 K in period II, ~3 K below the NAT point at 50 hPa. NAT formation occurs below 192.5 K, based on a supersaturation of 10, whereas ice particles are formed at equilibrium. The air pressure is 50 hPa throughout the trajectory. Initially, the two numerical solvers are compared, using an identical, detailed scheme for the calculation of heterogeneous reaction rates [Carslaw et al., 1995]. For all species excellent agreement was obtained between the two numerical solvers. The EBI model was used with a timestep of 20 minutes and 10 iterations. Model comparisons for O_3 and noon values of ClO are shown with solid (Gear) and dashed lines (EBI) in Figures 1b and 1d. Absolute differences between the two solvers are shown in Figures 1c and 1e for O_3 and ClO, respectively.

3.2 Assumptions in the aerosol phase

Calculation of the heterogeneous reaction rates with a global 3-D model requires several simplifying assumptions to limit the computational expense. In the detailed scheme (DETAIL) used in the box model described above, the initial liquid particle number density is 10 particles cm^{-3}, varying with changing temperature and pressure, whereas the aerosol number density is assumed to be constant at 10 particles cm^{-3} in the 3-D model. Also, in TM3 the temperature history of the particles is not considered and the aerosol phase is only determined by the surrounding temperature and the gas phase concentrations of HNO_3 and H_2O, ignoring the aerosol phase in the previous timestep. In other words, it is assumed that NAT forms and evaporates at the same temperature. This might result in an underestimation of the NAT abundance in comparison with the DETAIL scheme, since NAT is assumed to form at a supersaturation of 10 (equivalent to 192.5 K at 50 hPa) and only melts at the NAT point, which is 195 K at 50 hPa. This standard configuration (STAND), used in TM3,

has been compared to the DETAIL scheme to investigate the effect of these assumptions.

Table 1 Overview of reactions and reaction rate constants

Binary gas phase reactions:[1]

Reaction			**A**	**B**
$O + O_3$	→	$2\ O_2$	8.e-12	2060
$O(^1D) + H_2$	→	$OH + HO_2$	1.1e-10	0
$O(^1D) + H_2O$	→	2 OH	2.2e-10	0
$O(^1D) + N_2O$	→	2 NO	6.7e-11	0
$O(^1D) + N2O$	→	$N_2 + O_2$	4.9e-10	0
$O(^1D) + CH_4$	→	$OH + CH_3O_2$	1.5e-10	0
$3\ O(^1D) + CHCl_3$	→	3 Cl	2.3e-10	0
$2\ O(^1D) + CH_2Cl_2$	→	2 Cl	1.4e-10	0
O + OH	→	HO_2	2.2e-11	-120
$O + HO_2$	→	$OH + O_2$	3.e-11	-200
$O + H_2O_2$	→	$OH + HO_2$	1.4e-12	2000
$H + O_3$	→	$OH + O_2$	1.4e-10	470
$H + HO_2$	→	OH + OH	8.1e-11*.9	0
$H + HO_2$	→	$H_2 + O_2$	8.1e-11*.08	0
$H + HO_2$	→	$O + H_2O$	8.1e-11*.02	0
$OH + O_3$	→	$HO_2 + O_2$	1.6e-12	940
$OH + H_2$	→	$H_2O + H$	5.5e-12	2000
OH + OH	→	$O + H_2O$	4.2e-12	240
$OH + HO_2$	→	$H_2O + O_2$	4.8e-11	-250
$OH + H_2O_2$	→	$H_2O + HO_2$	2.9e-12	160
$HO_2 + O_3$	→	$OH + O_2$	1.1e-14	500
$HO_2 + HO_2$	→	$H_2O_2 + O_2$	2.3e-13	-600
$O + NO_2$	→	$NO + O_2$	6.5e-12	-120
$O + NO_3$	→	$NO_2 + O_2$	1.e-11	0
$H + NO_2$	→	NO + OH	4.e-10	340
$OH + NO_3$	→	$NO_2 + HO_2$	2.2e-11	0
$OH + HNO_2$	→	$NO_2 + H_2O$	1.8e-11	390
$OH + HNO_4$	→	$NO_2 + H_2O + O_2$	1.3e-12	-380
$OH + HNO_3$	→	$H_2O + HNO_3$	see note[2]	
$HO_2 + NO$	→	$NO_2 + OH$	3.5e-12	-250
$HO_2 + NO_3$	→	$OH + NO_2 + O_2$	1.2e-11	0
N + O2	→	NO + O	1.5e-11	3600
N + NO	→	N2 + O	2.1e-11	-100
$NO + O_3$	→	$NO_2 + O_2$	2.e-12	1400
$NO_3 + NO$	→	$2\ NO_2$	1.5e-11	-170
$NO_2 + O_3$	→	$NO_3 + O_2$	1.2e-13	2450
OH + CO	→	$HO_2 + CO_2$	$1.5e\text{-}13\cdot(1+0.6\cdot P_{atm})$	
$OH + CH_4$	→	$H_2O + CH_3O_2$	2.45e-12	1775

[1] Reaction rates constants are calculated according to: k(T) = A* exp(-B/T)

[2] $k = k_1 + \frac{k_3 \cdot [M]}{1 + k_3 \cdot [M] / k_2}$ with k1= 7.2e-15*exp(785/T), k2=4.1e-16*exp(1440/T), k3=1.9e-33exp(7275/T) , and [M] = the air density in [molec cm^{-3}]

Reaction			A	B
$OH + CH_2O$	→	$HO_2 + CO + H_2O$	1.e-11	0
$OH + CH_3OH$	→	$HO_2 + CH_2O + H_2O$	6.7e-12	600
$OH + CH_3O_2H$	→	$CH_3O_2 + H_2O$	3.8e-12*.7	-200
$OH + CH_3O_2H$	→	$CH_2O + H_2O + OH$	3.8e-12*.3	0
$HO_2 + CH_3O_2$	→	$CH_3O_2H + O_2$	3.8e-13	-800
$CH_3O_2 + CH_3O_2$	→	$CH_2O + CH_3OH + O_2$	2.5e-13	-190
$CH_3O_2 + NO$	→	$CH_2O + NO_2 + HO_2$	3.e-12	-280
$O + ClO$	→	$Cl + O_2$	3.e-11	-70
$O + OClO$	→	$ClO + O_2$	2.4e-12	960
$O + HCl$	→	$Cl + OH$	1.0e-11	3300
$O + HOCl$	→	$OH + ClO$	1.7e-13	0
$OH + Cl_2$	→	$Cl + HOCl$	1.4e-12	900
$OH + ClO$	→	$HO_2 + Cl$	1.1e-11*.94	-20
$OH + ClO$	→	$HCl + O_2$	1.1e-11*.06	-20
$OH + OClO$	→	$HOCl + O_2$	4.5e-13	-800
$OH + HCl$	→	$Cl + H_2O$	2.6e-12	350
$OH + HOCl$	→	$ClO + H_2O$	3.e-12	500
$HO_2 + Cl$	→	$HCl + O_2$	1.8e-11	-170
$HO_2 + Cl$	→	$ClO + OH$	4.1e-11	450
$HO_2 + ClO$	→	$HOCl + O_2$	4.8e-13*.97	-700
$HO_2 + ClO$	→	$HCl + O_3$	4.8e-13*.03	-700
$NO + OCLO$	→	$NO_2 + ClO$	2.5e-12	600
$Cl + O_3$	→	$ClO + O_2$	2.9e-11	260
$Cl + H_2$	→	$HCl + HO_2$	3.7e-11	2300
$Cl + H_2O_2$	→	$HO_2 + HCl$	1.1e-11	980
$Cl + CH_4$	→	$HCl + CH_3O_2$	1.1e-11	1400
$Cl + CH_2O$	→	$HCl + CO + HO_2$	8.1e-11	30
$Cl + CH_3OH$	→	$HO_2 + CH_2O + HCl$	5.4e-11	0
$Cl + OClO$	→	$2\ ClO$	3.4e-11	-160
$Cl + Cl_2O_2$	→	$Cl_2 + O_2 + Cl$	1.e-10	0
$Cl + HOCl$	→	$Cl2 + OH$	2.5e-12	130
$Cl + ClONO_2$	→	$Cl_2 + NO_3$	6.5e-12	-135
$ClO + NO$	→	$NO_2 + Cl$	6.4e-12	-290
$ClO + CH_3O_2$	→	$HO_2 + Cl + CH_2O$	3.3e-12	115
$O + BrO$	→	$Br + O_2$	1.9e-11	-230
$O + HBr$	→	$OH + Br$	5.8e-12	1500
$O + HOBr$	→	$OH + BrO$	1.2e-10	430
$OH + HBr$	→	$Br + H_2O$	1.1e-11	0
$HO_2 + Br$	→	$HBr + O_2$	1.5e-11	600
$HO_2 + BrO$	→	$Br + OH + O_2$	3.4e-12	-540
$Br + O_3$	→	$BrO + O_2$	1.7e-11	800
$Br + CH_2O$	→	$HBr + CO + HO_2$	1.7e-11	800
$Br + OClO$	→	$BrO + ClO$	2.6e-11	1300
$BrO + NO$	→	$NO_2 + Br$	8.8e-12	-260
$BrO + ClO$	→	$Br + OClO$	1.6e-12	-430
$BrO + ClO$	→	$Br + Cl + O_2$	2.9e-12	-220
$BrO + ClO$	→	$BrCl + O_2$	5.8e-13	-170
$BrO + BrO$	→	$2\ Br + O_2$	1.5e-12	-230

Ternary gas phase reactions:[1]

Reaction	k_0^{300}	*n*	k_∞^{300}	*m*	*A*	*B*
$O + O_2 + M \rightarrow O_3 + M$	6.e-34	2.3	-	-	-	-
$H + O_2 + M \rightarrow HO_2 + M$	5.7e-32	1.6	7.5e-11	0	-	-
$OH + OH + M \rightarrow H_2O_2 + M$	6.2e-31	1.	2.6e-11	0	-	-
$O + NO + M \rightarrow NO_2 + M$	9.e-32	1.5	3.e-11	0	-	-
$OH + NO + M \rightarrow HNO_2 + M$	7.e-31	2.6	3.6e-11	0	-	-
$OH + NO_2 + M \rightarrow HNO_3 + M$	2.5e-30	4.4	1.6e-11	1.7	-	-
$HO_2 + NO_2 + M \rightarrow HNO_4 + M$	1.8e-31	3.2	4.7e-12	1.4	2.1e27	10900
$NO_2 + NO_3 + M \rightarrow N_2O_5 + M$	2.2e-30	3.9	1.5e-12	0.7	2.7e-27	11000
$CH_3O_2 + NO_2 + M \rightarrow CH_3O_2NO_2 + M$	1.5e-30	4.0	6.5e-12	2.0	1.3e-28	11200
$Cl + NO_2 + M \rightarrow ClNO_2 + M$	1.3e-30	2.0	1.e-10	1.0	-	-
$ClO + NO_2 + M \rightarrow ClONO_2 + M$	1.8e-30	3.4	1.5e-11	1.9	-	-
$ClO + ClO + M \rightarrow Cl_2O_2 + M$	2.2e-32	3.1	3.5e-12	1.0	1.3e-27	8744
$BrO + NO_2 + M \rightarrow BrONO_2 + M$	5.2e-31	3.2	6.9e-12	2.9	-	-

Photodissociation reactions:[2]

O_2[3] + hν	→	O + O	N_2O + hν	→	N_2 + O
O_3 + hν	→	O_2 + O(^{1}D)	$CHCl_3$ + hν	→	3 Cl
O_3 + hν	→	O_2 + O	CH_2Cl_2 + hν	→	2 Cl
HNO_3 + hν	→	OH + NO_2	CH_3CCl_3 + hν	→	3 Cl
N_2O_5 + hν	→	NO_2 + NO_3	CH_3Cl + hν	→	Cl
$ClONO_2$ + hν	→	Cl + NO_3	CH_2O + hν	→	2 HO_2 + CO
NO + hν	→	N + O	CH_2O + hν	→	H_2 + CO
H_2O_2 + hν	→	OH + OH	H_2O + hν	→	OH + H
CH_3O_2H + hν	→	OH + HO_2 + CH_2O	HOBr + hν	→	OH + Br
Cl_2O_2 + hν	→	Cl + Cl + O_2	Br_2 + hν	→	Br + Br
HCl + hν	→	H + Cl	$BrONO_2$ + hν	→	Br + NO_3
Cl_2 + hν	→	Cl + Cl			
HOCl + hν	→	Cl + OH			
$ClNO_2$ + hν	→	Cl + NO_2			
NO_2 + hν	→	NO + O			

[1] Reaction rate constants k (molec cm^{-3} s^{-1}) are calculated as follows:

$$k_0(T) = k_0^{300} \cdot (T/300)^{-n}$$

$$k_\infty(T) = k_\infty^{300} \cdot (T/300)^{-m}$$

$$k(T,[M]) = \frac{k_0 \cdot [M]}{1 + k_0 \cdot [M]/k_\infty} \cdot 0.6^{1/1+\log\left(k_0 \cdot [M]/k_\infty\right)^2}$$

for temperature T and air density M (in molec cm^{-3})
The rate constants for the backward reactions are calculated as: A*exp(B/T)

[2] Photolysis rates are calculated as follows:

$$J = \int I(\lambda) \cdot \varphi(\lambda,T) \cdot \sigma(\lambda,T)\, d\lambda$$

$I(\lambda)$=actinic flux (1/s)
$\varphi(\lambda,T)$=quantum yield, values taken from JPL [1998]
$\sigma(\lambda,T)$=absorption cross section, values taken from JPL [1998] except for [5]
[3] Absorption cross sections for the Schumann Runge band are obtained from Allen and Frederick [1982]

$HNO_4 + h\nu$	→	$HO_2 + NO_2$		
$NO_3 + h\nu$	→	$NO + O_2$		
$NO_3 + h\nu$	→	$NO_2 + O$		
$OClO + h\nu$	→	$O + ClO$		
$BrCl + h\nu$	→	$Br + Cl$		

Heterogeneous reactions:

on NAT and ice:			*γ on NAT*	*γ on ice*
$N_2O_5 + H_2O$	→	$2\ HNO_3$	0.0003	0.01
$N_2O_5 + HCl$	→	$ClNO_2 + HNO_3$	0.003	0.03
$ClONO_2 + HCl$	→	$Cl_2 + HNO_3$	see text	0.3
$ClONO_2 + H_2O$	→	$HOCl + HNO_3$	see text	0.3
BrONO2 + H2O	→	$HOBr + HNO_3$	0.001	0.3
$BrONO_2 + HCl$	→	$BrCl + HNO_3$	0.3	0.3
$HCl + HOCl$	→	$H_2O + Cl_2$	see text	0.3
$HCl + HOBr$	→	$BrCl + H_2O$	0.1	0.3
$HBr + ClONO_2$	→	$BrCl + HNO_3$	0.3	0.3
$HBr + HOCl$	→	$BrCl + H_2O$	0.3	0.3
$HBr + HOBr$	→	$Br_2 + H_2O$	0.1	0.1

on/in liquid aerosol[1]*:*

$N_2O_5 + H_2O$	→	$2\ HNO_3$
$ClONO_2 + HCl$	→	$Cl_2 + HNO_3$
$ClONO_2 + H_2O$	→	$HOCl + HNO_3$
$BrONO_2 + H_2O$	→	$HOBr + HNO_3$
$HCl + HOCl$	→	$H_2O + Cl_2$
$HCl + HOBr$	→	$BrCl + H_2O$
$HBr + HOCl$	→	$BrCl + H_2O$
$HBr + HOBr$	→	$Br_2 + H_2O$

[1] see text

Figure 1. Comparison of the idealized trajectory runs using the EBI chemical scheme and a solver using Gear's method. (a) shows the temperature along the trajectory, with the ice frost temperature (T_{ice}) and NAT equilibrium temperature (T_{nat}) indicated by dashed lines and symbols I and II denoting two cold spells with temperatures below T_{ice} and T_{nat}, respectively. (b) and (d) show the volume mixing ratios of O_3 and ClO at noon, respectively (ppbv). Solid lines represent the results of the Gear method, dashed lines denote the EBI results. (c) and (e) show the absolute difference in O_3 and ClO (ppbv) between the model using the Gear method and the EBI model.

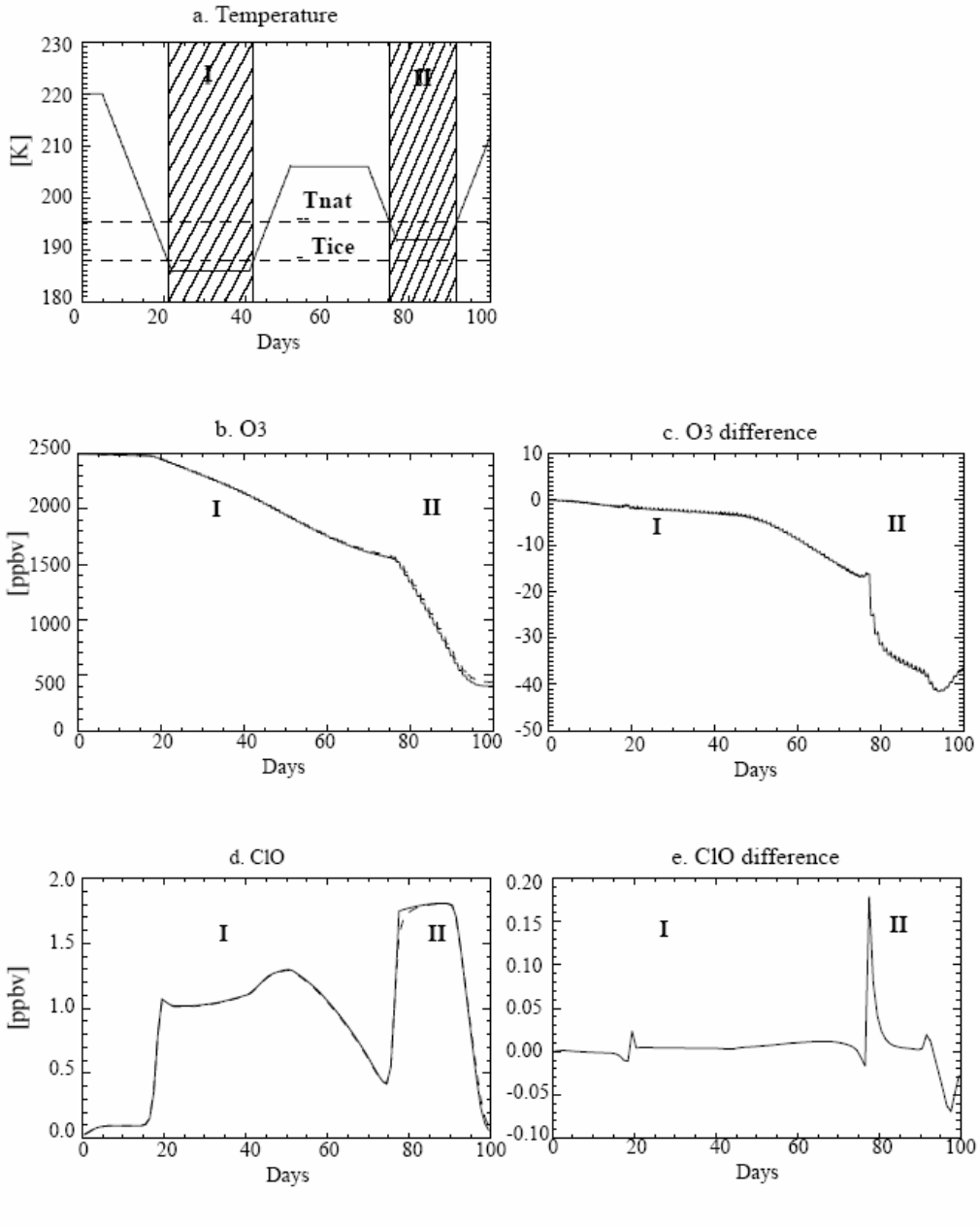

In addition to the differences related to the model simplifications, uncertainties exist regarding the phase of the aerosol between the ice frost point and the NAT equilibrium temperature. Several box model runs have been carried out with different assumptions regarding the aerosol phase between the NAT and ice melting temperatures to see what their effect is on chlorine partitioning and ozone depletion. An overview of all test runs and their assumptions is given in Table 2. Both the STAND and DETAIL parameterizations assume that NAT particles form at a supersaturation ratio of 10 of HNO_3 with respect to NAT, which is equivalent to ~3 K undercooling, and the remaining 9 particles are in the liquid phase. Three other assumptions have been tested:

- In the LIQUID run no NAT is assumed to form and the aerosol remains liquid until the ice frost point.
- The MNAT run assumes that only NAT is present below its melting temperature (10 particles cm^{-3})
- The MIX run assumes the formation of 1 particle cm^{-3} of NAT below its melting temperature without the assumption of undercooling, while the other particles remain liquid.Two trajectories have been used for this sensitivity test: the previously described idealized trajectory and a similar trajectory, with higher temperatures during cold period II of the trajectory (195 K instead of 192 K). The results of ClO and $ClONO_2$ (noon values) and O_3, from day 75 onwards, are shown in Figure 2. During the first part of the trajectory, when particles are mostly either liquid or water ice, all schemes yield the same results for both the chlorine species and O_3. Whenever water ice forms, chlorine is fully converted into ClO_x (=ClO, Cl_2 and Cl_2O_2) within a day, independent of the assumptions. The lack of sunlight prevents large ozone depletion at this stage. As can be expected, differences appear when temperatures are between the melting points of ice and NAT, as occurs during period II in the trajectories. Note that during cold periods in the Arctic vortex these temperatures are common.

First we find that the STAND and the DETAIL schemes compare well in both trajectories. Thus the assumptions in TM3, i.e. a constant aerosol number density and ignoring the phase history of the particles, do not have a significant influence on the O_3 concentrations and on chlorine activation, especially near the threshold of NAT formation. However, the particle history might have a larger influence on the partitioning of species when the temperature changes occur on smaller timescales.

In the STAND and DETAIL trajectory experiments NAT is formed at temperatures below 192.5 K, with liquid aerosol present simultaneously. Therefore, the resulting species concentrations are similar to the results of the MIX run in the lower temperature trajectory. In the trajectory with higher temperatures during period II, at 195 K, no NAT is formed in the STAND and DETAIL model versions and they yield the same results as the LIQUID run.

Comparing the MNAT and LIQUID results, production of ClO and ozone depletion are stronger when only NAT is formed at temperatures close to the NAT equilibrium temperature, while the LIQUID test case shows stronger ozone depletion in the lower temperature trajectory. At 195 K the NAT surface area is much larger than the area of liquid aerosol, whereas the liquid aerosol volume grows exponentially with decreasing temperatures. At 192 K the liquid particle surface is only about 5 times smaller than that of a NAT particle at the same pressure and gas phase concentrations. This was also found by Carslaw et al. [1997]. In addition, the fast reaction of HCl with HOCl in liquid aerosol is a factor of 8 slower on NAT particles at 192 K [Hanson et al., 1994; Hanson and Ravishankara, 1993]. Remarkably, the MNAT experiments (yellow lines) show that this can even lead to more chlorine activation and ozone loss at 195 K than

at 192 K. In the lower temperature trajectory the noon ClO concentrations decrease after initial production, because $ClONO_2$ is completely activated through the heterogeneous reactions with HCl and H_2O. Therefore, during the integration Cl_2 can only be produced from the relatively slow reaction of HCl with HOCl. As a consequence, the ClO production cannot compensate for the gas phase loss of ClO through the HCl production by the CH_4+Cl reaction, and ClO decreases in time. In the higher temperature trajectory not all $ClONO_2$ is activated at once, so that chlorine activation can continue for a longer time period and more ozone loss is calculated at 195 K than at 192 K when only NAT is present. Although this model situation may not be very realistic, since the influx from neighbouring regions would prevent $ClONO_2$ from becoming completely depleted, these results clearly demonstrate the sensitivity and non-linearity of temperature change on chlorine activation and ozone loss.

In the MIX experiments the largest chlorine activation and ozone depletion is calculated in both trajectories. This is due to the simultaneous presence of NAT and liquid aerosol. The freezing out of NAT provides a large particle surface area and fast processing of HCl and $ClONO_2$, whereas the reaction of HOCl and HCl in liquid aerosol is able to rapidly convert the remaining reservoir chlorine. It should be noted that a very small difference is found in chlorine activation and ozone loss between the two temperature regimes in the MIX experiment, due to the full conversion of chlorine reservoir species, which occurs already in the higher temperature trajectory. The difference in ozone loss between all assumptions regarding the aerosol phase is largest in the trajectory where the minimum temperature in part II is 195 K, close to the NAT melting temperature. Thus, the uncertainties regarding the phase of the aerosol have a potentially larger influence on the modeling of ozone loss at temperatures close to the NAT melting temperature.

Table 2. Model assumptions, related to freezing of PSC particles between the ice frost point - 3 K and the NAT equilibrium temperature. Model results are depicted in Figure 2.

Test run	Phase history/ varying number density ?	Temperature of NAT formation	NAT [cm^{-3}]	Liquid aerosol [cm^{-3}]
DETAIL	Yes	At $T < T_{nat} - 3$ K	~ 1	~ 9
STAND	No	At $T < T_{nat} - 3$ K	max. 1	min. 9
LIQUID	No	None	0	10
MNAT	No	At $T < T_{nat}$	10	0
MIX	No	At $T < T_{nat}$	max. 1	min. 9

Figure 2. Calculated O_3 (ppbv) (a, b), ClO at noon (c, d) and $ClONO_2$ at noon mixing ratios (e,f) during period II of the idealized trajectory using the assumptions in Table 2.

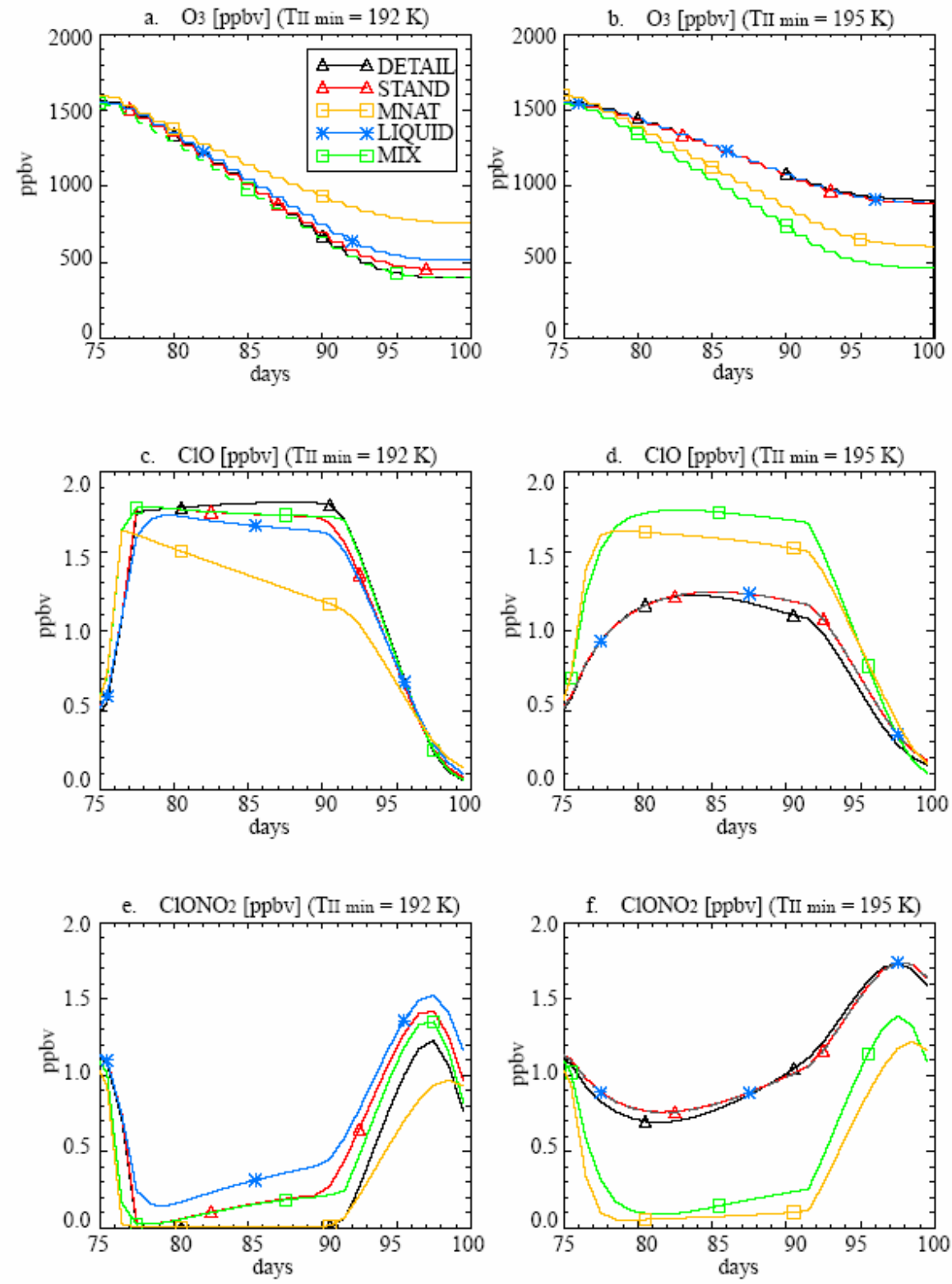

4 Analysis of calculated ozone fields of February and March, 1997

4.1 Total Ozone

The Arctic winter stratosphere in 1996-1997 was characterized by low temperatures below the PSC formation threshold, especially during late winter. Pawson and Naujokat [1999] compared this winter to a 32 year record of stratospheric meteorological analyses. Their analysis shows that the vortex region began to cool mid- January, with favorable conditions for PSC formation. It also shows that during March record low temperatures occurred nearly each day of the month at the 30 hPa and 50 hPa pressure levels. The core of this persistent springtime polar vortex, which remained strong and symmetric until late April, was cold enough for formation of type I PSCs until late March [Coy et al., 1997]. Consequently, high concentrations of ClO were detected by the Microwave Limb Sounder (MLS) [Santee et al., 1997] and strong ozone loss was reported from several measuring and modeling studies [Manney et al. 1997; Müller et al. 1997b; Newman et al. 1997; Lefèvre et al., 1998. See also the Nov. 15., 1997, special issue of the Geophysical Research Letters.]
In our study the TM3 model, including the STAND chemistry routine, is initialized on October 1, 1996, and integrated until the end of March of the next year. Initialization was based on the results at October 1, 1996, of a multi-year run of the TM3 model, starting in October 1994 [Bregman et al., 1999]. The initial ozone concentrations were adjusted by fitting the modelled profiles to TOMS total ozone measurements of October 1, 1996.
Model results of total ozone on March 27, 1997, are compared to observations by three satellite instruments in Figure 3. The GOME instrument is a nadir-viewing UV-VIS spectrometer on board the ERS-2 satellite. For this comparison assimilated GOME data (level 4) were used [Eskes et al., 1999] . The TOMS instruments were flown on board the ADEOS satellite and the NASA Earth Probe (EP) satellite. These instruments are identical and yield similar results, with ADEOS TOMS giving values ~1% higher than EP-TOMS [Newman et al., 1997]. The EP-TOMS shows differences with the Dobson network of 1 to 1.5 % [R.D. McPeters, personal communication]. Since the model only extends up to 10 hPa, upper stratospheric ozone has been determined from zonally averaged climatological profiles, based on ozone sonde and satellite measurements between 1980-1991 [Fortuin and Kelder, 1998], resulting in an additional 30 DU at the poles and 60 DU in the tropics. Overall, the simulated total ozone field and spatial pattern agree well with the observations, however, the model O_3 columns are overestimated upto 60-100 DU within the vortex and upto 20 DU at mid-latitudes. Adjusting the model at the top with climatological values of O_3 instead of instantaneous observations, has an effect on the total column of ozone as well. Using 5% less ozone, in accord with the Northern Hemisphere annual standard deviations in the climatology [Fortuin and Kelder, 1998], resulted in a decrease of 20-30 DU within the vortex and 5-10 DU at mid-latitudes.

Figure 3. Column ozone measured by three satellite instruments and calculated by the TM3 model on March 27, 1997. Upper right: ADEOS TOMS level 3 data. Lower right: Earth Probe TOMS level 3. Lower left: GOME level 4. Upper left: TM3 results.

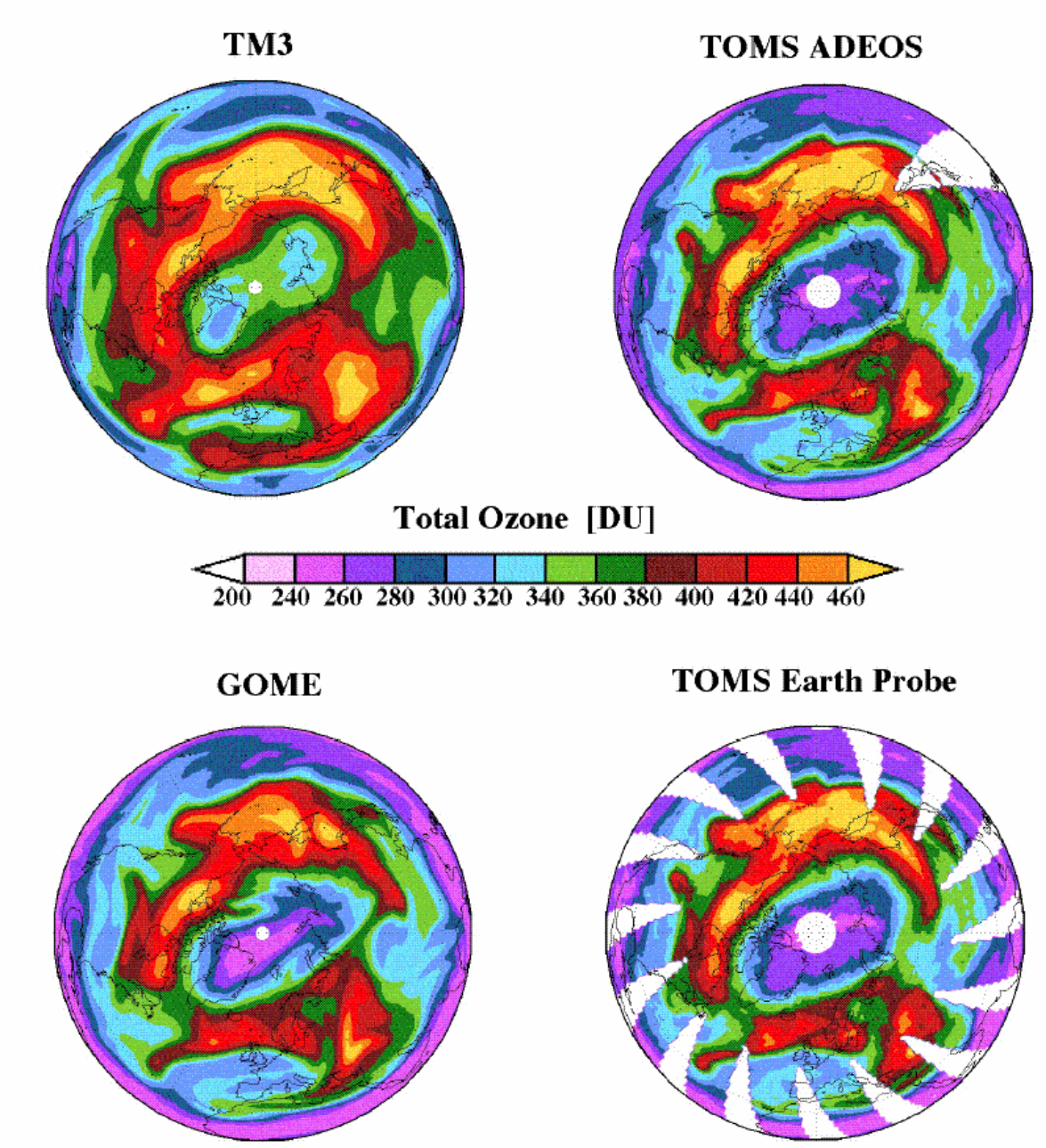

4.2 Ozone profiles

Several ozone sonde observations of the same day are compared to the model results in Figure 4. Profiles have been sampled above Aberystwyth (the observation method is described by Reid et al. [1996]), Ny Ålesund [Steinbrecht et al., 1999], Payerne, Keflavik, Sodankylä and De Bilt. The model results agree fairly well with the magnitude and height of the ozone peak found in the observations except for Ny Alesund (Spitsbergen). At this location the model underestimates O_3 above 200 hPa,

in line with what is found in the comparison of total ozone (Figure 3). From Figure 3 it can be seen as well that Spitsbergen was located near the vortex edge. A detailed inspection of this figure shows that at this location the TM3 model does not capture the sharp O_3 gradient between the ozone depleted vortex and the adjacent O_3 maximum, as a consequence of limited model resolution. In general however, especially between 30 and 73 hPa, the model is in good agreement with all of the observed profiles. An O_3 overestimation is found for the uppermost layer, where climatological mean values are used to constrain the model. In the lowermost stratosphere, the model overestimates O_3 in Aberystwyth and De Bilt, both at mid-latitudes. At the tropopause (200-300 hPa) ozone is overestimated in comparison with several of the profiles. The latter two effects are probably related to uncertainties in transport processes in the lowermost stratosphere [Bregman et al., 1999]. All of these features contribute to the higher O_3 columns as compared to the satellite observations depicted in Figure 3. Furthermore, the vertical fine structure, such as observed over Sodankylä between 70 and 150 hPa, is not captured by the model, due to its relatively coarse vertical resolution.

Figure 4. Ozone sonde observations on March 27 1997 (solid lines), compared to model results of the same day (dashed lines; the triangles denote the centre of the model levels). Observations have been carried out at Aberystwyth, Ireland (52.4N, 4.1W), Ny Ålesund, Spitsbergen (78.9N, 12.0E), Payerne, Switzerland (46.8N, 7.0E), Keflavik, Iceland (64.0N, 22.6W), Sodankylä, Finland (67.4N, 26.7E) and De Bilt, the Netherlands (52.1N, 5.2E)

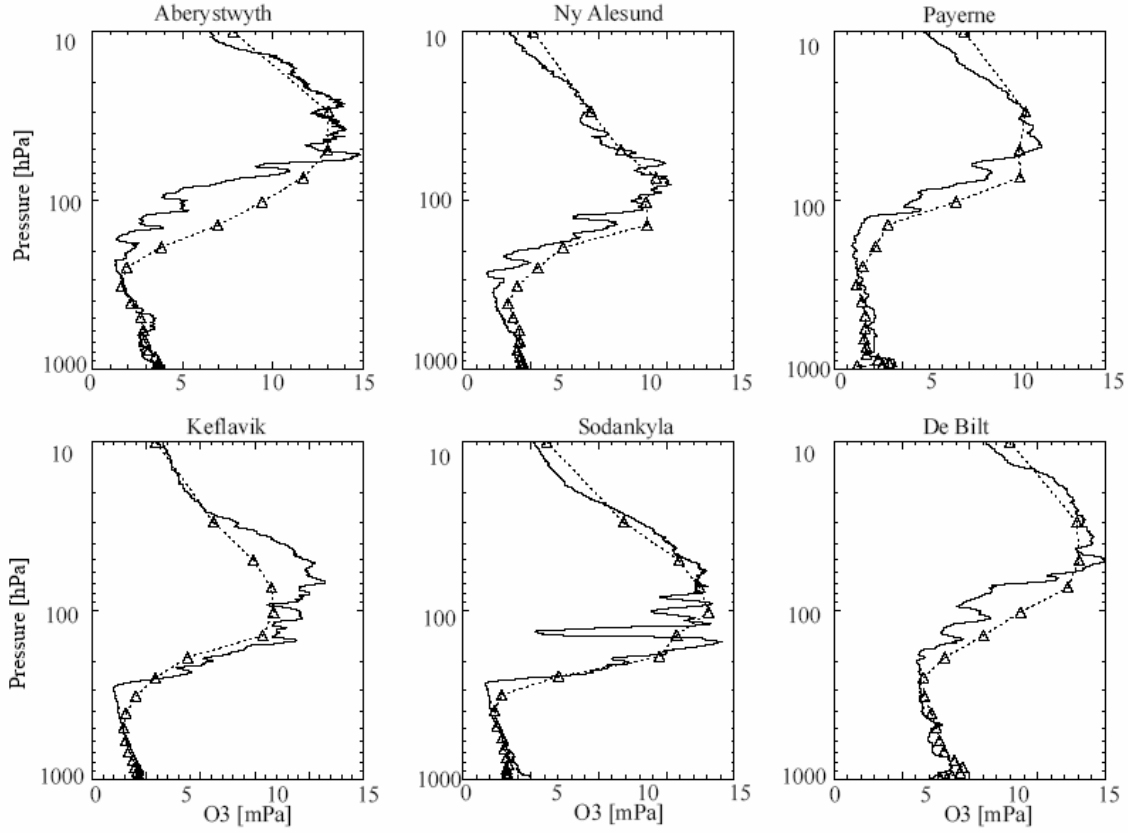

4.3 Ozone loss

Next, we discuss the chemical ozone loss during this winter. The upper plot of Figure 5 shows the 30 and 40 PV isolines on the 475 K level for March, 31, 1997. These lines mark the edge of the vortex, which is defined as the isoline of highest PV-gradients on a surface of equal potential temperature. The middle plot shows the chemical ozone depletion at 50 hPa, separately integrated for each gridbox over the period of February 1 to March 31, 1997. The maximum chemical ozone depletion is found at the sunlit edge of the vortex region, which is to be expected. These values should be conceived as an upper limit of calculated ozone destruction, if no advection of ozone depleted air would have taken place. The maximum destruction is 1.3 ppmv, which equals 22 ppbv/day. The ozone depleted air has been transported throughout the vortex, and this has resulted in decreased ozone concentrations throughout the polar vortex by the end of March. The lower plot shows the ozone change over this time period as calculated from the full-chemistry run minus the results of a 'transport-only'-run, in which ozone was treated as a passive tracer. These latter results can be compared to ozone loss rates derived from observations. Inside the vortex, ozone depletion is 0.8 ppmv at most at the 50 hPa level, which is on average 13 ppbv d^{-1}. This is considerably lower than that derived from measurements. Sinnhuber et al. [1998] derived ozone loss rates of 22 ppbv d^{-1} at the 475 K level during February and March, derived from ground based measurements above Ny Ålesund (79.8˚ N, 11.9˚ E). Similar values were obtained by Kreher et al. [1999] between 475 K and 460 K for inner vortex air above Kiruna (67.9˚ N, 21.1˚ E). Schulz et al. [1999] derived maximum ozone loss rates in the first weeks in March of 45 ppbv d^{-1} during the MATCH campaign. On average they inferred a loss of ~20 ppbv d^{-1} during February and March. Knudsen et al. [1998] derived an ozone depletion of 1.24 ppmv throughout the vortex at the 475 K level from 154 ozone sonde measurements within the vortex, although their calculations include January as well. All of these measurements accounted for downward transport of O_3 through diabatic cooling. From December to March, we calculate a maximum loss of 35 DU in the stratosphere, which is considerably less than the 92 DU derived by Knudsen et al. [1998] between January and March and the loss calculated by Müller et al. [1997b] in the same period from measurements by HALOE. They calculated loss rates by comparing observed ozone to simultaneous observations of the chemically conserved tracer HF. In general the model appears to underestimate the ozone loss rates derived from observations.

Figure 5. PV values at the 475 K potential temperature level (a). Chemical ozone destruction integrated for each gridbox from February 1 to March 31, 1997, at the 50 hPa model level given in ppmv (b). Calculated ozone loss in ppmv from February 1 to March 27 as a result of the difference between O_3 - O_3 as a passive tracer (c)

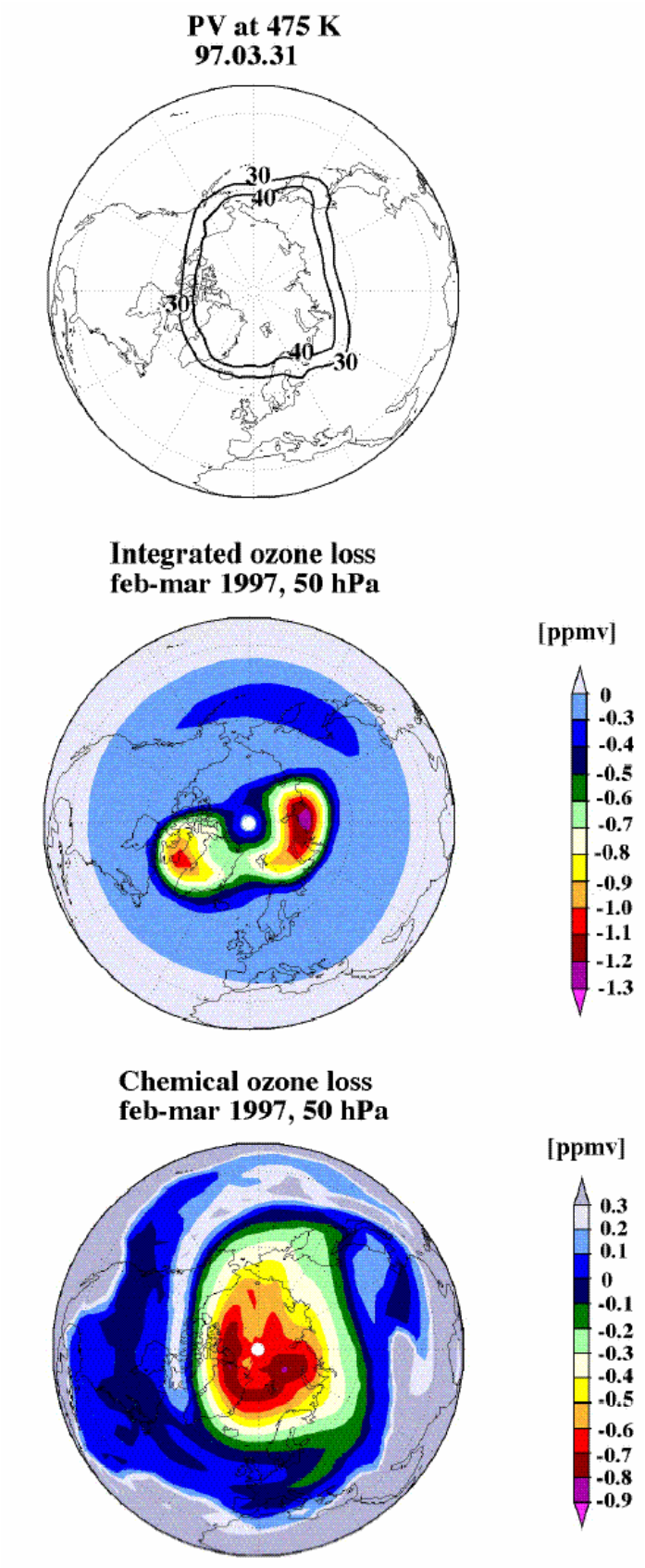

5 The role of heterogeneous chemistry

5.1 ClO mixing ratios

Since ozone loss inside the polar vortex is mainly determined by the ClO dimer and BrO-ClO cyles [Chipperfield and Pyle, 1998], an underestimation of ozone loss is likely to be caused by underestimated ClO and, to a lesser extend, BrO concentrations. Vertical profiles of ClO have been measured throughout the northern hemisphere by MLS on the UARS satellite [Santee et al., 1998] during the 1996/97 winter.
We compare observations of enhanced ClO in the Arctic vortex, sampled on the 46 hPa level of February 20 and February 26, 1997, with model results on 50 hPa. Only daytime ClO measurements were used by Santee et al. [1998] to compose a plot for the northern hemisphere (Figure 6a). A realistic comparison was obtained by using the local noon model results of these dates. The ClO enhancement, as measured by MLS, is qualitatively reproduced by TM3. On both days two maxima appear, both in the measurements and in the model, located over Greenland and Northern Russia. TM3, however, underestimates the measurements by as much as 1.0 ppbv on different occasions. The single profile precision and accuracy of the MLS level 4 data observations are 0.4 ppbv and 10%, respectively [Santee et al., 1997], however, by averaging several profiles, the precision in the maxima over Greenland and Russia is improved to 0.1-0.2 ppbv. Therefore, the difference cannot be explained by possible errors in the observations alone. A similar run, in which the heterogeneous reactions were turned off, illustrated that nearly all ClO calculated by the model in this comparison originates from heterogeneous chemistry. The partitioning of chlorine on February 26th shows that both $ClONO_2$ and HOCl are nearly fully converted at the location of the ClO maxima (together 0.2 ppbv), but 0.6-0.8 ppbv HCl out of 3.3 ppbv Cl_y is still present. The remaining inorganic chlorine is in the form of Cl_2O_2.
The box model study showed that calculated chlorine activation and ozone depletion are strongly influenced by assumptions regarding the phase of the aerosol between the ice frost temperature and the NAT temperature, especially close to the NAT temperature. It was shown that the strongest production of ClO is found when NAT is assumed to form at its melting point, with 1 particle cm^{-3} freezing and the rest of the aerosol remaining in the liquid phase. A sensitivity study was carried out for 26 February using these assumptions on the aerosol phase, resulting in a maximum increase of 0.8 ppbv ClO. The difference with the standard run is shown in figure 8a. Neither in the atmosphere nor in the laboratory are NAT particles detected ubiquitously between the ice frost point and the NAT point [Peter, 1997]. Assuming an overall freezing of NAT below its melting point is likely to give an overestimation of ClO and the resulting value should therefore be considered as an upper limit regarding the uncertainty of the aerosol phase and its effect on the production of ClO.
In addition to these uncertainties related to the aerosol phase, we discuss the previously mentioned model uncertainties affecting heterogeneous reaction rates. Bregman et al. [1997] showed with a box model that, within realistic uncertainty ranges, varying the total amount of chlorine and the temperature has the largest impact on ClO. In this study, the values of inorganic chlorine (Cl_y) and temperature have been varied within the uncertainty range to see whether this may explain the discrepancies with the measurements.

Figure 6. Measured average daytime ClO mixing ratios (ppbv) from MLS at 46 hPa on February 26, 1997 (a) and February 20, 1997 (c). Modelled ClO mixing ratios (ppbv) at 50 hPa at local noon on the same days (b+d).

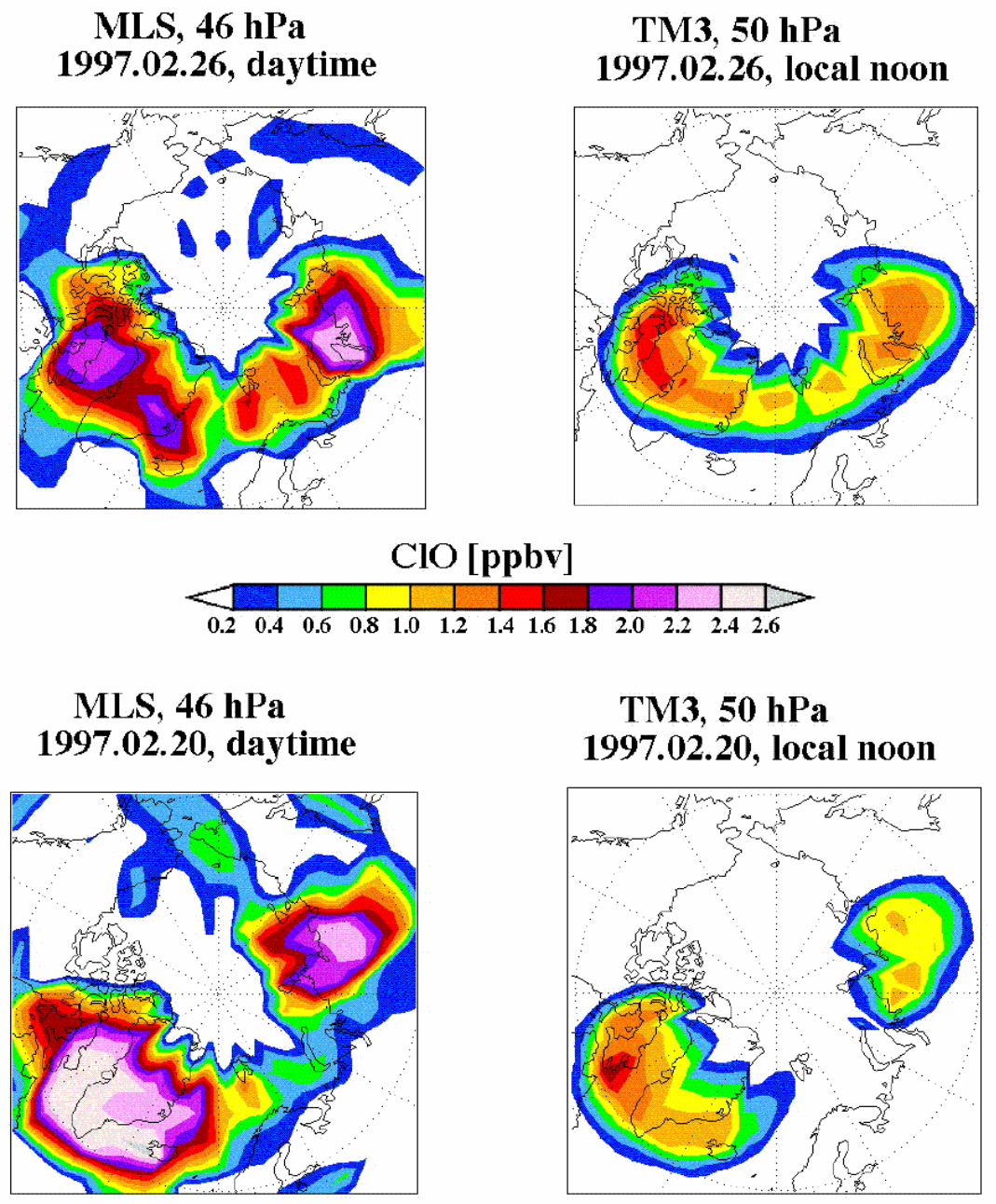

For February, 25th, 1997, Strunk et al. [1998] derived the age of air and Cl_y concentrations from organic chlorine species and SF_6 observations within the vortex. Their results are compared to our model results in Figure 7. Polynomial fits have been drawn through both the observations and the model results. The differences between them range from 380-630 pptv. A sensitivity study has been carried out by adding 500 pptv Cl_y to the model in each gridbox. This results in 3.8 ppbv Cl_y at the location of the maximum ClO in figure 6, which is slightly higher compared to the Cl_y maximum calculated by Strunk et al. [1998].
The temperature variability is also known to affect heterogeneous reaction rates. Subgrid scale temperature variations can cause errors in the calculation of

heterogeneous chemistry and ozone depletion, since the rate of these processes increases non-linearly with decreasing temperature [Murphy and Ravishankara, 1994]. The ECMWF analysis data, used as meteorological input for the TM3 model, indeed show discrepancies with temperature sonde measurements [Knudsen, 1996]. Especially at PSC formation temperatures (T < 195 K), temperatures are on average overestimated in the ECMWF analyses. The average biases (sonde temperature - ECMWF temperature) and the standard deviations found by Knudsen et al. [1996] at PSC formation temperatures are –0.6 K (±1.49 K), –1.1 K (±1.75 K), –1.3 K (±1.93 K) and –1.6 K (±2.26 K) at the 100 hPa, 70 hPa, 50 hPa, and 30 hPa levels, respectively.

Figure 7. Cl_y within the polar vortex derived from observations (asterisks) and and calculated with TM3 (dots) for 25 February 1997. Polynomial fits are indicated by solid and dashed lines respectively.

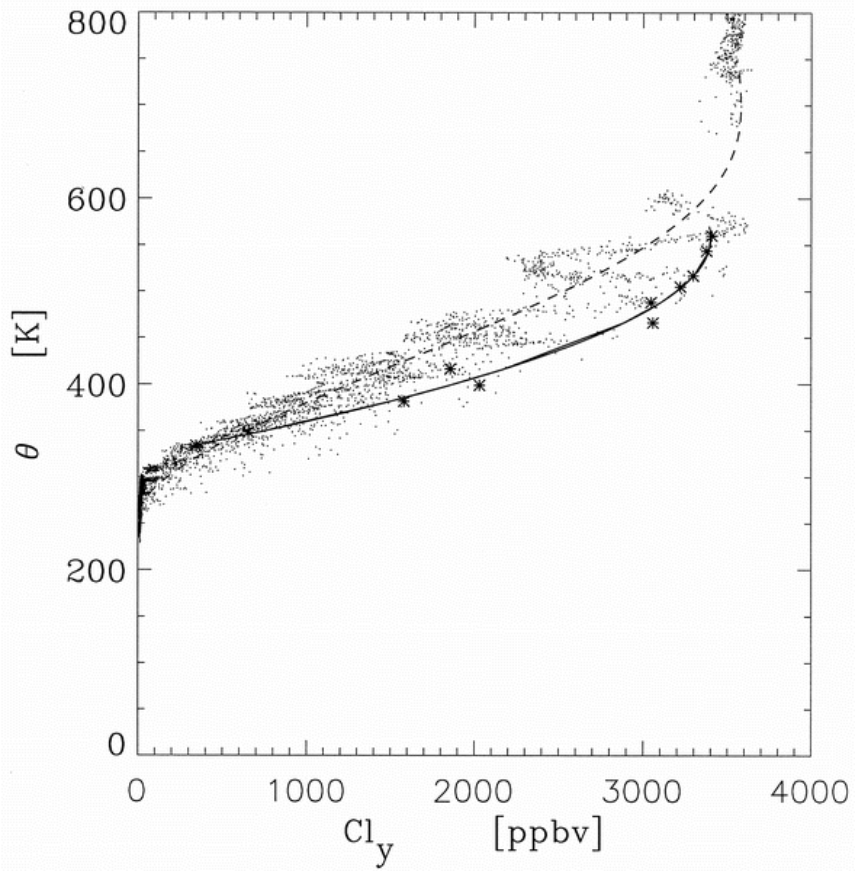

The differences in ClO with the standard run are shown in Figure 8 for the three test cases: NAT formation below its equilibrium temperature; maximum chlorine abundance; and minimum temperatures. An additional run was carried out in which both the lower temperature limit and the maximum amount of Cl_y are implemented. Both the runs with maximum NAT formation and minimum temperatures significantly enhance the amount of ClO in the model. Any other assumption regarding the freezing of NAT only reduces chlorine activation, as was shown in our box model study. The discrepancies of ECMWF temperatures with temperature sondes on the other hand, show high variability [Knudsen, 1998]. Hence, considering the non-linear temperature dependency of heterogeneous reaction rates, the temperature uncertainty might well exceed the uncertainty range assumed in this study and it is probably more important than the aerosol phase uncertainty. A thorough

assessment is needed which also takes into account the standard deviation of the temperature biases. A small part of the enhancement in ClO in the upper plots of figure 8 is due to the enhancement of denitrification, which only occurs when NAT is formed.

Figure 8. Difference of calculated ClO volume mixing ratios (ppbv) from several test simulations compared with the standard model version at 50 hPa, on 26 February 1997, local noon. Upper left: formation of NAT at its equilibrium temperature. Upper right: temperatures decreased. Lower left: 0.5 ppbv increase in inorganic chlorine. Lower right: both lower temperatures and increase in Cl_y (see text for details).

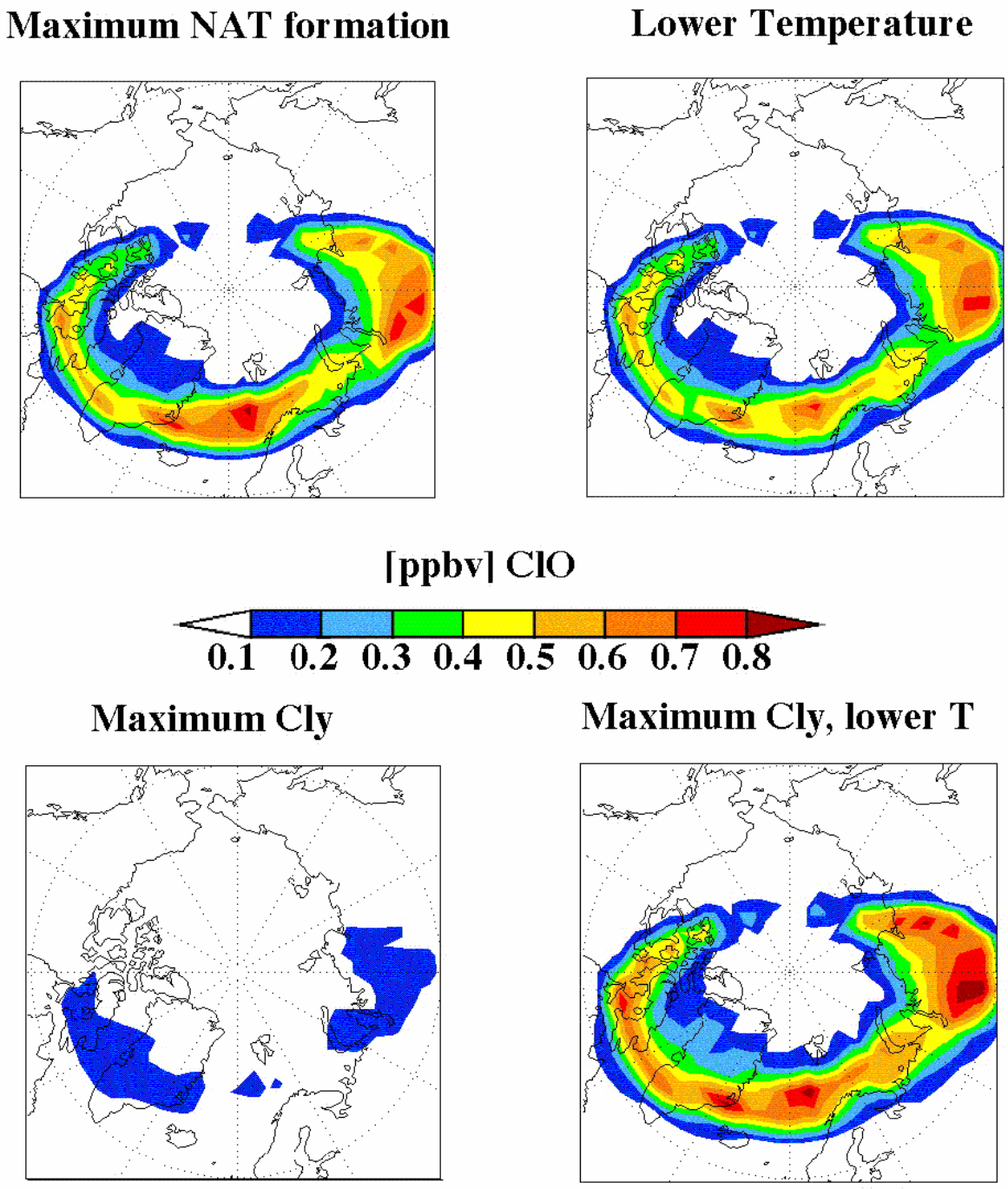

Overall, denitrification was small, because temperatures did not decrease below the ice frost point. ClO is enhanced due to the 0.5 ppbv Cl_y increase, as shown in the lower left plot of figure 8, but this effect is small compared to the other uncertainties. Since not all chlorine is activated continuously, the surplus Cl_y increases ClO by less than 0.5 ppbv.
By combining the lower temperature and maximum Cl_y abundance in the model, the differences between modelled and observed ClO can be explained, although a small discrepancy remains. Besides the errors in the MLS observations that were mentioned before, subgrid scale processes which are not captured by the model, such as the additional temperature uncertainty [Knudsen, 1998] or lee-waves which may cause local temperature decreases of 10 K or more [Carslaw et al., 1998], can possibly explain the remaining differences.

5.2 Ozone depletion rates

Maximum ozone depletion was calculated for all sensitivity simulations by substracting the results of the 'ozone as a passive tracer' run from those of the full-chemistry runs. The chemical loss that affects the 50 hPa level at the end of March was calculated over February and March, 1997. The results are shown in table 3. Whereas both the temperature decrease and NAT increase have large effects on the calculation of ozone depletion, the large surplus in chlorine only has a small effect because ClO is not fully activated. At lower temperatures, when more chlorine activation takes place, the effect of a chlorine increase is much larger than in the standard run (0.5 ppbv·day^{-1} additional ozone depletion instead of 0.3 ppbv·day^{-1}).

Table 3. Sensitivity simulations with TM3. Results indicate maximum modelled ozone depletion during the months of February and March, 1997, on the 50 hPa level.

Test run:	**Maximum $-\Delta O_3$ 50 hPa [ppbv d^{-1}] from Feb-Mar 1997**
Standard run	14
NAT formation at equilibrium	21
More Cl_y (6%)	17
Temperature lowered	20
Temperature lowered and increased Cl_y	25

For this winter, the uncertainties in aerosol phase and temperature largely determine the uncertainty in calculated chlorine activation and ozone depletion. The model agreement with the measurements improves significantly when temperature is lowered. When maximum Cl_y is assumed as well, ozone depletion is overestimated compared to the observations.
In addition to the discussed uncertainties affecting heterogeneous chemistry, there are uncertainties in the gas phase ClO chemistry. The most important uncertainty influencing ozone depletion is that of the Cl_2O_2 absorption cross section [Fish and Burton, 1997]. Ruhnke et al. [1999] showed with a 3-D model that the absorption cross section of Cl_2O_2 represents an uncertain factor for the lower stratosphere, and ozone depletion in March 1997 is decreased by 15% at 20 km, when different absorption cross sections are applied. In this study, however, their upper limit

absorption cross sections Cl_2O_2 have already been used. Uncertainties in the HCl production channel from the ClO + HO_2 and ClO + OH reactions have only a small influence in the lower stratosphere [Ruhnke et al., 1999] and are not discussed here.

6 Discussion and conclusions

We have developed a computationally fast chemistry scheme using a parameterization of heterogeneous chemistry suitable for a 3-D CTM. The results are in excellent agreement with those of a numerically very accurate chemical scheme.
A box model study compares various parameterizations of NAT formation between the ice frost point and the NAT equilibrium temperature. It shows that maximum chlorine activation and ozone depletion, both at 192 K and at 195 K, is calculated when NAT is assumed to form at its equilibrium temperature, and when liquid particles exist at the same time. Ubiquitous presence of NAT between the ice frost point and the NAT equilibrium temperature is unlikely and assuming the formation of NAT throughout the stratosphere right below its equilibrium temperature, with liquid aerosol present simultaneously, is not realistic. The resulting calculated chlorine activation should be considered as an upper limit of the surplus ClO that can be modelled by making assumptions on the aerosol phase.
Implementation of the chemistry scheme in a 3-D transport model yields quite good agreement with ozone observations, but production of ClO and ozone depletion are underestimated using the model standard configuration. Adjustment of the microphysical scheme, so that it produces the highest chlorine activation, significantly increases ClO. However, lowering the temperature by only ~1K at PSC formation temperatures, results in a similar increase. Considering that the difference between ECMWF analysed temperatures and sonde measurements has not only negative biases but also a large variability, the temperature uncertainty might be even more important than shown here, whereas the microphysical effect is most likely overestimated. The temperature uncertainty therefore appears to be the main problem to realistically model ozone depletion with a 3-D model, and it will therefore be difficult to study the impact of uncertainties in aerosol phase with a 3-D model. Not only the ECMWF temperatures, also the UKMO temperatures often used in models, show a warm bias at PSC temperatures [Knudsen, 1996]. Therefore, underestimation of ClO production and subsequent ozone depletion by models using these temperatures is likely. A more accurate uncertainty estimate can not be derived from our results, and an assessment accounting for the variability of temperature biases would be useful. When both the temperature biases and the upper uncertainty limit of Cl_y are implemented, the discrepancies with ClO observations remain within the uncertainty ranges of the observations, although ozone depletion is overestimated compared to observations.
In winters with different temperature regimes, the results of such a sensitivity study may be different. Under extremely cold circumstances, such as in the Antarctic springtime stratosphere, full chlorine activation is likely to occur, and both the microphysical and temperature uncertainties (of ~1 K) might have a smaller effect on ozone loss, whereas uncertainties in chlorine abundance are probably more important in such a case. During a winter with higher temperatures, above or close to the NAT equilibrium temperature, the assumption of more NAT formation in the model may affect the calculations of chlorine activation and ozone loss more strongly. Our box model study shows a large difference in O_3 depletion at 195 K, using different parameterizations of NAT formation. Therefore, the effects on large scale calculations under different winter temperature regimes needs further investigation.

Acknowledgements

The authors thank A. Piters at KNMI and the Langley-DAAC centre for providing total ozone from the GOME and TOMS instruments, respectively, and M. Santee for providing MLS data. P. von der Gathen, E. Kyro, M.Gil, R. Stübi, M. Allaart, and G. Vaughan are acknowledged for providing ozone profile observations through the NILU database, and M. Strunk kindly provided us with values of Cl_y. We thank M. Chipperfield for his denitrification routine and B. Knudsen for calculations of radiosonde - ECMWF temperature biases. Miranda van den Broek was supported by the NWO GO-2 programme under project number eo-022. Bram Bregman was supported by the European Union (DG-XII) under contracts No. ENV4-CT95-0155 and No. ENV4 CT97 0542.

7 References

Allen, M., and J.E. Frederick, Effective photodissociation cross sections from molecular oxygen and nitric oxide in the Schumann-Runge bands, J. Atm. Sci., 39, 2066-2074, 1982.

Bekki, S., and J.A. Pyle, A two-dimensional modeling study of the volcanic eruption of Mount Pinatubo, J. Geophys. Res., 99, 18861-18,869, 1994.

Brasseur, G.P., X. Tie, P.J. Rasch, and F. Lefèvre, A three-dimensional simulation of the Antarctic ozone hole: Impact of anthropogenic chlorine on the lower stratosphere and upper troposphere, J. Geophys. Res., 102, 8909-8930, 1997.

Bregman, A., M.M.P. van den Broek, K.S. Carslaw, R. Müller, T. Peter, M.P. Scheele, and J. Lelieveld, Ozone depletion in the late winter lower Arctic stratosphere: Observations and model results, J. Geophys. Res., 102, 10815-10828, 1997.

Bregman, A., J. Lelieveld, M.M.P. van den Broek, P.C. Siegmund, H. Fischer, and O. Bujok, The N_2O and O_3 relationship in the lowermost stratosphere: a diagnostic for mixing processes as represented by a three-dimensional chemistry-transport model, , J. Geophys. Res., 105, 17,279-17,290, 2000

Carslaw, K.S., B.P. Luo, and Th. Peter, an Analytic Expression for the Composition of Aqueous HNO_3-H_2SO_4 stratospheric aerosol including gas phase removal of HNO_3, Geophys. Res. Lett., 22, 1877-1880, 1995.

Carslaw, K.S., Th. Peter, and R. Müller, Uncertainties in reactive uptake coefficients for solid stratospheric particles-2. Effect on ozone depletion, Geophys. Res. Lett., 24, 1747-1750, 1997.

Carslaw, K.S., M. Wirth, A. Tsias, B.P. Luo, A. Dörnbrack, M. Leutbecher, H. Volkert, W. Renger, J.T. Bacmeister, E. Reimer, and Th. Peter, Increased stratospheric ozone depletion due to mountain-induced atmospheric waves, Nature, 391, 675-678, 1998.

Chipperfield, M.P., and J.A. Pyle, Model sensitivity studies of Arctic ozone depletion, J. Geophys. Res., 103, 28,389-28,403, 1998

Coy, L., E.R. Nash, and P.A. Newman, Meteorology of the polar vortex: Spring 1997, Geophys. Res. Lett., 24, 2693-2696, 1997.

Crutzen, P.J., and F. Arnold, Nitric acid cloud formation in the cold Antarctic stratosphere: a major cause for the springtime 'ozone hole', Nature, 324, 651-655,1986.

Curtis, A.R., and W.P. Sweetenham, Facsimile/Chekmat User's Manual, Computer Science and Systems Division, Harwell Laboratory, Oxford, 135 pp, 1987.

Daniel, J.S., S.M. Schauffler, W.H. Pollock, S. Solomon, A. Weaver, L.E. Heidt, R.R. Garcia, E.L. Atlas, and J.F. Vedder, On the age of stratospheric air and inorganic chlorine and bromine release, J. Geophys. Res., 101, 16,757-16,770, 1996.

DeMore, W.B., S.P. Sander, C.J. Howard, A.R. Ravishankara, D.M. Golden, C.E. Kolb, R.F. Hampson, M.J. Kurylo, and M.J. Molina, Chemical Kinetics and Photochemical Data for Use in

Stratospheric Modeling, Evaluation Number 12, Jet Propulsion Laboratory, National Aeronautics and Space Administration, 1997.

Dentener, F.J., J. Feichter, and A. Jeuken, Simulation of the transport of Radon^{222} using on-line and off-line global models at different horizontal resolutions: a detailed comparison with measurements, Tellus, 51B, 573-602, 1999.

Dye, J.E., D. Baumgardner, B.W. Gandrud, S.R. Kawa, K.K. Kelly, M. Loewenstein, G.V. Ferry, K.R. Chan, and B.L. Gary, Particle size distributions in arctic polar stratospheric clouds, growth and freezing of sulfuric acid droplets and implications for cloud formation, J. Geophys. Res., 97, 8015-8034, 1992.

Eskes, H.J., A.J.M. Piters, P.F. Levelt, M.A.F. Allaart, and H.M. Kelder, Variational assimilation of total-column ozone satellite data in a 2D lat-lon tracer-transport model, 3560-3572, 1999.

Farman, J.C., B.G. Gardiner, and J.D. Shanklin, Large losses of total ozone in Antarctica reveal seasonal ClO_x/NO_x interaction, Nature, 315, 207-210, 1985.

Fish, D.J., and M.R. Burton, The effect of uncertainties in kinetic and photochemical data on model predictions of stratospheric ozone depletion, J. Geophys. Res., 102, 25,537-25,542, 1997.

Fortuin, J.P.F., and Kelder, H., An ozone climatology based on ozonesonde and satellite measurements, J. Geophys. Res., 103, 31,709-31,734, 1998.

Ganzeveld, L.N., J. Lelieveld, and G-J. Roelofs, A dry deposition parameterization for sulfur oxides in a chemistry and general circulation model, J. of Geophys. Res., 103, 5679-5694, 1998.

Hanson, D.R., and K. Mauersberger, Vapor pressures of HNO_3/H_2O Solutions at Low Temperatures, J. Phys. Chem., 92, 6167-6170, 1988.

Hanson, D.R., A.R. Ravishankara, and S. Solomon, Heterogeneous reactions in sulfuric acid aerosols: a framework for model calculations, J. Geophys. Res., 99, 3615-3629, 1994.

Hanson, D.R., and A.R. Ravishankara, Reactive uptake of $ClONO_2$ onto sulfuric acid due to reaction with HCl and H_2O, J. Phys. Chem., 98, 5728-5735, 1994.

Hanson, D.R., and A.R. Ravishankara, heterogeneous chemistry of bromine species in sulfuric acid under stratospheric conditions, Geophys. Res. Lett. 22, 385-388, 1995.

Hanson, D.R., A.R. Ravishankara, and E.R. Lovejoy, Reaction of $BrONO_2$ with H_2O on submicron sulfuric acid aerosol and the implications for the lower stratosphere, J. Geophys. Res., 101, 9063-9069, 1996.

Harries, J. E., J. M. Russell III, A. F. Tuck, L. L. Gordley, P. Purcell, K. Stone, R. Bevilacqua, M. R. Gunson, G. Nedoluha, and W. A Traub, Validation of Measurements of Water Vapor from the Halogen Occultation Experiment, HALOE, J. Geophys. Res., 101, 10,205-10,216, 1996.

Hertel, O., R. Berkowicz, J. Christensen, and Ø. Hov, Test of two numerical schemes for use in atmospheric transport-chemistry models, Atmosph. Env., 27a, 16, 2591-2611, 1993.

Houweling, S., F.D. Dentener, and J. Lelieveld, The impact of nonmethane hydrocarbon compounds on tropospheric photochemistry, J. Geophys. Res., 103, 10,673-10,696, 1998.

Huthwelker, Th., Th. Peter, B.P. Luo, S.L. Clegg, K.S. Carslaw, and P. Brimblecombe, solubility of HOCl in water and aqueous H_2SO_4 to stratospheric temperatures, J. Atm. Chem., 21, 81-95, 1995.

Jones, A.E., and J.D. Shanklin, Continued decline of total ozone over Halley, Antarctica, since 1985, Nature, 376, 409-411, 1995.

Keim, E.R., M. Loewenstein, J.R. Podolske, D.W. Fahey, R.S. Gao, E.L. Woodbridge, R.C. Wamsley, S.G. Donelly, L.A. Del Negro, C.D. Nevison, S. Solomon, K.H. Rosenlof, C.J. Scott, M.K.W. Ko, D. Weisenstein, and K.R. Chan, Measurements of the $NO_y - N_2O$ correlation in the lower stratosphere: Latitudinal and seasonal changes and model comparisons, J. Geophys. Res., 102, 13,193-13,212, 1997.

Knudsen, B.M., Accuracy of arctic stratospheric temperature analyses and the implications for the prediction of polar stratospheric clouds, Geophys. Res. Lett., 23, 3747-3750, 1996.

Knudsen, B.M., N. Larsen, I.S. Mikkelsen, J.-J. Morcrette, G.O. Braathen, E. Kyrö, H. Fast, H. Gernandt, H. Kanzawa, H. Nakane, V. Dorokhov, V. Yushkov, G. Hansen, M. Gil, and R.J. Shearman, Ozone depletion in and below the Arctic vortex for 1997, Geophys. Res. Lett., 25, 627-630, 1998.

Kreher, K., G.E. Bodeker, H. Kanzawa, H. Nakane, and Y. Sasano, Ozone and temperature profiles measured above Kiruna inside, at the edge of, and outside the Arctic polar vortex in February and March 1997, Geophys. Res. Lett., 26, 715-718, 1999.

Lary, D.J., and J.A. Pyle, Diffuse Radiation, Twilight, and Photochemistry - I, J. Atm. Chem., 13, 373-392, 1991.

Lefèvre, F., F. Figarol, K.S. Carslaw, and T. Peter, The 1997 Arctic ozone depletion quantified from three-dimensional model simulations, Geophys. Res. Lett. 25, 2425-2428,1998.

Luo, B.P. , K.S. Carslaw, Th. Peter, and S.L. Clegg, Vapour pressures of $H_2SO_4/HNO_3/HCl/HBr/H_2O$ solutions to low stratospheric temperatures, Geophys. Res. Lett. 22, 247-250, 1995.

Manney, G.L, L. Froidevaux, M.L. Santee, R.W. Zurek, and J.W. Waters, MLS observations of Arctic ozone loss in 1996-1997, Geophys. Res. Lett., 24, 2697-2700, 1997.

Müller, R., Th. Peter, P.J. Crutzen, H. Oelhaf, G.P. Adrian, Th. V. Clarmann, A. Wegner, U. Schmidt, and D. Lary, Chlorine chemistry and the potential for ozone depletion in the Arctic stratosphere in the winter of 1991/92, Geophys. Res. Lett., 21, 1427-1430, 1994.

Müller, R., P.J. Crutzen, J.-U. Grooβ, C. Brühl, J.M. Russell III, H. Gernandt, D.S. McKenna, and A. Tuck, Severe chemical ozone loss in the Arctic during the winter 1995-1996, Nature, 389, 709-712, 1997a.

Müller, R., J.-U. Grooβ, D.S. McKenna, P.J. Crutzen, C. Brühl, J.M. Russell II, and A.F. Tuck, HALOE observations of the vertical structure of chemical ozone depletion in the Arctic vortex during winter and early spring 1996-1997, Geophys. Res. Lett., 24, 2717-2720, 1997b.

Murphy, D.M., and A.R. Ravishankara, Temperature averages and rates of stratospheric reactions, Geophys. Res. Lett., 21, 2471-2474, 1994.

Newman, P.A., J.F. Gleason, R.D. McPeters, and R.S. Stolarski, Anomalously low ozone over the Arctic, Geophys. Res. Lett., 24, 2689-2692, 1997.

Nightingale, R.W., A.E. Roche, J.B. Kumer, J.L. Mergenthaler, J.C. Gille, S.T. Massie, P.L. Bailey, D.P. Edwards, M.R. Gunson, G.C. Toon, B. Sen, J-F. Blavier, and P.S. Connell, Global CF_2Cl2 measurements by UARS cryogenic limb array etalon spectrometer: Validation by correlative data and a model, J. Geophys. Res., 101, 9711-9736, 1996.

Pawson, S., and B. Naujokat, The cold winters of the middle 1990s in the northern lower stratosphere, J. Geophys. Res., 104, 14,209-14,222, 1999.

Peter, Th., Microphysics and heterogeneous chemistry of polar stratospheric clouds, Annu. Rev. Phys. Chem., 48, 785-822, 1997.

Portmann, R.W., S. Solomon, R.R. Garcia, L.W. Thomason, L.R. Poole, and M.P. McCormick, Role of aerosol variations in anthropogenic ozone depletion in the polar regions, J. Geophys. Res., 101, 22991-23006, 1996.

Prather, M.J., Numerical advection by conservation of second-order moments, J. Geophys. Res., 91, 6671-6681, 1986.

Reid, S.J., G. Vaughan, A.R.W. Marsh, and H.G.J. Smit, Accuracy of Ozonesonde Measurements in the Troposphere, J. Atm. Chem., 25, 215-226, 1996.

Rex, M., N.R.P. Harris, P. von der Gathen, R. Lehmann, G.O. Braathen, E. Reimer, A. Beck, M.P. Chipperfield, R. Alfier, M. Allaart, F. O'Connor, H. Dier, V. Dorokhov, H. Fast, M. Gil, E. Kyrö, Z. Litynska, I.S. Mikkelsen, M.G. Molyneux, H. Nakane, J. Notholt, M. Rummukainen, P. Viatte, and J. Wenger, Prolonged stratospheric ozone loss in the 1995-96 Arctic winter, Nature, 389, 835-838, 1997.

Roche, A.E., J.B. Kumer, R.W. Nightingale, J.L. Mergenthaler, G.A. Ely, P.L. Bailey, S.T. Massie, J.C. Gille, D.P. Edwards, M.R. Gunson, M.C. Abrams, G.C. Toon, C.R. Webster, W.A. Traub, K.W. Jucks, D.G. Johnson, D.G. Murcray, F.H. Murcray, A. Goldman, and E.C. Zipf, Validation of CH_4 and N_2O measurements by the cryogenic limb array etalon spectrometer instrument on the Upper Atmosphere Research Satellite, J. Geophys. Res., 101, 9679-9710, 1996.

Ruhnke, R., W. Kouker, Th. Reddmann, H. Berg, G. Hochschild, G. Kopp, R. Krupa, and M. Kuntz, The vertical distribution of ClO at Ny-Ålesund during March 1997, Geophys. Res. Lett., 7, 839-843, 1999.

Santee, M.L., G.L. Manney, L. Froidevaux, R.W. Zurek, and J.W. Waters, MLS observations of ClO and HNO_3 in the 1996-97 Arctic polar vortex, Geophys. Res. Lett., 24, 2713-2716, 1997.

Schulz, A., J. Steger, M. Rex, N. Harris, G.O. Braathen, E. Reimer, R. Alfier, A. Beck, M. Alpers, J. Cisneros, H. Claude, H. De Backer, H. Dier, V. Dorokhov, H. Fast, S. Godin, G. Hansen, Y. Kondo, E. Kosmidis, E. Kyro, M.J. Molyneux, G. Murphy, H. Nakane, C. Parrondo, F. Ravegnani, C. Varotsos, C. Vialle, V. Yushkov, C. Zerefos, and P. von der Gathen, Match observations in the Arctic winter 1996/1997: High stratospheric ozone loss rates correlate with low temperatures deep inside the polar vortex, Geophys. Res. Lett.,27, 205-208,2000.

Sinnhuber, B-M., J. Langer, U. Klein, Uwe Raffalski, K. Künzi, and O. Schrems, Ground based millimeter-wave observations of Arctic ozone depletion during winter and spring of 1996/97, Geophys. Res. Lett., 25, 3327-3330, 1998.

Solomon, S., R.R. Garcia, F.S. Rowland, and D.J. Wuebbles, On the depletion of Antarctic ozone, Nature, 321, 755-758, 1986.

Steinbrecht, W., R. Neuber, P. v.d. Gathen, P. Wahl, T.J. McGee, M.R. Gross, U. Klein, and J. Langer, Results of the 1998 Ny-Alesund Ozone Measurements Intercomparison NAOMI, submitted to Geophys. Res. Lett., 1999.

Strunk, M., A. Engel, M. Muller, and U. Schmidt, Estimates of total inorganic chlorine (Cly) using a sulfur hexafluoride derived age, Polar stratospheric ozone 1997, proceedings of the fourth European symposium, 22 to 26 September, Schliersee, Bavaria, Germany, edited by N.R.P. Harris, I. Kilbane-Dawe and G.T. Amanatidis, 1998.

Thomason, L.W., L.R. Poole, and T. Deshler, A global climatology of stratospheric aerosol surface area density deduced from Stratospheric Aerosol and Gas Experiment II: 1984-1994, J. Geophys. Res., 102, 8967-8976, 1997.

Tiedtke, M., A comprehensive mass flux scheme for cumulus parameterization in large-scale models, Mon. Wea. Rev., 117, 1779-1800, 1989.

Woodbridge, E.L., J.W. Elkins, D.W. Fahey, L.E. Heidt, S. Solomon, T.J. Baring, T.M. Gilpin, W.H. Pollock, S.M. Schauffler, E.L. Atlas, M. Loewenstein, J.R. Podolske, C.R. Webster, R.D. May, J.M. Gilligan, S.A. Montzka, K.A. Boering, and R.J. Salawitch, Estimates of total organic and inorganic chlorine in the lower stratosphere from in situ and flask measurements during AASE II, J. Geophys. Res., 100, 3057-3064, 1995.

World Meteorological Organization (WMO), Scientific Assessment of ozone depletion: 1994, Global Ozone Research and Monitoring Project – report no. 37, 1995.

World Meteorological Organization (WMO), Scientific Assessment of ozone depletion: 1998, Global Ozone Research and Monitoring Project – report no. 43, 1999.

CHAPTER III

The impact of model grid zooming on tracer transport in the 1999/2000 Arctic polar vortex

Published in Atmospheric Chemistry and Physics, 3, 1833-1847 (2003), with M.K. van Aalst[1], A. Bregman[2], M. Krol[1], J. Lelieveld[3], G.C. Toon[4], S. Garcelon[5], G.M. Hansford[5], R.L. Jones[5] and T.D. Gardiner[6] as co-authors.

[1] Institute for Marine and Atmospheric Research (IMAU), Utrecht, the Netherlands
[2] Royal Netherlands Meteorological Institute (KNMI), De Bilt, the Netherlands
[3]Max-Planck-Institut für Chemie (MPI), Mainz, Germany
[4]Jet Propulsion Laboratory (JPL), Pasadena, USA
[5]Cambridge University, Cambridge, UK
[6]National Physical Laboratory (NPL), Teddington, UK

Abstract

We have used a 3D chemistry transport model to evaluate the transport of HF and CH_4 in the stratosphere during the Arctic winter of 1999/2000. Several model experiments were carried out with the use of a zoom algorithm to investigate the effect of different horizontal resolutions. Balloon-borne and satellite-borne observations of HF and CH_4 were used to test the model. In addition, air mass descent rates within the polar vortex were calculated and compared to observations.
Outside the vortex the model results agree well with the observations, but inside the vortex the model underestimates the observed vertical gradient in HF and CH_4, even when the highest available resolution (1˚ × 1°) is applied. The calculated diabatic descent rates agree with observations above potential temperature levels of 450 K. These model results suggest that too strong mixing through the vortex edge could be a plausible cause for the model discrepancies, associated with the calculated mass fluxes, although other reasons are also discussed.
Based on our model experiments we conclude that a global 6°x9° resolution is too coarse to represent the polar vortex, whereas the higher resolutions, 3°×2° and 1°×1°, yield similar results, even with a 6°×9° resolution in the tropical region.

1 Introduction

Both 2D and 3D Chemistry Transport Models (CTMs) are widely used to evaluate the understanding of atmospheric processes and to study how possible future changes in emissions will affect the composition and state of the atmosphere. One important focus of stratospheric research with CTMs is the depletion of ozone, notably in the polar vortex and at mid-latitudes. Both transport and chemical processes influence the ozone concentration, while its variability is mainly determined by dynamics [Chipperfield and Jones, 1999]. To model stratospheric ozone and to estimate chemical ozone loss, it is therefore of great importance that ozone transport is modeled realistically.

Several studies tested modeled transport and investigated the related key model properties.

In a 2-D latitude-longitude study on ozone depletion, Edouard et al. [1996] found a large impact of increasing horizontal resolution. Searle et al. [1998] repeated this study with contradictory results. Since both these studies concentrate on ozone depletion, both chemistry and transport are expected to influence this result.

One method to evaluate model transport separately is by simulating long-lived tracers, which can then be tested against observations. HF, for example, is such a tracer, which is used in this study. In an earlier model evaluation, Chipperfield et al. [1997] also simulated HF. They found a good agreement with observations, except in polar air where HF columns were underestimated. Rind et al., [1999] used CFC-11 and SF_6 to evaluate model transport across the tropopause and found no improvement when they increased the vertical resolution of their general circulation model (GCM). They suggested that dynamical properties such as wave drag and top altitude of the model should be improved with priority. Mahowald et al. [2002] point out that the choice of the vertical coordinate system, based on pressure or isentropes, impacts tracers such as water vapor and the age of air in the tropical stratosphere, with the isentropic coordinate system giving less diffusive and more realistic model results. A recent model intercomparison among 2D models and 3D CTMs showed that the calculated age of air was too low in almost all models [Hall et al., 1999]. However, more recent analysis showed that the descent rates inside the polar vortex in the 3D CTMs SLIMCAT and REPROBUS agreed reasonably well with observations [Greenblatt et al., 2002]. Plumb et al. [2002] modeled transport of N_2O in the polar vortex for the same winter using the CTM MATCH. They found that N_2O was overestimated in the lower stratospheric vortex and suggested that cross-vortex boundary transport was not accurately calculated or that inner-vortex mixing was too intense. It was suggested that this was related to the underlying meteorological data, since doubling their original horizontal resolution of 2.8ºx2.8º did not make a difference. Another study of N_2O and NO_y transport during this winter showed that increasing the vertical resolution did not improve the comparison of model results with observations either [Considine et al., 2003].

In this study we explore the effect of horizontal resolution and of using a zoom region on tracer distributions in more detail by model simulations of HF and CH_4 during the 1999/2000 winter, focusing on the Arctic polar vortex. We also evaluate diabatic descent rates to interpret the calculated tracer distributions. We employ the newly developed chemistry transport model TM5 [Krol et al., 2003] to simulate HF and CH_4. TM5 contains a 2-way nesting zooming algorithm [Krol et al., 2001], which is employed here to study the effect of resolution changes on transport. HF and CH_4 are long-lived in the stratosphere and have lifetimes over 1 year below 10 hPa, and are

therefore solely influenced by transport on shorter timescales. HF is produced in the upper stratosphere by photochemical breakdown of CFCs. It has no chemical sinks in the stratosphere and its only known loss mechanism is downward transport and subsequent wet deposition in the troposphere. CH_4 has the inverse profile, with higher values in the troposphere due to emissions at the earth surface from biogenic and anthropogenic activity. Concentrations drop with increasing altitude due to chemical loss by photo-dissociation and reaction with OH, O^1D and Cl in the stratosphere and reaction with OH in the troposphere.
An important reason to focus on the 1999/2000 winter is the availability of observations of HF and CH_4 from the combined SOLVE (Sage III Ozone Loss and Validation Experiment) and THESEO (THird European Stratospheric Experiment on Ozone) campaigns. Furthermore, a distinct polar vortex formed in the lower stratosphere after December 1st [Manney and Sabutis, 2000], which provides a good test case to study the isolation of the vortex.
We investigate modeled tracer distributions employing three different horizontal resolutions in the northern hemisphere, ranging from 9° longitude by 6° latitude to 1° longitude by 1° latitude. Van Aalst et al. [2003] carried out a model study with the same experimental set-up, using the MA-ECHAM climate model with assimilated meteorological data of the same time period.
The model experiments and the observations used are described in Section 2. Section 3 presents the model results and compares with the observations. A sensitivity test on the model initialization is carried out in paragraph 3.6. Discussion and conclusions follow in Section 4.

2 Model experiments

2.1 Model description

We have used the new global three-dimensional transport model, version 5 (TM5). The model is an extended version of the TM3 model that has been used in several previous stratospheric studies [Van den Broek et al., 2000; Bregman et al., 2000; Bregman et al., 2001]. The new model is able to zoom horizontally over a certain area, e.g. Europe or the polar vortex, by selectively increasing the horizontal resolution. Krol et al. [2001] explain the mass conserving two-way nesting algorithm and show first model results for tropospheric ^{222}Rn.
Figure 1 gives an impression of the zooming options in TM5 used in this study. Meteorological input for the model is provided by six-hourly ECMWF (European Centre for Medium-Range Weather Forecasts) forecast fields of temperature, surface pressure, wind and humidity. The data extend up to 0.2 hPa. The method to calculate mass fluxes from ECMWF winds has recently been improved [Bregman et al., 2003]. We used a 33-layer subset of the 60 layer fields that are taken into account in the ECMWF model, with a reduced number of levels in the tropospheric boundary layer and above 70 hPa. Before October 12 1999 the ECMWF model used 50 vertical layers from which we derived a subset of 30 layers. Near the surface the model levels are defined as terrain following sigma coordinates whereas the layers above 100 hPa are defined at pressure surfaces. A hybrid of the two is used between the lower levels and the lower stratosphere. An example of the vertical grid in TM5, assuming a surface pressure of 1000 hPa, is shown in Figure 2 together with the original ECMWF grid.

Figure 1. An illustration of the horizontal zoom grid of TM5. Zoom option Gl96_NH32 is shown here.

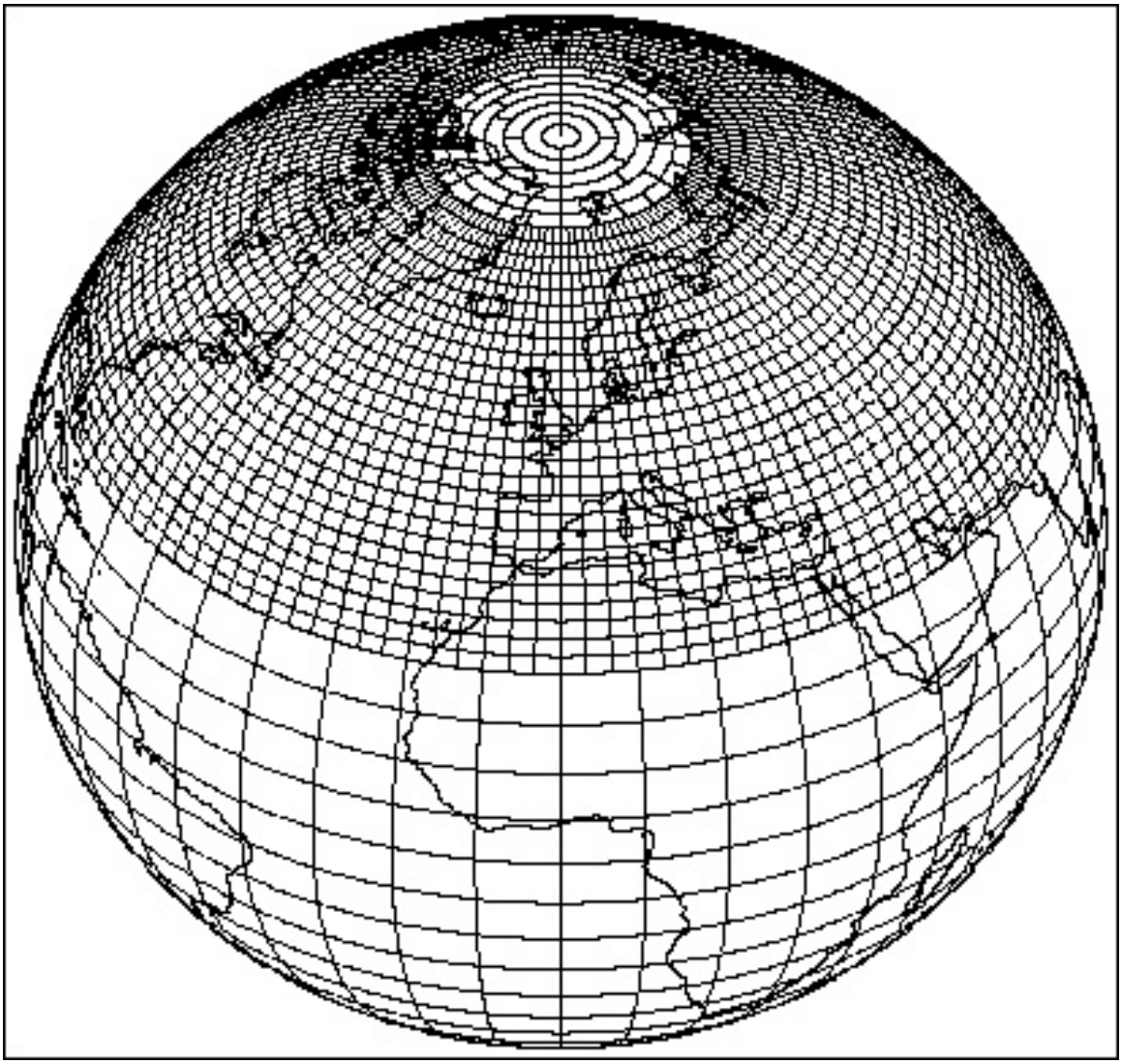

A mass flux advection scheme, using first order slopes [Russell and Lerner, 1981], is used to calculate tracer transport. A dynamical time step of 1800 s is applied for the coarsest grid (6 ˚ latitude by 9˚ longitude). For the 1˚ by 1˚ resolution a time step of 225 s is employed. Over the poles, the grid is reduced to avoid numerical instability through violation of the Courant Friedrichs-Lewy (CFL) condition (see figure 1). The physical parameterization of boundary layer diffusion and convection are identical to those of the TM3 model [Peters et al., 2002], For instance, convection is calculated with the Tiedtke [1989] mass flux parameterization for cumulus clouds, including entrainment and detrainment in updrafts and downdrafts.

Figure 2.The vertical grid of TM5 and the original ECMWF vertical grid.

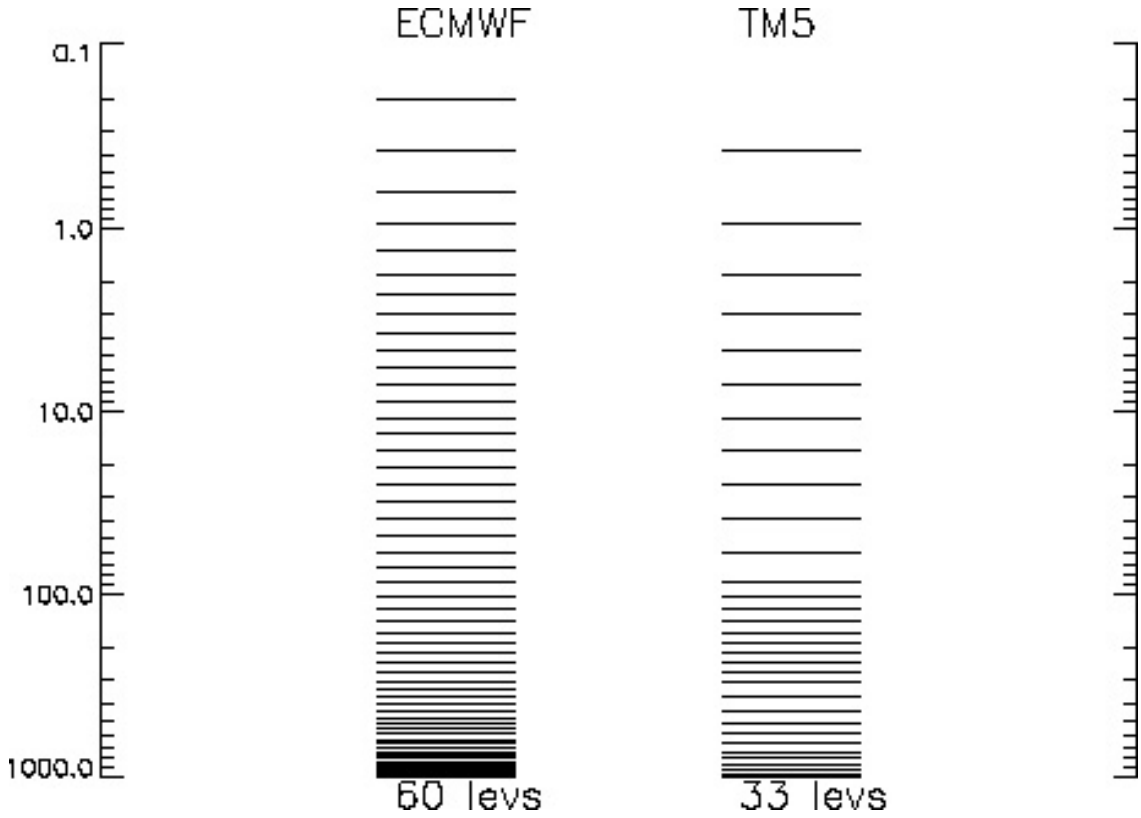

2.2 Experimental set-up

In this study, HF, and CH_4 are simulated for the Arctic winter of 1999-2000. Four zooming options have been investigated (see Table 1), with a horizontal model resolution ranging from 9˚ longitude by 6˚ latitude globally, up to 1° by 1 ˚ from 30˚ to 90˚ N.

Table 1. An overview of the different horizontal resolutions used in this study

	Region 1 (global) lon × lat	**Region 2 (zoom) lon × lat**
Gl_96	9° × 6°	
Gl96_NH32	9° × 6°	3°× 2° (24°N - 90°N)
Gl_32	3° × 2°	
Gl32_NP11	3° × 2°	1°× 1° (30°N - 90°N)

The model integrations start at September 1 1999. Initialization is based on zonally averaged observations of the HALOE (HALogen Occultation Experiment) sunset sweep of 7 August to 22 September 1999, which ranged from 73.9°N to 63.5°S. In regions for which observations are not available (at the poles, in the troposphere and in a gap in the HALOE data between 43°N and 62°N), the initial concentrations are linearly inter- or extrapolated from nearby latitudes. In the vertical direction, we prescribe tropospheric values of 0 ppbv HF and 1.76 ppmv CH_4, distributed slightly

over the two hemispheres by adding a 0.02 ppmv sine function. A log-pressure interpolation is applied when no HALOE data are available at a certain altitude. Removal of HF by wet deposition has been implemented in TM5 by assuming a lifetime of 5 days below 400 hPa, as in Chipperfield et al. [1997]. In the top two levels CH_4 and HF are constrained with monthly zonally averaged UARS data [Randel et al., 1998], since chemical production (of HF) and destruction (of CH_4) are not included in the model. Sensitivity runs carried out by Van Aalst et al. [2003] show that stratospheric washout of HF and prescribing the top boundary concentrations for both tracers have only a small or negligible effect on the tracer fields for the integration period considered in this study. In addition, they found that ignoring chemical destruction of CH_4 causes a small deviation of less than 10 %, and only above 20 hPa.

2.3 Observations during the 1999-2000 winter

The lower stratosphere was extremely cold during the Arctic winter of 1999-2000, especially in the early winter. Despite these low temperatures, the lower stratospheric vortex was weak until December and formed slowly compared to other cold winters. In the upper and middle stratosphere, a distinct vortex was already discernable on November 1st. By the end of December, the vortex was established throughout the stratosphere [Manney and Sabutis, 2000].
Several measurements of CH_4 and HF were used for comparison with the model results.
(i) The balloon-borne Tunable Diode Laser Absorption Spectrometer (TDLAS) measured in-situ profiles of CH_4. The flights took place on January 28th, February 9th, 13th and 27th, and March 25th 2000 and samples were taken inside, outside and at the edge of the vortex [Garcelon et al., 2002]. (ii) Balloon-borne observations of HF and CH_4 were carried out with the JPL MkIV interferometer [Toon et al., 1999] in the inner vortex; both at the start of vortex formation on December 3 1999 and close to vortex break up on March 15 2000. (iii) The HALOE instrument observed both CH_4 and HF, collecting 8-15 profiles each day at two latitude bands [Russell et al., 1993]. Usually, HALOE observations do not extend poleward far enough to reach the vortex, but on February 20 2000 at 56°N some profiles were obtained at the edge of the vortex.
All these observations have been compared with the TM5 results. In addition, diabatic descent rates within the vortex, calculated by the model, have been compared with those derived from CH_4 observations [Greenblatt et al., 2002].

3 Results

3.1 HALOE HF profiles

The HALOE instrument has sampled many mid-latitude profiles of HF during the '99-'00 winter. The errors within the HALOE HF profiles are small. The mean difference between HALOE HF and correlative balloon underflight measurements is less than 7% in the altitude range between 5 hPa and 50 hPa [Russell et al., 1996]. All available Northern hemispheric mid-latitude HALOE HF observations from December 1999 to March 2000 have been compared to the modeled fields. North of 30º N, 649 profiles were measured in total. The bulk of the measurements were carried out outside the polar vortex. Figures 3a and 3b show the correlations of these

observations with the TM5 model results. The TM5 results have been matched with the measurements by using the results of the model gridbox and time zone (within 12 hours) in which the HALOE data were observed. Since the HALOE instrument produces a high vertical resolution compared to the TM5 model, HALOE observations within one TM5 vertical layer have been averaged. Figure 3a shows all correlations for 3 different horizontal model resolutions: 9ºx6º (Gl96), 3ºx2º (Gl32) and 1ºx1º (Gl32_NP11, with 3ºx2º south of 30ºN). Independent of resolution, the correlation between the model results and the observations is good. The gl69 run shows the largest scatter with a tendency to underestimate the tracer distribution. The results from higher resolutions show much less scatter. Note that the correlation hardly improves any further when going from a 3°x2° to a 1°x1° resolution. Nevertheless, significant variability is present, even at the highest resolution. We have separated these relationships in time, latitude, and pressure to investigate the origin of this variability. Figure 3b shows the results from the gl23 run.

Figure 3a. Correlation between HALOE observations and TM5 model output for three different model resolutions: Gl96 (9°x6°), Gl32 (3°x2°) and Gl32_NP11 (1°x1°, 3°x2° south of 30°N), from December 1999 to March 2000, north of 30°N and pressure < 150hPa. The number of profiles used is given as well.

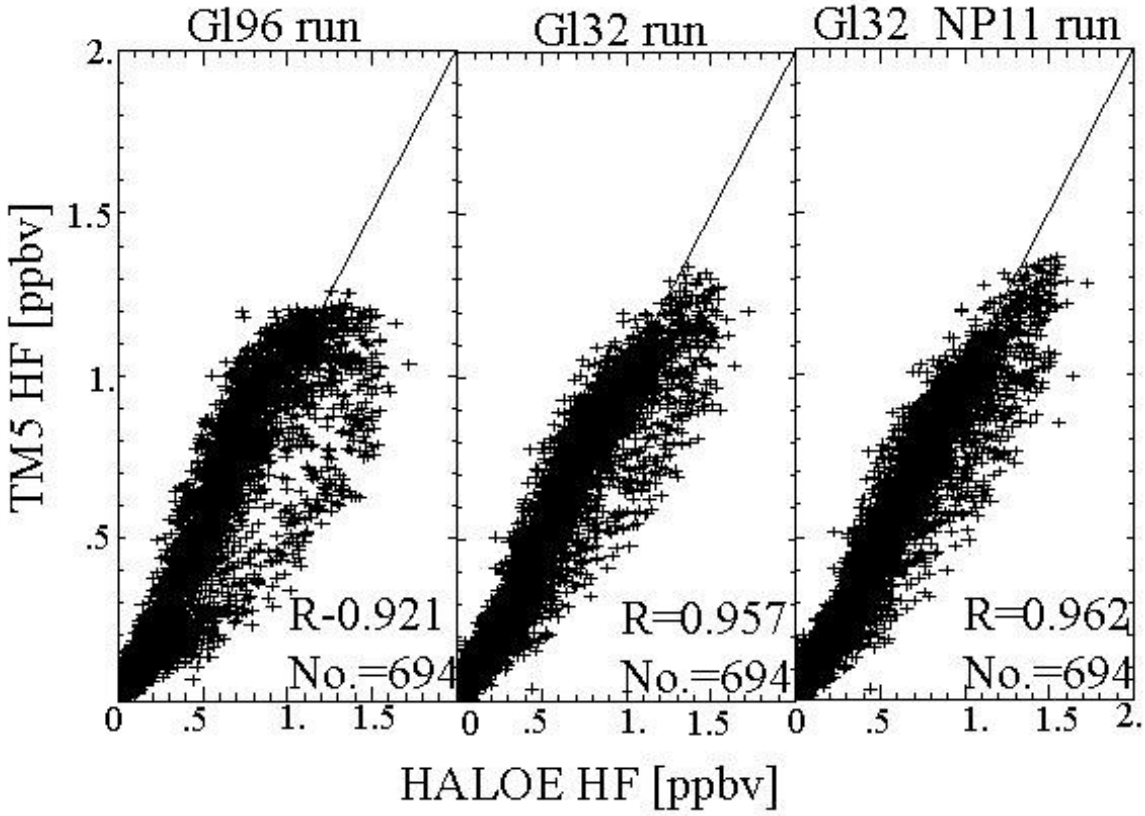

The significant underestimation becomes primarily visible at the end of the winter (March) at high latitudes between 50 – 100 hPa. We have selected March, 15, 2000 to show that the samples of this 'branch' of data originate from the polar vortex (white crosses). We therefore compared the model results with all HALOE profiles on March 15 on an equivalent latitude grid at a potential temperature level of 500 K in Figure 3c. One can clearly see that the model deviates at high equivalent latitudes. The agreement is good at midlatitudes where all observations fall within the model

variability (2σ) for each equivalent latitude bin. This indicates that the model deviations only occur in polar vortex air.

Figure 3b. Correlation between HALOE observations and TM5 model output for the Gl32 run, divided among 4 time periods (Dec '99-Mar '00), 4 latitudes (30-40°N, 40-50°N, 50-60°N and 60-63°N) and 4 altitude regions (150-100 hPa, 100-50 hPa, 50-10 hPa, 10-1 hPa). For the different time periods and latitudes, the number of profiles is given as well (15 comparisons per profile). The white crosses denote observations of March 15, between 100 and 50 hPa.

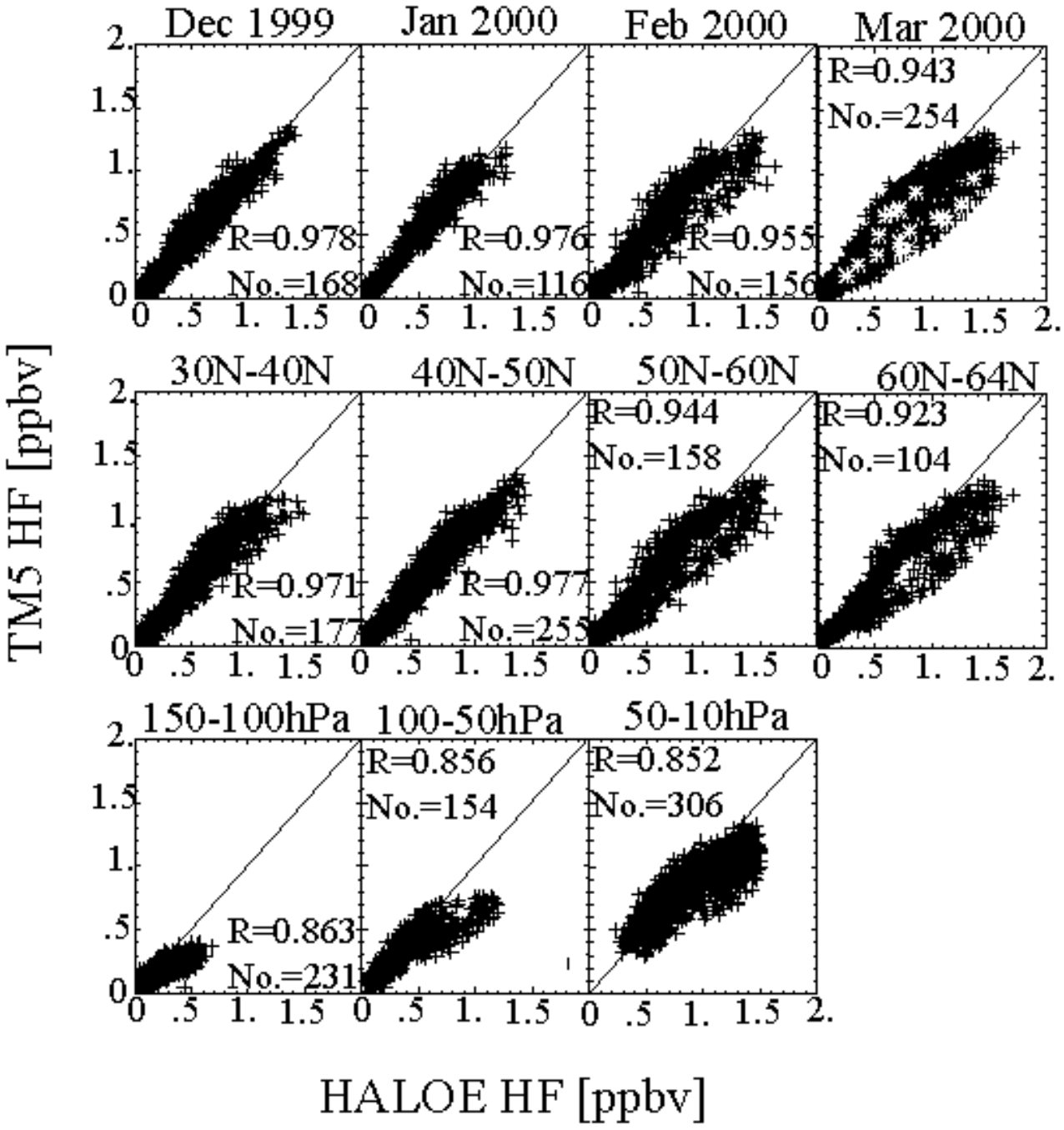

Fig 3c. HF volume mixing ratio from HALOE observations (grey dots) and TM5 simulations (black dots), along equivalent latitude. Results are shown for March 15 2000 on the 500 K potential temperature level. The vertical bars denote the model variability (2σ) for each equivalent latitude bin (2°).

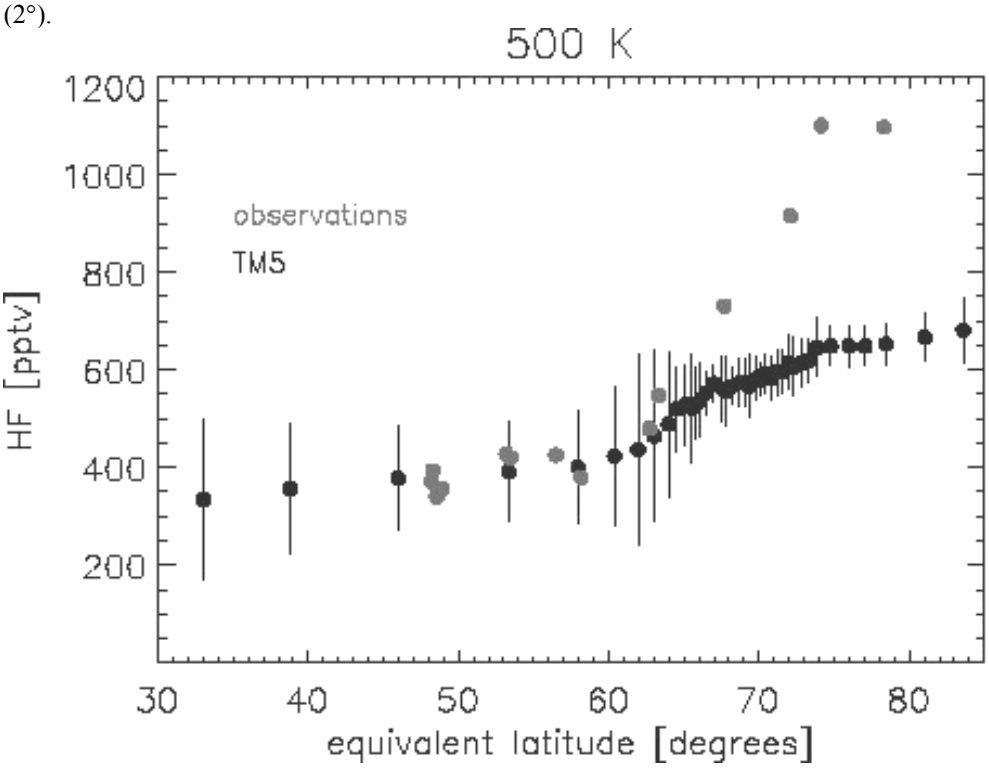

3.2 TDLAS CH_4 observations in/out of the vortex

As a next step, we compared modeled CH_4 profiles to CH_4 profiles that have been measured by means of the balloon-borne TDLAS spectrometer, both inside and outside the polar vortex. The result is shown in Figure 4a. The estimated error for the observations is about 10% [Garcelon et al., 2002]. Clearly, as in Figure 3, the model results compare reasonably well with the observations outside the vortex, whereas the model results within and at the inner edge of the vortex indicate significant overestimation. As in figure 3, it is remarkable that the model results are very similar for all zooming experiments, including the 1° by 1° resolution. The Gl_96 run shows the largest overestimation, implying that this resolution is too coarse for a realistic representation of the tracer distribution.
The good agreement between model and observations outside the vortex was also indicated by the HALOE profile comparisons, especially below 10 hPa (see Figure 3). However, inside and at the edge of the vortex the CH_4 vertical gradient increases with time, which is obviously not fully captured by the model.
Figure 4b shows the modeled horizontal gradients on a pressure level of approximately 75 hPa across the vortex edge between Kiruna, the site of the balloon observation, and central Europe on February 13 2000. The coarser Gl_96 model run results in a gradient of ~0.1 ppmv between Kiruna and central Europe, whereas the Gl_32 and NP_11 runs gives a larger gradient of ~0.2 ppmv. Nevertheless, these gradients are smaller than the differences between the model and the observation at this altitude, which is about 0.35 ppmv (see figure 4a). The 1º by 1º run does show a sharper gradient, as can be expected, with more distinct features. This may be important when species with large concentration gradients over the vortex edge are studied.

Figure 4a. Modeled CH_4 [ppmv] compared to TDLAS profiles, on 28 January, 9, 13 and 27 February and 25 March 2000.

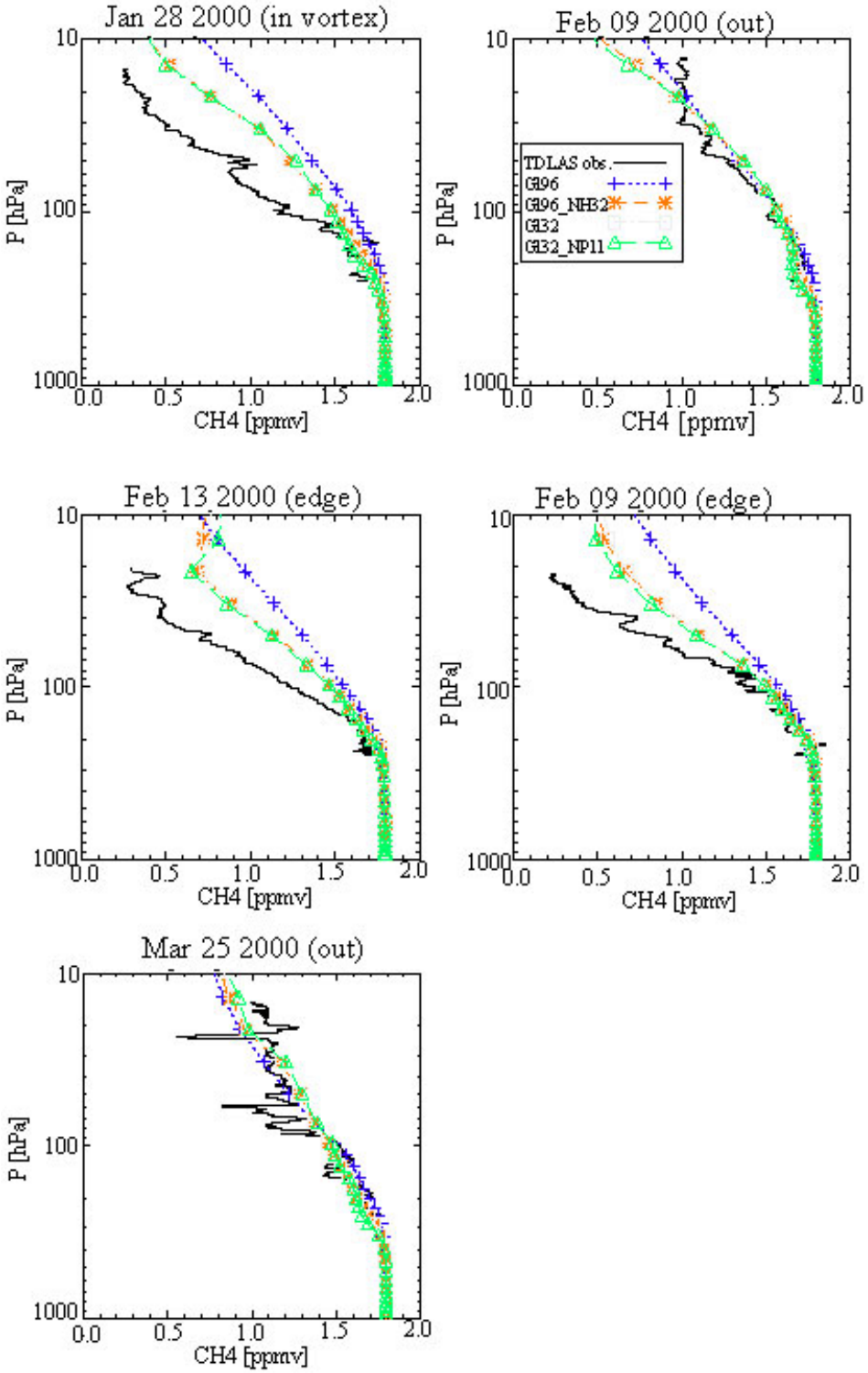

Figure 4b. Horizontal field of CH_4 [ppmv] around Kiruna on February 13 2000, at a pressure level of ~75 hPa. The three model runs, NP_11, Gl_32 and Gl_96 show how gradients across the vortex edge are affected by the model resolution.

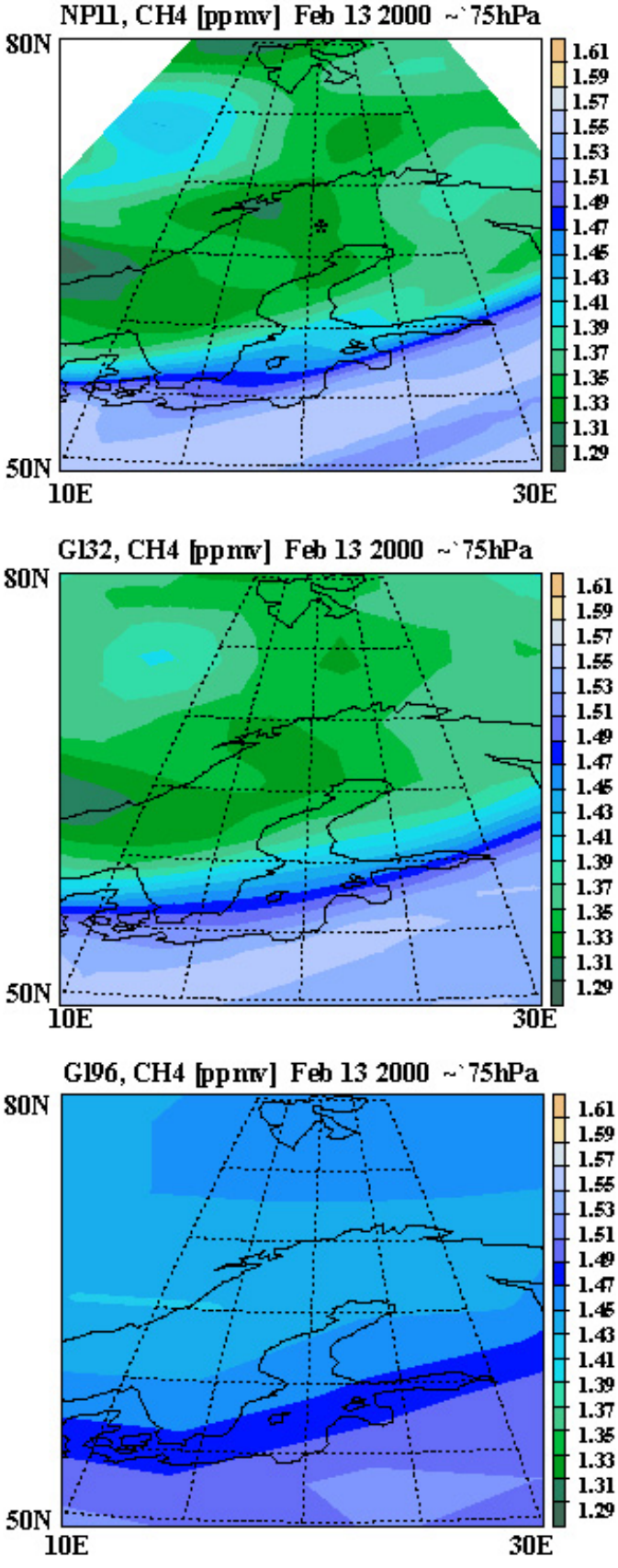

3.3 MkIV inner vortex observations in early and late winter

In Figure 5 TM5 results are compared to HF and CH_4 measurements by the MkIV interferometer, focusing here on the lower stratosphere. The observations were carried out inside the polar vortex in the beginning of winter, on December 3, when the vortex was just formed in the lower stratosphere, and on March 15 2000, just before the vortex break-up. Also in this comparison, HF is consistently underestimated and CH_4 is overestimated, both at the beginning and at the end of winter, and the differences between the model runs are similar to the earlier comparisons.

Figure 5. Modeled HF [ppbv] and CH_4 [ppmv] compared to MkIV profiles on December 3rd 1999 and March 15th 2000.

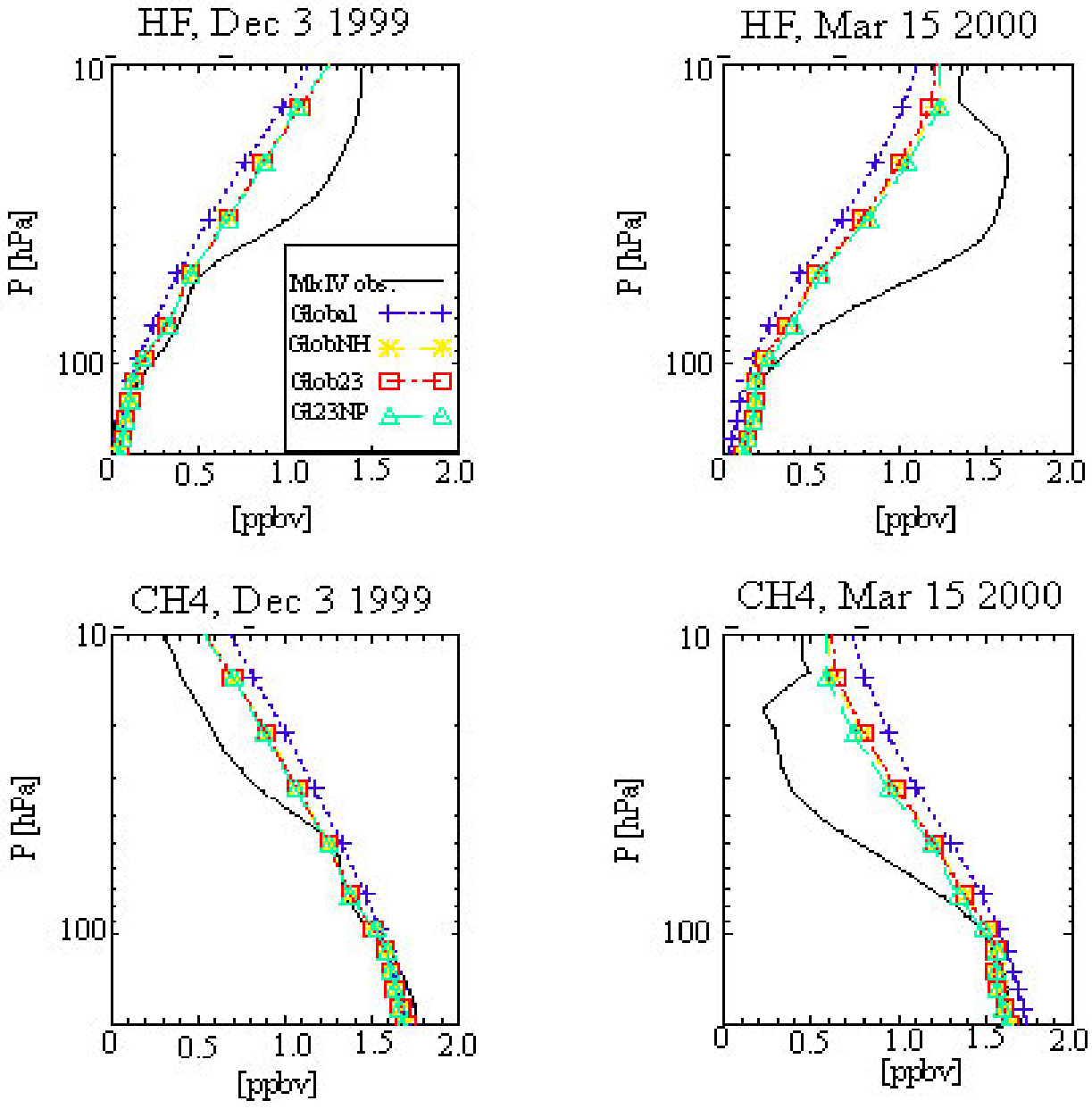

However, on December 3, the difference between model and observation occurs only above 50 hPa while by March 15, the difference is seen throughout the lower stratosphere. Above 15 hPa HF steeply decreases and CH_4 increases on March 15. PV maps indicate that the MkIV observations above 15 hPa were at the edge of, or outside, the vortex, which explains the gradient reversal. The discrepancies found so early in winter suggest a potential impact from inaccuracies in the initial tracer field. Later we will demonstrate the sensitivity of the model results for the initial tracer fields.

3.4 HALOE HF longitude cross section

Fifteen HALOE HF sunrise profiles, observed on February 20 2002 at 56°N, have been compiled in a longitudinal graph and are compared with TM5 results (Figure 6). The HALOE observations comprise both vortex and non-vortex air. For example, the feature with increased HF values between 90°E and 60°E and 50 hPa and 10 hPa represents air from the vortex edge. An increased vertical gradient in HF is visible below this area, between 100 hPa and 20 hPa. Another small feature of increased HF is discernable near 100 hPa, around 150°E - 180°E.
More obvious than in the previously discussed profile comparisons, the Gl_96 run is too coarse to simulate transport within or across the edge of the vortex, since none of the observed longitudinal features is captured (Figure 6b). All other model runs capture the observed longitudinal features well and again they produce similar results. On the other hand, the model underestimates the vertical gradient between 100 hPa and 1 hPa at all longitudes, and especially inside the vortex between 150°E and 180°E. This is in agreement with the profile comparisons discussed above (Figure 4 and 5). The discrepancy between 10 and 1 hPa is also visible in the late winter mid-latitude profiles shown in figure 3 and may be attributed to the mixing of vortex air with mid-latitude air.
The vortex air sampled at 56°N was situated at the edge, which can be seen from the modeled latitudinal cross-sections at 50°N and 62°N (not shown here). The representation of the vortex edge may contribute to the discrepancies with the observations there, due to the large gradients of HF across the edge of the vortex. At 62°N for example, situated more inside the vortex, the sharp vertical gradient matches much better with the HALOE observations at 56°N (see also van Aalst et al. [2003]).

3.5 Descent rates

One likely cause of the model-observations discrepancies could be the underestimate of the diabatic descent by the model. To evaluate the possible origin of these discrepancies, we calculated the modeled vertical descent rates inside the vortex from December 1 to March 1 2000 and compared those with observed descent rates (i.e. derived from observations). It should be kept in mind that such comparisons do not separate vertical and horizontal transport, so that deviations can be caused by inaccuracies in the mass flux representation in TM5 in both directions. The observed descent is derived from a number of CH_4 observations inside the vortex and agrees with calculations carried out with a large number of N_2O observations [Greenblatt et al., 2002].

Figure 6. Modeled HF [ppbv] compared to HALOE observations on 00-02-20, longitudinal cross section at 56° N.

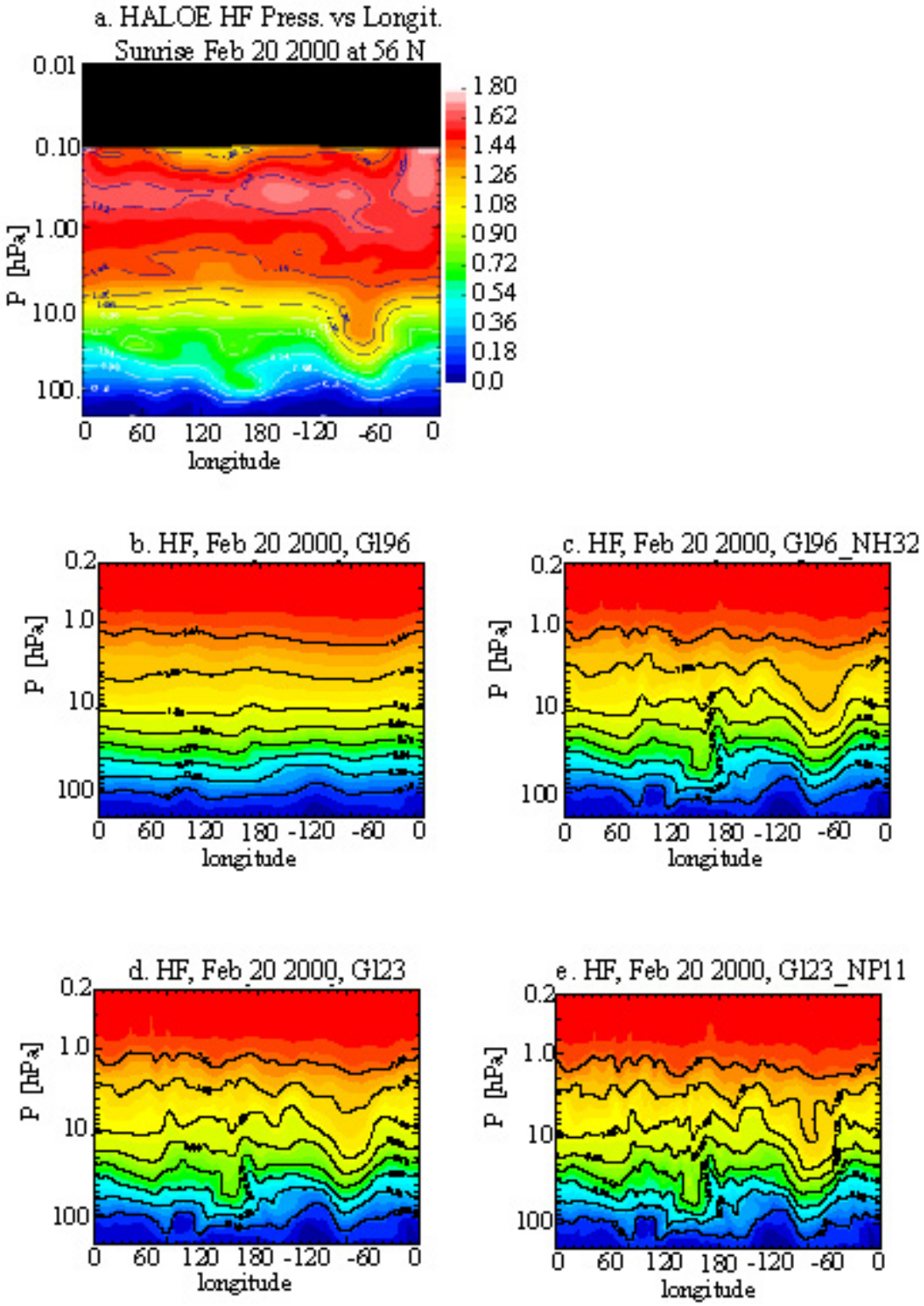

Figure 7 shows the decrease of potential temperature along five CH_4 isopleths throughout the winter. The black lines shows inner vortex descent calculated from five observed profiles of CH_4 during the SOLVE/THESEO campaign [Greenblatt et al., 2002]. The grey lines represent the descent of CH_4 calculated with TM5. On each first day of the month, zonal winds and PV gradients were used to calculate vortex average profiles of potential temperature and CH_4 (see also van Aalst et al. [2003]). We restricted the sampling to those profiles that were located within the vortex in the full altitude range between 100 and 10 hPa. Inner vortex air was selected by sampling within the area bordered by the steepest gradient in PV, according to the ECMWF forecasts.

Figure 7. Potential temperature throughout the winter of 1999-2000 along CH_4 isopleths for observations [Greenblatt et al., 2002] in dotted lines, with the triangles representing the profile observations, and for model results on each first day of the month (circles connected by solid lines) from all zooming options.

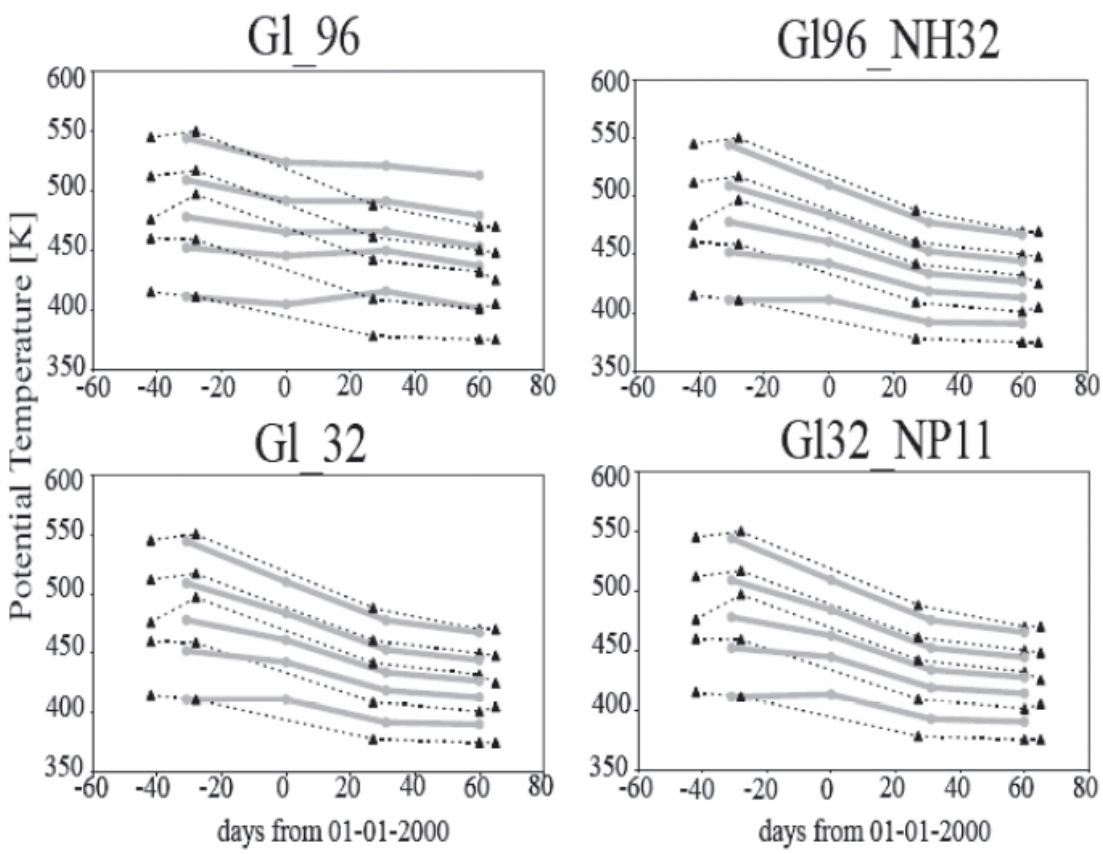

Figure 7 shows that, except for the "Gl_96" run, the calculated descent rates during the winter agree quite well with those observed, except in the layer below θ~450 K, which is the layer undergoing the highest ozone loss. The discrepancy increases closer to the vortex lower boundary, i.e. ~400 K, especially in early winter. Largest descent takes places from December to January, slowing down in February and being close to zero after the first of March. Increasing the horizontal resolution in the zooming experiments, either in the tropics or in the polar region, has no effect on these results. Initially, modeled potential temperature on December 1 1999 has been synchronized with the observed θ profiles. Note that at the start of this calculation on December 1, the offset in potential temperature for comparable CH_4 volume mixing ratios is about 50 K above 500 K. Around 450 K the offset is 20 K, whereas the offset has

disappeared around 400 K and layers below. Thus, the model does not simulate the tracer fields above 450 K correctly, at the start of this comparison on December 1st. This is in agreement with the modeled overestimation of CH_4 and underestimation of HF with respect to the MkIV observations on December 3rd, illustrated in figure 5. Similar pre-winter offsets are also found with the 3-D CTMs REPROBUS and SLIMCAT using the same set of observations [Greenblatt et al., 2002]. Greenblatt et al. [2002] compared modeled and observed descent rates in a similar way as discussed here. Both models showed similar descent rates as TM5, although REPROBUS descent is somewhat faster than the observed descent in the beginning of winter in the lower stratosphere. In addition, similar results are found with the MA-ECHAM model [van Aalst et al., 2003].

3.6 Sensitivity of the initialization

The model validation gives arguments to question the influence of the initial fields on the tracer distribution, as mentioned earlier. The initialization of the model on September 1 1999 was based on the HALOE observations of August and September 1999. The northernmost latitude in this field is 73.9°N. Therefore the species concentrations in the polar region outside the observed area were extrapolated from this latitude. Despite this caveat, the method was applied to use as much observations as possible. Another option for initialization is the use of 3D model output fields of full chemistry runs.
To test the impact of the initial fields we have performed a run with the Gl32 resolution, starting on October 20 1999 and using an initialization provided by the full chemistry ARPROBUS climate model [WMO, 1999]. A CTM model study using the same initialization and meteorological input showed a good agreement with inner vortex CH_4 profiles [G. Berthet and F. Lefèvre, personal communication].
Figure 8 shows a comparison with the TDLAS and MkIV balloon observations similar to figures 4a and 5, with the old and new initialization. The new initialization has resulted in consequently lower CH_4 concentrations. Inside the vortex, this means that the model gives more realistic results. The deviation with the two TDLAS profiles sampled outside the vortex is small as well, in both model runs.
Figure 9 shows the dependence of the correlation between HALOE observations and TM5 results on the initialization. All data from December 1999 – March 2000, north of 30°N have been included. As mentioned earlier, the bulk of these observations are outside the polar vortex. From these results it can be seen that the original HALOE initialization gives a slightly better correlation with the observations. The ARPROBUS initialization gives lower model concentrations. In agreement with the HF comparisons (Figure 3a, b and c), the samples showing overestimation all originate from the polar vortex. The shift caused by the ARPROBUS initialisation results in better agreement for polar vortex air and slightly worse agreement for extra-vortex air, although the correlation remains good. Thus, this figure clearly shows that the initialization does have an effect on the results. However, it does not affect the relative difference between mid-latitudes and the polar vortex.

Figure 8. TDLAS and MkIV balloon-borne observations of CH_4 from December 3 to March 25 2000 compared to TM5 output with two different initialisations. The TDLAS measurements are both inside and outside the vortex, whereas the MkIV measurements are all sampled inside the vortex.

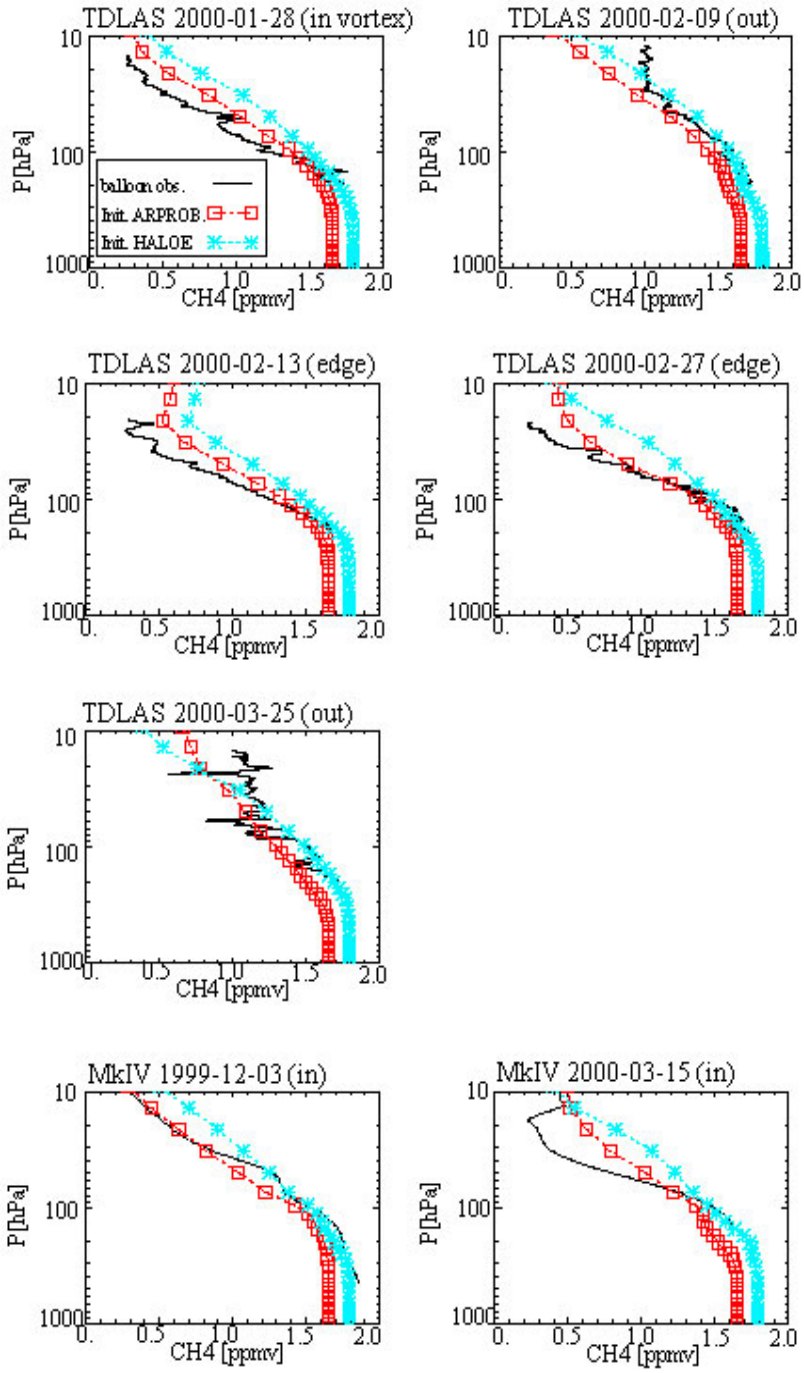

Figure 9. Correlation between HALOE observations and TM5 model output from December 1999 to March 2000, for two different initializations. These are described in detail in the text.

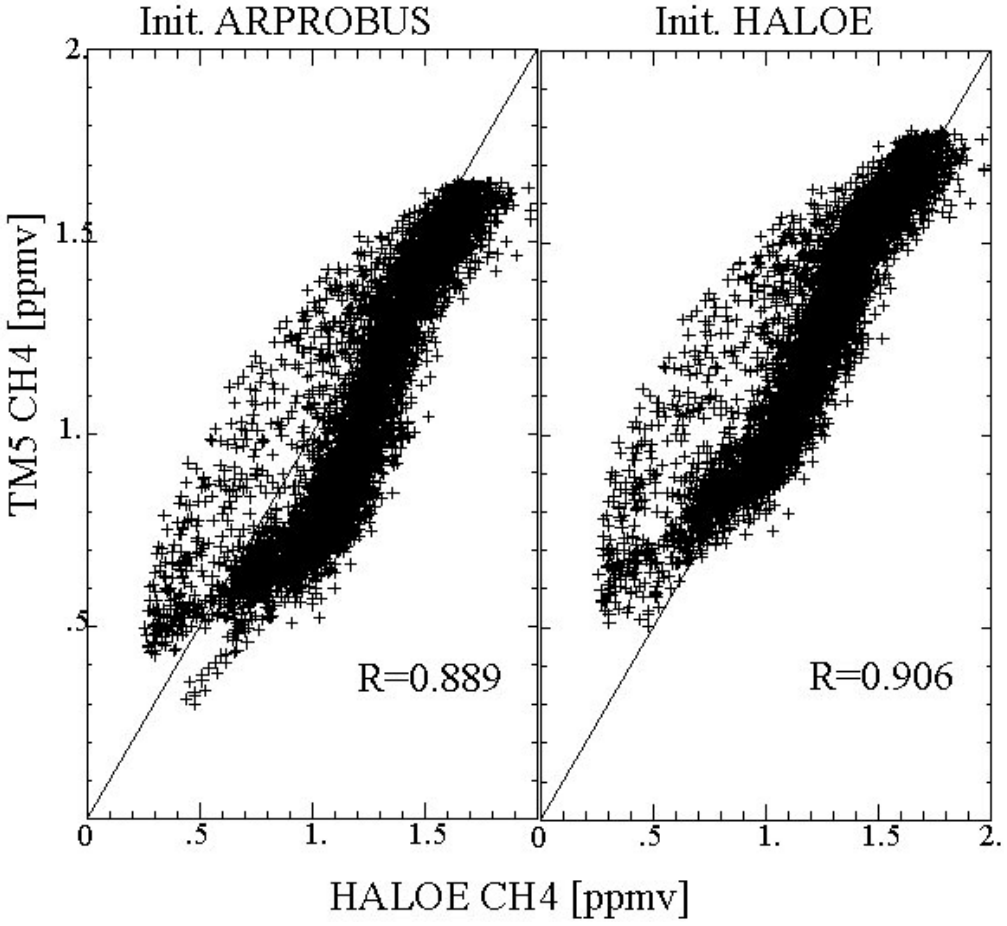

4 Discussion and conclusions

We have evaluated the 3D chemistry transport model TM5 with the stratospheric tracers HF and CH_4 during the Arctic winter of 1999/2000 and tested the new model zooming algorithm. The results of our model experiments, applying three different resolutions of 6°x9°, 3°x2° and 1°x1°, have been compared to observations. As can be expected, the coarsest resolution of 6˚ latitude by 9˚ longitude produces relatively large errors. The longitudinal variation as compared to the HALOE HF observations near the vortex edge, and inner vortex descent are simulated unrealistically with this resolution. Such discrepancies should be considered since many climate model integrations are performed with similar resolutions [e.g. Pawson et al., 2000, Austin et al., 2003]. Outside the vortex, the results of the 2º by 3º run agree better with the observations. Remarkably, the tracer profiles are similar if a 6º by 9º resolution is used in the southern hemisphere and tropics instead of 2º by 3º. Apart from the significant improvement when increasing the resolution from 9° by 6° to 3° by 2°, further increase of the horizontal resolution does not improve, or worsen, the comparison with the observations in this model set-up. Nevertheless, differences between the 3°×2° and the 1°×1° runs arise close to large gradients such as the vortex edge, which may be important when species with larger concentration gradients are studied.

The close resemblance between the results of the uniform 3°×2° run and the northern hemisphere 3°×2° run shows the applicability of the TM5 zooming algorithm. Thus, high-resolution simulations become feasible. It is intended to compare these simulations to observations from measurements campaigns and satellite instruments in the (lower) stratosphere.

The model comparisons with balloon and satellite profiles measured inside the vortex give an underestimation of HF and subsequent overestimation of CH_4 for each resolution. Our model analysis shows that these model deviations are restricted to polar vortex air. Outside, the HF and CH_4 distribution are simulated in agreement with observations.

Comparisons with observed tracer isopleths show reasonable agreement in vortex descent for the higher grid resolutions. However, this comparison does not separate horizontal and vertical model transport, so that both may have contributed to the discrepancies. A way to separate horizontal and vertical transport was described by Considine et al. [2003]. They isolated the vertical model transport by eliminating tracer concentration gradients along the isentropic model levels. Their conclusions point towards compensating errors in the vertical and the horizontal transport.

Additional aspects of the exerimental set-up may have contributed to the inner vortex discrepancy. Firstly, it can be ruled out that these discrepancies are caused by uncertainties in boundary conditions at the top and bottom of the model and tropospheric rain-out, as was investigated by van Aalst et al. [2003].

Secondly, some of the comparisons between model and measurements in early winter suggest that the initialization could be in error. The combined time series of the calculated and observed CH_4 and HF profiles (figure 4a and 5) show that the inner vortex discrepancy already starts during early winter (note that the discrepancy is already present on December 3). We tested whether a different initialization was able to explain the discrepancies. A better agreement with observations was indeed achieved within the vortex region, explaining the early winter offset. It, however, leads to a worse agreement at mid-latitudes (figure 9). Thus, an inaccurate initialization may lead to an offset, but it cannot fully explain the discrepancies found in the vertical gradient and over time.

Another possible reason for the model discrepancies could be found in the vortex formation. The ECWMF data extend only to 0.2 hPa where observations become sparse. Since the vortex was already formed on November 1 in the upper stratosphere [Manney and Sabutis, 2000], this region is very critical when simulating the early winter vortex. It may indicate that either diabatic descent or horizontal transport is not well represented in the model, thus the underlying meteorology from ECMWF does not properly represent the downward or horizontal transport in the polar vortex. In this study, we increased the horizontal resolution of TM5 up to 1°x1° for a relatively large area (northward of 30°N). Nevertheless, the discrepancies remain, which may be an indication that the accuracy of the mass fluxes as provided by ECMWF is insufficient [Considine et al., 2003; Plumb et al., 2002]. Recent studies indicate that errors in the stratospheric circulation in assimilated meteo fields exist that may play a crucial role here, e.g. during the formation of the winter vortex [Kawa et al., 2003].

Finally, other model characteristics such as the vertical resolution, the advection scheme and the reduced grid used in the polar region have not been investigated. All of these parameters are being addressed with the TM5 model by including all (60) ECMWF model layers, by removal of the reduced grid and by using a higher order advection scheme [Bregman et al., manuscript in preparation].

Acknowledgements

The authors wish to express their gratitude to the HALOE team for providing us with their observations. We thank the other members of the TDLAS and MkIV teams, especially I.H. Howieson, N.R. Swann and P.T. Woods from the National Physical Laboratory. Benedikt Steil, Christoph Brühl from the Max Planck Institute for Chemistry in Mainz and J. Greenblatt, at Princeton University, are thanked for fruitful discussions. The second initialization was provided by Gwenael Berthet and Franck Lefèvre, for which we thank them. We also thank Arjo Segers and Peter van Velthoven from the Royal Netherlands Meteorological Institute for providing the software to process the meteorological fields. Bram Bregman is funded by the EC project TOPOZ III EVK2-CT-2001-00102.

5 References

J. Austin, D. Shindell, S. R. Beagley, C. Brühl, M. Dameris, E. Manzini, T. Nagashima, P. Newman, S. Pawson, G. Pitari, E. Rozanov, C. Schnadt, and T. G. Shepherd, Uncertainties and assessments of chemistry-climate models of the stratosphere, *Atmos. Chem. Phys., 3*, 1-27, 2003

Bregman, A., J. Lelieveld, M. van den Broek, H. Fischer, P. Siegmund and O. Bujok, The N_2O and O_2 relationship for mixing processes as represented by a three-dimensional chemistry-transport model, *J. Geophys. Res., 105*, 17,279-17,290, 2000.

Bregman, A., M.C. Krol, H. Teyssedre, W.A. Norton, A. Iwi, M. Chipperfield, G. Pitari, J.K. Sundet and J. Lelieveld, Chemistry-Transport model comparison with ozone observations in the midlatitude lowermost stratosphere, *J. Geophys. Res., 106*, 17,479-17,496, 2001.

Bregman, A., A. Segers, M. Krol, E. Meijer, and P. van Velthoven, On the use of mass-conserving wind fields in chemistry-transport models, *Atm. Chem. Phys., 3*, 447-457, 2003.

Chipperfield, M.P., M. Burton, W. Bell, C.P. Walsh, T. Blumenstock, M.T. Coffey, J.W. Hannigan, W.G. Mankin, B. Galle, J. Mellqvist, E. Mahieu, R. Zander, J. Notholt, B. Sen and G.C. Toon, On the use of HF as a reference for the comparison of stratospheric observations and models, *J. Geophys. Res., 102*, 12,901-12,919, 1997.

Chipperfield, M.P. and R.L. Jones, Relative influences of atmospheric chemistry and transport on Arctic ozone trends, *Nature, 400*, 551-553, 1999.

Considine, D.B., S.R. Kawa, M.R. Schoeberl, and A.R. Douglass, N_2O and NO_y observations in the 1999/2000 Arctic polar vortex: Implications for transport processes in a CTM, *J. Geophys. Res., 108*, 10.1029/2002JD002525, 2003.

Edouard, S., B. Legras, F. Lefèvre and R. Eymard, The effect of small-scale inhomogeneities on ozone depletion in the Arctic, *Nature*, *384*, 444-446, 1996.

Garcelon, S., T.D. Gardiner, G.M. Hansford, N.R.P. Harris, I.H. Howieson, R.L.Jones, J.D. McIntyre, J.A. Pyle, A.D. Robinson, N.R. Swann and P.T. Woods, Investigation of CH_4 and CFC-11 vertical profiles in the Arctic vortex during the SOLVE/THESEO 2000 campaign, *poster presentation at EGS,* Nice, 2002.

Greenblatt, J.B., H.J. Jost, M. Loewenstein, J. R. Podolske, D.F. Hurst, J. W. Elkins, S. M. Schauffler, E.L. Atlas, R.L. Herman, C.R. Webster, T.P. Bui, F.L. Moore, E.A. Ray, S. Oltmans, H. Voemel, J.-F. Blavier, B. Sen, R.A. Stachnik, G.C. Toon, A. Engel, M. Mueller, U. Schmidt, H. Bremer, R.B. Pierce, B.-M. Sinnhuber, M. Chipperfield, F. Lefevre, Tracer-based determination of vortex descent in the 1999-2000 Arctic winter, *J. Geophys. Res.*, *107*, 10.1029/201JD000937, 2002.

Hall, T. M., D.W. Waugh, K.A. Boering, R.A. Plumb, Evaluation of transport in stratospheric models, *J. Geophys. Res., 104*, 18,815-18,839, 1999.

Kawa, S.R., R. M. Bevilacqua, J. J. Margitan, A. R. Douglass, M. R. Schoeberl, K. W. Hoppel and B. Sen, Interaction between dynamics and chemistry of ozone in the setup phase of the Northern Hemisphere polar vortex, *J.Geophys. Res., 108*, 10.1029/2001JD001527, 2003

Krol, M.C., W. Peters, P.J.F. Berkvens and M.A.Botchev, A New Algorithm for two-way nesting in global models: Principles and Applications, in: *Proc. 2nd Int. Conf. Air Pollution Modeling and Simulation*, April 9-12, 2001, Champs-sur-Marne (ed. Sportisse, B.) 225-235 (Springer, Berlin, Heidelberg and New York, 2002)

Krol, M.C., J. Lelieveld, D.E. Oram, G.A. Sturrock, S.A. Penkett, C.A.M. Brenninkmeier,V. Gros, J. Williams and H.A. Scheeren, Continuing emissions of methyl chloroform from Europe, *Nature, 421*, 131-135, 2003.

Mahowald, N.M., R.A. Plumb, P.J. Rasch, J. del Corral, F. Sassi and W. Heres, Stratospheric transport in a 3-dimensional isentropic coordinate model, *J. Geophys. Res., 107*, 10.1029/2001JD001313, 2002

Manney, G.L. and J.L. Sabutis, Development of the polar vortex in the 1999-2000 Arctic winter stratosphere, *Geophys. Res. Lett., 27*, 2,589-2,592, 2000.

Pawson, S., K. Kodera, K. Hamilton, T.G. Shepherd, S.R. Beagley, B.A. Boville, J.D. Farrara, T.D. A. Fairlie, A. Kitoh, W.A. Lahoz, U. Langematz, E. Manzini, D.H. Rind, A.A. Scaife, K. Shibata, P. Simon, R. Swinbank, L. Takacs, R.J. Wilson, J.A. Al-Saadi, M. Amodei, M. Chiba, L. Coy, J. de Grandpré, R.S. Eckman, M. Fiorino, W.L. Grose, H. Koide, J.N. Koshyk, D. Li, J. Lerner, J.D. Mahlman, N.A. McFarlane, C.R. Mechoso, A. Molod, A. O'Neill, R.B. Pierce, W.J. Randel, R.B. Rood, and F. Wu, The GCM-Reality Intercomparison Project for SPARC (GRIPS): Scientific issues and initial results, *Bull. Am. Meteor. Soc., 81*, 781-796, 2000.

Peters, W., M.Krol, F. Dentener, A.M. Thompson, and J. Lelieveld, Chemistry-transport modeling of the satellite observed distribution of tropical tropospheric ozone, *Atmospheric Chemistry and Physics, 2*, 103-120, 2002.

Plumb, R.A., W. Heres, J.L. Neu, N.M. Mahowald, J. del Corral, G.C. Toon, E.R. Ray, F. Moore, A.E. Andrews, Global tracer modeling during SOLVE: High latitude descent and mixing, *J. Geophys. Res.*, *107*, 10.1029/2001JD001023, 2002

Randel, W.J., F. Wu, J.M. Russell III, A. Roche, and J.W. Waters, Seasonal cycles and QBO variations in stratospheric CH_4 and H_2O observed in UARS HALOE data, *J. Atmos. Sci., 55*, 163-185, 1998.

Rind, D., J. Lerner, K. Shah, and R. Suozzo, Use of on-line tracers as a diagnostic tool in general circulation model development 2. Transport between the troposphere and stratosphere, *J. Geophys. Res., 104*, 9,151-9,167, 1999

Russell, G.L., and J.A. Lerner, A new finite-differencing scheme for the tracer transport equation, *J. Appl. Meteorol., 20*, 1,483-1,498, 1981.

Russell, J.M. III, L.L. Gordley, J.H. Park, S.R. Drayson, D.H. Hesketh, R.J. Cicerone, A.F. Tuck, J.E. Frederick, J.E. Harries, and P.J. Crutzen, The Halogen Occultation Experiment, *J. Geophys. Res., 98*, 10,777-10,797, 1993.

Russell, J.M. III, L.E. Deaver, M. Luo, R.J. Cicerone, J.H. Park, L.L. Gordley, G.C. Toon, M.R. Gunson, W.A. Traub, D.G. Johnson, K.W. Jucks, R. Zander and I.G. Nolt, Validation of hydrogen fluoride measurements made by the Halogen Occultation Experiment from the UARS Platform, *J. Geophys. Res.*, 101, 10,163-10,174, 1996.

Searle, K.R., M.P. Chipperfield, S. Bekki and J.A. Pyle, The impact of spatial averaging on calculated polar ozone loss: I. Model Experiments, *J. Geophys. Res., 103*, 25,397-25,408, 1998.

Tiedtke, M., A comprehensive mass flux scheme for cumulus parameterization in large-scale models, *Mon. Wea. Rev., 117*, 1779-1800, 1989.

Toon, G. C., J.-F. Blavier, B. Sen, B., J.J. Margitan, C.R. Webster, R.D. May, D. Fahey, R. Gao, L. Del Negro, M. Proffitt, J. Elkins, P.A. Romashkin, D.F. Hurst, S. Oltmans, E. Atlas, S. Schauffler, F. Flocke, T.P. Bui, R.M. Stimpfle, G.P. Boone, P.B. Voss, R.C. Cohen, Comparison of MkIV balloon and ER-2 aircraft measurements of atmospheric trace gases, *J. Geophys. Res., 104*, 26,779-26,790, 1999.

Van Aalst, M.K., M.M.P. van den Broek, A. Bregman, C. Brühl, B. Steil, G.J. Roelofs and J. Lelieveld, Trace gas transport in the 1999/2000 Arctic vortex: comparison of nudged GCM runs with observations, *Atm. Chem. Phys. Discuss.*, 3, 2465-2497, 2003.

Van den Broek, M.M.P., A. Bregman and J. Lelieveld, Model study of stratospheric chlorine activation and ozone loss during the 1996/1997 winter, *J. Geophys. Res., 105*, p. 28,961-28,977, 2000.

World Meteorological Organization (WMO), *Scientific Assessment of ozone depletion:1998, Global ozone research and monitoring project*, WMO Rep. 44, 1999.

CHAPTER IV

Implementing Growth and Sedimentation of NAT particles in a global Eulerian Model

published in Atmospheric Chemistry and Physics Discussions, p. 3089-3126, June (2004), and submitted to Atmospheric Chemistry and Physics, with J.E. Williams[1] and A. Bregman[2] as co-authors.

[1] Eindhoven University, Eindhoven, Netherlands
[2] The Royal Netherlands Meteorology Institute (KNMI), De Bilt, Netherlands

Abstract

Here we present a concise and efficient algorithm to mimic the growth and sedimentation of Nitric Acid Trihydate (NAT) particles in the polar vortex in a state-of-the-art 3D chemistry transport model. The particle growth and sedimentation are calculated using the microphysical formulation of Carslaw et al. [2002]. Once formed, NAT particles are transported in the model as tracers in the form of size-segregated quantities. Two different approaches were adopted for this purpose: one assuming a fixed particle number density ('FixedDens') and the other assuming a discrete set of particle diameter values ('FixedRad'). Simulations were performed for three separate 10-day periods during the 1999-2000 Arctic winter and compared to the results of an existing Lagrangian model study, which uses similar microphysics in a computationally more expensive method for the simulation of NAT particle growth. The resulting maximum particle sizes for both our approaches compare favourably at 96hPa with those obtained from this previous model study, and also *in-situ* observations related to the size of large NAT particles. Comparisons were made with a standard equilibrium approach and the differences in the redistribution of HNO_3 were found to be substantial. For both approaches the performance of the algorithm is rather insensitive to both the number of size bins and the shape of the size distribution. However, the percentage of HNO_3 sequestered into NAT is critically dependent on the total number density of particles prescribed for each size bin.

1 Introduction

Shortly after the discovery of the ozone hole in the mid 1980's, it was recognized that denitrification (i.e. the uptake and subsequent sedimentation of HNO_3 within Polar Stratospheric Clouds (PSC's)) both increases and prolongs stratospheric ozone loss [Crutzen and Arnold, 1986; Fahey et al., 1989, Fahey et al., 1990]. Although this process is considered to be most important for the Antarctic winter stratosphere, as a consequence of lower temperatures, Shindell et al. [1998] have postulated that any possible future stratospheric cooling could result in an increase in the importance of denitrification in the Arctic winter stratosphere. Moreover, during the last decade, observational evidence of this vertical redistribution of HNO_3 in the Arctic stratosphere has also been found [e.g. Fahey et al., 1990; Sugita et al., 1998; Waibel et al., 1999], where it has been shown that such a redistribution can lead to an increase in Arctic ozone loss [Rex et al., 1997; Waibel et al., 1999].

More recently, during the Arctic winter of 1999/2000, which is one of the coldest currently on record [Manney and Sabutis, 2000], both extensive nitrification [Koike et al., 2002] and denitrification [Popp et al., 2001; Santee et al., 2000; Kleinböhl et al., 2003] were observed. Again, large ozone loss was also derived for this winter using both model experiments [Sinnhuber et al., 2000] and *in-situ* observations of ozone [Richard et al., 2001]. Model results attributed 21-30% of ozone loss at the 460 K potential temperature level to denitrification [Davies et al., 2003]. The presence of large HNO_3-containing particles was recorded directly by means of NOy measurements on board the NASA ER-2 aircraft [Northway et al., 2002a] and aerosol extinction measurements by the SAGE III satellite [Poole et al., 2003]. The Multiangle Aerosol Spectrometer Probe (MASP) instrument took in-situ samples of large PSC particles [Fahey et al., 2001; Brooks et al., 2003]. These particles ranged from 2-22 μm in diameter, with a bi-modal distribution. Since the sedimentation of large particles (> 5μm radius) is significantly faster than that of small particles, the presence of large particles increases the rate at which HNO_3 is redistributed.

To date, atmospheric models have typically described denitrification using a rather simplified approach. For instance, most chemistry transport models (CTM's) neglect to include PSC particles as transported species. Instead, a constant or equilibrium PSC particle size and number density are prescribed during the model runs [e.g. Chipperfield, 1999; Koike et al., 2002]. Several of these model studies have concluded that such a simple parameterization of denitrification maybe inadequate for modelling Arctic wintertime ozone loss [Kleinböhl et al., 2003; Sinnhuber et al., 2000]. Therefore, agreement between model results and observations may simply be fortuitous. For instance, Koike et al. [2002] were able to represent NOy measurements during the 1999/2000 winter with a CTM using an average NAT particle radius of 5 μm and fixed particle number density of 5×10^{-3} cm^{-3}. Although this radius falls within the range of observed radii for large particles, the particle number density was overestimated by a factor of ~20 [c.f. Fahey et al., 2001]. Thus, the finding that large NAT particles exist with correspondingly low particle number densities has introduced a strong constraint regarding the description of NAT particles in atmospheric models. A proper description of NAT particles is essential to modelled ozone loss in a cooling climate. It has been demonstrated that current CTM's significantly underestimate the temperature sensitivity of ozone loss during the last two decades [Rex et al., 2004]. This partly reflects shortcomings in NAT representation in global chemistry climate or transport models.

Certain non-equilibrium model studies have been carried out for the same winter. For

example, Jensen et al. [2002] used 1-D model simulations of NAT growth and transport. They tested the sensitivity of the model results towards a number of input parameters, of which the lifetime of the NAT cloud was found to be the most important. The first 3-D model study to include non-equilibrium growth and simultaneous sedimentation of NAT particles was that of Carslaw et al. [2002], where a Lagrangian microphysical algorithm was coupled to the SLIMCAT CTM for particle transport. This study was unique in that the authors were able to represent the radii of the large particles measured by Fahey et al. [2001]. This algorithm was also used in combination with the full-chemistry CTM to simulate the entire 1999/2000 winter and yielded results for denitrification that were consistent with observations [Mann et al., 2003]. One disadvantage of using a Lagrangian method for simulating NAT particles may be that the algorithm is prohibitively expensive for multiple year or long-term climate runs when using complex atmospheric models. Therefore, the development of a concise, computationally efficient method, which transports NAT mass according to size, is required but has yet to be developed. In this paper we aim to address this issue by introducing a computationally inexpensive algorithm designed for use in CTM's, describing nonequilibrium growth, sedimentation of NAT particles and subsequent transport of the size-segregated particles as chemical tracers, following the parameterization developed by Carslaw et al. [2002]. We will show consistent results from two different approaches describing growth and transport of NAT, which both yield realistic HNO_3 redistribution, NAT particle sizes and particle number densities. In Section 2, the CTM and the algorithms for both approaches are described. Section 3 shows the results in comparison to observations and other model studies. Several sensitivity studies are carried out and described in Section 4 and, finally, the discussion and conclusions are presented in Section 5.

2 Model description

2.1 The TM5 model

For our purpose we use the recently developed global three-dimensional transport model, version 5 (TM5). This model has been used previously for several studies of both the troposphere [e.g. Krol et al., 2004; Krol et al., 2003] and stratosphere [van den Broek et al., 2003]. It has been developed by modification of the existing TM3 model, which has also been used for a number of stratospheric chemistry and transport studies [van den Broek et al., 2000; Bregman et al. 2000; Bregman et al., 2001]. The main improvement is the inclusion of a zooming algorithm and the vertical extension of the model domain up to 0.2 hPa, with a higher vertical resolution. In this study we apply a 2º latitude by 3º longitude horizontal resolution for all model runs. The transport of tracers in TM5 is driven by six-hourly forecast fields for temperature, surface pressure, wind, humidity and convective mass flux taken from the European Centre for Medium-Range Weather Forecasts (ECMWF) operational data. The method to calculate mass fluxes from ECMWF winds has recently been improved [Bregman et al., 2003]. We used a 33-layer subset of the 60 layer fields that are taken into account in the ECMWF model, with a reduced number of levels in the tropospheric boundary layer and above 70 hPa. Near the surface the model levels are defined as terrain following sigma coordinates whereas the layers above 100 hPa are defined at pressure surfaces. A hybrid of the two is used between the lower troposphere and the lower stratosphere.
The mass flux advection scheme contains first order slopes [Russell and Lerner, 1981]

or second-order moments [Prather, 1986]. A model time step of 1800s is applied, resulting in dynamical and chemical time steps of 900 s. In contrast to previous model configurations of TM3 and TM5 no reduced grid is applied in the polar region. Instead, the time step in the advection scheme is decreased iteratively to prevent violation of the Courant Friedrichs-Lewy (CFL) condition [Bregman et al., manuscript in preparation].
To focus solely on the redistribution of HNO_3 and performance of the NAT algorithm in this theoretical study no gas phase chemistry was active for any of the runs. This allows us to compare the results with those of Carslaw et al. [2002]. Nitric Acid Dihydrate (NAD) is not accounted for as it is thought to result in a small effect in terms of NO_y redistribution when temperatures fluctuate around 190K due to the associated higher HNO_3 equilibrium pressure [Jensen et al., 2002]. For the Arctic vortex, the coldest temperatures typically only fall to the values needed for NAD formation for a few days, therefore NAD particles never grow to appreciable sizes and thus do not sediment. No supercooled ternary solution (STS) is included as to avoid the transport of additional tracers (i.e. H_2SO_4 and liquid aerosol). The initial profiles used for HNO_3 and H_2O were set at 8 ppbv and 5 ppmv, respectively, for the entire column in all runs, similar to those used for the Lagrangian study by Carslaw et al, 2002. This [HNO_3] in the stratosphere is based on extensive measurements [Kleinböhl et al., 2003] and considered to be a lower limit for the average stratospheric [HNO_3] available.

2.2 The algorithm for NAT growth and sedimentation

The key aspect of our algorithm is the calculation of NAT particle growth in combination with the transport of NAT as tracers that are segregated by size. This is done by distributing the NAT particles between a number of size bins. The particle number density per size bin (n_{bin} [cm^{-3}]) and particle radius (r, [m]) define the NAT mass according to equations (1) and (2):

$$m_p = \frac{[NAT]}{n_{bin}} \tag{1}$$

Where [NAT] is the concentration of NAT [g cm^{-3}], and m_p is the mass [g $particle^{-1}$]

$$r^3 = \frac{m_p}{\rho_{NAT}} \cdot \frac{3}{4\pi} \tag{2}$$

Where ρ_{NAT} is the density of NAT = 1.626×10^6 g m^{-3} [Drdla et al., 1993]

To implement the exact calculation of the NAT properties within a Eulerian model, the advection of another model property, besides mass, would be required, e.g. the NAT number density. This would however result in a double amount of tracers, thereby dramatically decreasing the model efficiency. Furthermore, the separate transport of two quantities that are linked to each other, but are allowed to have different model gradients, will give severe numerical problems during advection. For example, a number density of NAT could exist in a model grid box while no mass of NAT is present. Therefore, we have only included the transport of NAT mass while assumptions are made regarding the particle number density per size bin (n_{bin}) or the radius (r). Firstly, we introduce an approach that assumes a fixed n_{bin} per size bin (hereafter referred to as 'FixedDens'). Secondly, we introduce an approach that assumes that each particle that resides in a specific size bin has the average radius for

that size bin (hereafter referred to as 'FixedRad'). In contrast to these two nonequilibrium approaches, we also discuss the equilibrium approach, which is adopted by most previous model studies [e.g. Koike et al., 2002].

The process of NAT particle growth and sedimentation within TM5 is clarified in the schematic given in Figure 1. Any differences that occur between 'FixedDens' and 'FixedRad' are denoted in red. These differences are described in more detail in Sections 2.3 and 2.4. The schedule is valid for each model grid box in which temperature is low enough for the presence of NAT. Both approaches describe the formation of NAT, particle growth/evaporation, particle sedimentation and the particle size spectrum in an identical manner. NAT particles are allowed to exist in the model only when temperature ≤ 200 K and latitude > 50ºN. After initialization of the model, fresh formation of NAT particles only occurs if the first size bin is empty.

In most CTM's, NAT formation is assumed to occur either on ice particles [e.g. Kleinböhl et al., 2003] or at supersaturation of the surrounding HNO_3-containing air with respect to NAT, usually by a factor of 10 [e.g. Koike et al., 2002]. The exact formation mechanism of NAT has still not yet been fully elucidated from the detailed microphysical studies that have been performed, meaning there is still some debate regarding NAT formation [Drdla, 2003, Knopf et al., 2002, Tabazadeh et al., 2003]. For this reason we adopt a simple approach where, in the base run of our model, particles initially form in the first size bin with a radius of 0.1 μm and a particle number density of 5.75×10^{-5} cm^{-3} (process (1) in Figure (1)) when the temperature is below the NAT equilibrium temperature T_{NAT} [Hanson and Mauersberger, 1988]. Both a doubling of the initial radius and enlarging the threshold for NAT formation by assuming a super saturation by a factor of 10, made no significant change to our results (not shown).

The growth and evaporation of NAT is calculated using the algorithm adopted from Carslaw et al. [2002] (process (2) in Figure (1)). Before implementation of this algorithm into a 3D model run, we first tested the formulation using a box model and successfully reproduced the particle sizes and sedimentation rates for NAT as those shown in Carslaw et al, [2002]. An assumption we make is that the calculation of growth across all size bins starts with the smallest size bin. After growth, the NAT particles are re-binned across the size spectrum, meaning that the mass distribution also changes accordingly (process (3) in Figure (1)). The assumptions used regarding the calculation of r and n_{bin} from the NAT mass are different in both methods and are explained in more detail in Sections 2.3 and 2.4, below. After the re-binning step, a stoichiometric $\Delta[HNO_3]_g$ is calculated according to the increase or decrease of NAT in each grid box (process (4) in Figure (1)). Since both r and n_{bin} are needed for the calculation of the sedimentation rate, differences occur between both approaches (process (5) in Figure (1)), before sedimentation is described (process (6) in Figure (1)). Numerical diffusion due to vertical layering is limited by applying first-order slopes [Russell and Lerner, 1981] to the sedimentation calculation. The calculation of NAT growth and sedimentation is followed by the advective transport of all tracers, i.e. HNO_3 and the NAT mass per size bin (process (7) in Figure (1)). After this advective transport of the modelled species the NAT growth subroutine starts again with the calculation of either r ('FixedDens') or n_{bin} ('FixedRad') from the transported NAT mass (process (8) in Figure 1)).

Figure 1. Schematic diagram for the calculation of growth and sedimentation of NAT particles using the 'FixedRad' and 'FixedDens' algorithms. The black text indicates the general approach whereas the red text indicates differences between approaches 'FixedRad' and 'FixedDens'. See Section 2.2 for more details

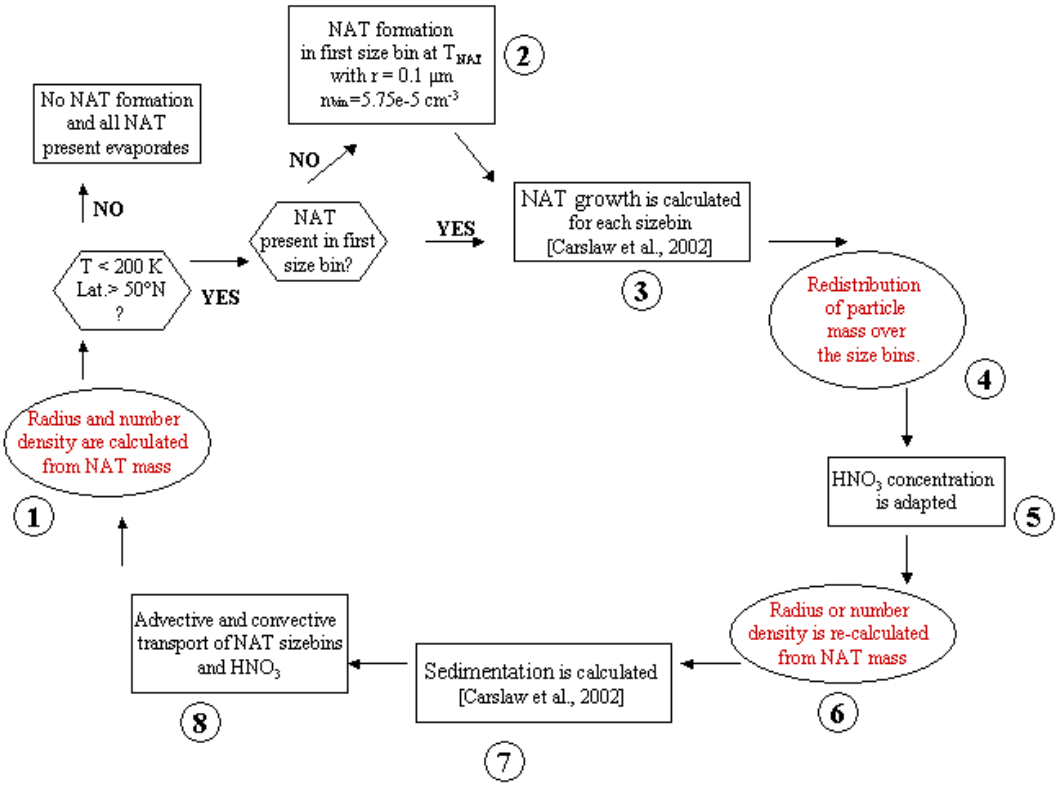

2.3 The 'FixedDens' approach

In this approach r is calculated for each respective size bin from the transported particle mass and the constant n_{bin} value, by using equations (1) and (2). This means that we need to assume that n_{bin} remains constant for each size bin across the entire size bin spectrum after the initial formation of NAT particles. All particles within the same size bin are assumed to grow or evaporate by the same amount. After NAT growth, re-binning of the particles occurs if Δr is large enough for the size bin limit to be exceeded. During this process, the mass of NAT is conserved.
A drawback of this method is that a constant size distribution is applied, whereas in reality the size distribution will change during the growth and evaporation of the NAT particles. Since the radius r is related to n_{bin} through the particle mass (Equations (1) and (2)), an underestimated n_{bin} may lead to an overestimation of r, or the reverse. To diminish this effect, we chose n_{bin} so that the total number density is in close agreement with observed values of large particles [Fahey et al., 2001] after a 10-day simulation. The effect of these assumptions has been investigated using several sensitivity studies and the findings are discussed in Section 4.

2.4 The 'FixedRad' approach

In this second approach the n_{bin} of each size bin is calculated using the transported particle mass together with equations (1) and (2). Here, we assume that the NAT

particle radius (r) equals the average radius of each respective size bin. To allow the transfer of particles between size bins an n_{bin} threshold is required, otherwise an explosion of small particles occurs as a consequence of resetting r equal to the average bin radius at each time step. The required time step would be unrealistically small to solve this numerical problem. Particle growth and sedimentation are calculated in an identical manner as for the 'FixedDens' approach. After growth, any Δr is immediately converted into an increase in n_{bin} using the associated increase in NAT mass (see Eqn. 2). If the re-calculated n_{bin} exceeds the n_{bin} threshold for any particular size bin then the excess n_{bin} is transferred (as mass) to the next size bin. During this step mass is conserved, leading to an instantaneous reduction in the transferred n_{bin} as a consequence of the instantaneous increase in r, which is set equal to the bin average. This continues until the NAT particulate mass resides across the entire size bin spectrum. An advantage of this approach is that a realistic size distribution, with n_{bin} changing per size bin, may be introduced into the scheme. In the 'FixedDens' scheme this would introduce a fluctuation in the number of particles during transfer across the size bins, either introducing a mass inconsistency or an artificial change of the radius. Moreover, not all particles within one size bin need to move to the next size bin after particle growth. However, an associated disadvantage is that the growth or evaporation of particles is actually calculated as a change in n_{bin} instead of r, in first instance, introducing some diffusivity in the size spectrum. Whereas the n_{bin} thresholds move the particles upward to the next size bin during a period of growth, continual evaporation would result in a very small n_{bin} value, which essentially indicates the emptying of the size bin. Combined with the advective transport of particles, the result of the n_{bin} thresholds is that not all size bins are at the n_{bin} limit at any one time and location, which is more realistic than the assumption of constant n_{bin} in the 'FixedDens' method. The assumption that the radius of resident NAT particles in any size bin equals the average radius of that size bin has some influence on the particle growth. Depending on whether n_{bin} represents a NAT mass above or below the average r, a small over- or underestimation of growth may occur. Several sensitivity studies to assess the impact of these assumptions are discussed in Section 3.

2.5 Equilibrium approach

To date, CTM models have adopted a simplified way to parameterize denitrification. Typically, a constant r and n_{bin} of NAT are prescribed [Chipperfield et al., 1999; Koike et al., 2001], or alternatively, calculated assuming an equilibrium particle size [Sinnhuber et al., 2000; Davies et al., 2003]. In all these studies, NAT mass is not transported and it is determined at each time step whether NAT formation is possible. This is in strong contrast to the nonequilibrium methods introduced above, which allow the NAT particles to grow and be transported within a fixed number of size bins.

To allow a direct comparison to be made between all the methods discussed here, we performed two model runs using such a simplified approach, which we refer to as the equilibrium approach.

3 Description of the model runs

3.1 Simulation period

Model runs were carried for three separate 10-day time intervals during the 1999/2000 winter period, these being the 10th – 20th January, 24th January – 3rd February and 16th –26th February, respectively. The end dates of these periods coincide with the NAT particle observations made by the NOAA NOy and MASP instruments [Fahey et al., 2001; Brooks et al., 2003] and also allow us to make a direct comparison with the results of a Lagrangian modelling study of NAT formation for identical periods [Carslaw et al., 2002]. Figure 2 depicts the minimum temperatures from the ECMWF 6-hour forecast fields at two potential temperature levels, 380 K and 475 K, during this winter. From there it can be seen that the minimum temperature at 475 K is continuously below 193 K, which approximately equals T_{NAT}, during the first two simulation periods. The first period, 10th –20th January, experienced the coldest stratospheric temperatures of all the three chosen intervals with T< 191 K throughout the period at 475 K.

3.2 The base run

A base run was defined to allow a direct comparison to be made between the two methods introduced in Sections 2.3 and 2.4. During this run NAT was formed at the NAT equilibrium temperature [Hanson and Mauersberger, 1988] with an initial radius of 0.1 μm and an initial n_{bin} of

Figure 2. Minimum temperatures in the ECMWF 6-hour forecast data on the 380 K and 475 K levels during January and February 2000.

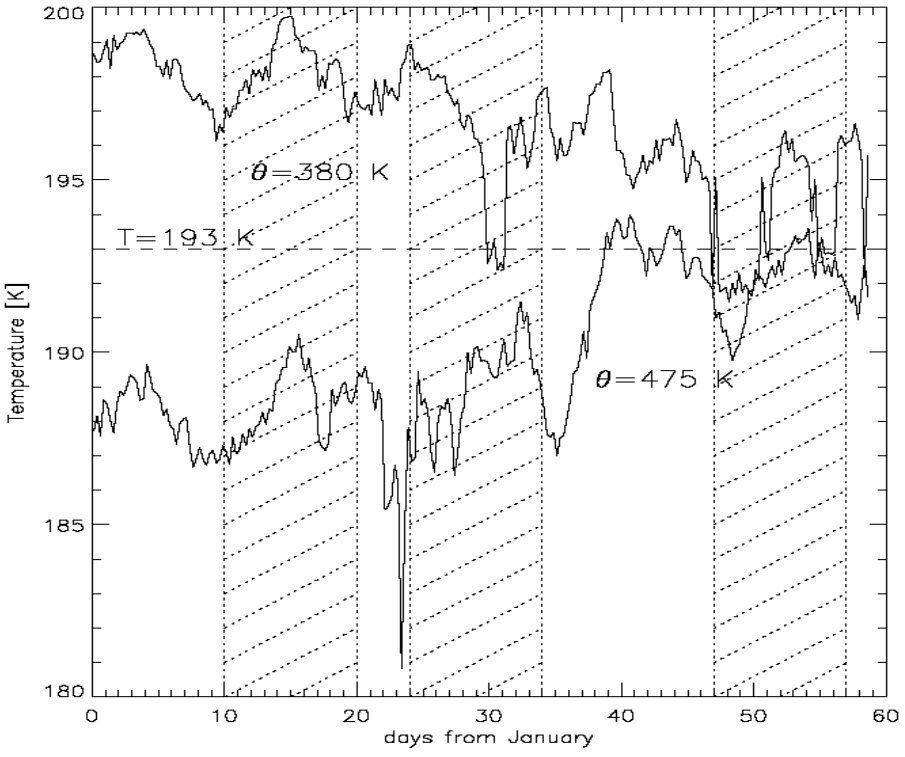

5.75×10^{-5} cm^{-3} (i.e.) equal to n_{bin} of the first size bin. In total 5 size bins were defined, with the thresholds for n_{bin} being set equal to those shown in Table 1 below. The minimum, maximum and average r values, along with the average number concentrations assumed for each bin, are also given for both methods. The n_{bin} values were chosen so that the sum of the particle number concentrations equalled 2.3×10^{-4} cm^{-3}, based on the number density of large particles observed by Fahey et al. [2001] during the same Arctic winter. Since the particles which reside in size bin #5 (i.e. $r >$ 10 μm) lie outside the particle sizes observed during these measurements, this total number concentration was distributed over all size bins where $r < 10$ μm so as not to underestimate particle number concentrations between 0-20 μm diameter. Figure 3a shows the resulting size distribution (black line).

3.3 Sensitivity Studies

To investigate the stability, performance and constraints of both approaches, a series of sensitivity tests were performed and the resulting denitrification was examined. All sensitivity studies were performed for the first 10-day interval of 10^{th}-20^{th} January 2000, where the unusually cold temperatures ensured the existence of NAT particles in the model for the entire simulation period. The sensitivity studies can be grouped into four main categories: (i) comparison against an equilibrium model which neglects NAT growth and transport, (ii) the influence of the n_{bin} limit, (iii) the influence of the number of size bins (and thus tracers) and (iv) the influence of differently shaped size spectra.

Table 1**:** Prescribed radii size limits, average radius, size bin particle density (n_{bin}) and number concentrations used for the base run. Values are given for each respective bin. Within the 'FixedDens' approach, n_{bin} is fixed, whereas the 'FixedRad' approach uses them to set mass thresholds for each bin (see Section 2.4). Simulations were performed for all three chosen intervals using each approach.

Size bin number	1	2	3	4	5
Minimum r [μm]	0	0.2	2	6	12
Maximum r [μm]	0.2	2	6	12	25
Average r [μm]	0.1	1.1	4	9	18.5
Number density per size bin [10^{-5} cm^{-3}]	5.75	5.75	5.75	5.75	5.75
Number concentration. [10^{-5} cm^{-3} μm^{-1} diameter]	14.4	1.597	0.719	0.48	0.221

Details regarding the constraints of the sensitivity runs are given in Table 2 below, while the related size distributions are shown in Figure 3. Figure 3a shows the size distribution of the standard run (black line) plus the size distributions used for the sensitivity tests with higher (blue) and lower (red) total number density, which are discussed in Section 4.2.2. The size distributions for the runs with 7, 10 and 18 bins are shown in Figures 3b-d, respectively, and their results are discussed in Section 4.2.3. Figures 3e-f show the differently shaped size distributions consisting of 7 bins, whose results are discussed in Section 4.2.4.

Figure 3. Plots of particle number concentration [cm^{-3} μm^{-1}] versus particle diameter [μm] for all sensitivity runs performed for the 'FixedDens' and 'FixedRad' approaches: (a) base run (black), with the higher (blue, $4x10^{-4}$ cm^{-3}) and lower (red, $4x10^{-5}$ cm^{-3}) total number density spectra overlayed, (b) 7 bins, (c) 10 bins, (d) 18 bins, (e) and (f) 7 bin model run with differently shaped size distributions: standard (black), negative (blue) in Figure e, and positive slope (green) and observed distribution (red) [Fahey et al., 2001] in Figure f (see text for more details). The total number density for runs (b-f) was similar as for the base run. See Sections 4.2.2 and 4.2.3 for more details.

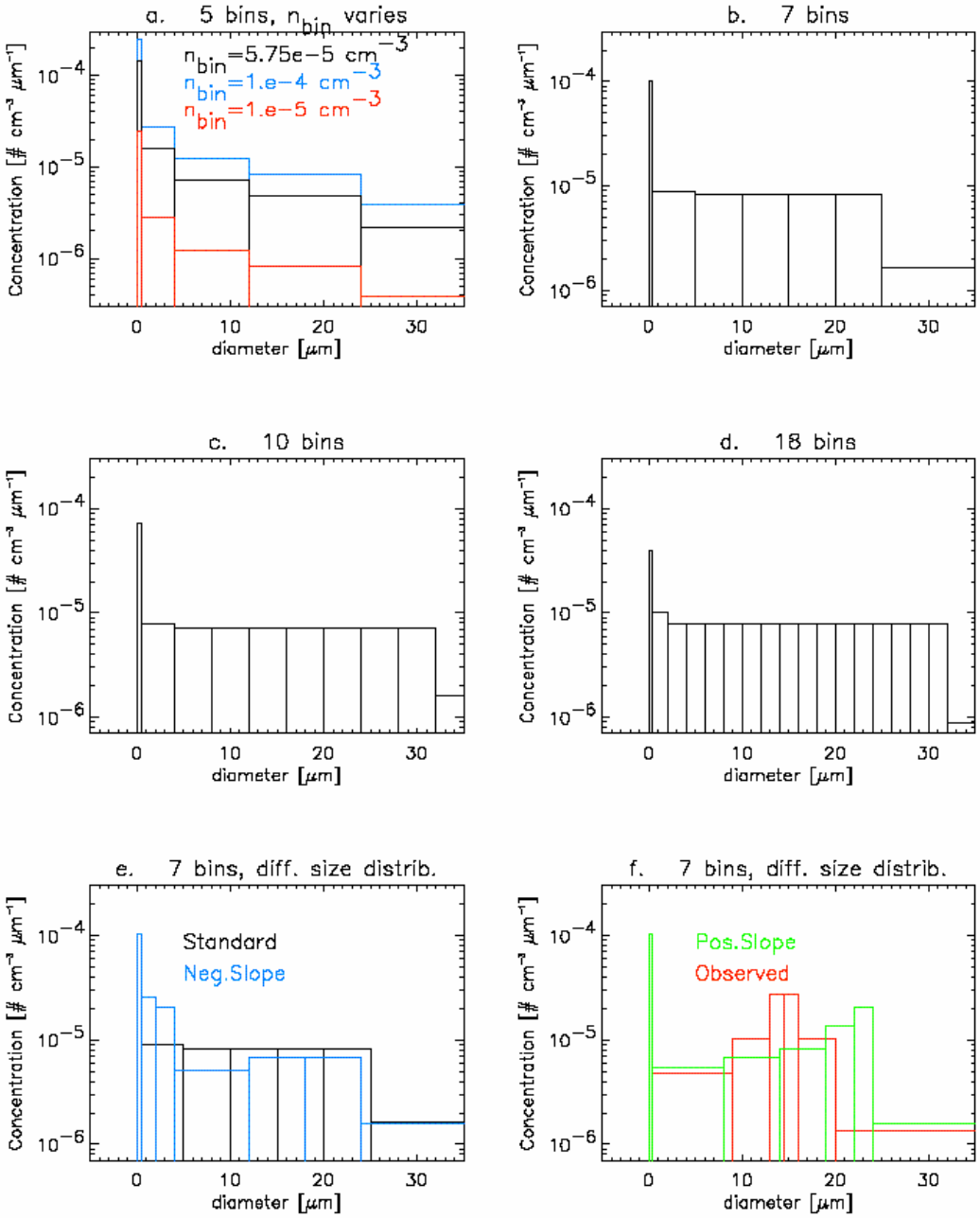

Table 2: Definition of the sensitivity runs conducted regarding the number of size bins, the total particle number density at the end of the simulation, the particle number concentrations in each bin (n_{bin}), and the initial diameter.

	Definition of the Model Run	No. size bins	Total particle number density [1x10^{-4} cm^{-3}]	Number density per size bin n_{bin} [1x10^{-5} parts cm^{-3}]	Init. diam. [μm]
I	Base	5	2.3	5.75	0.2
II	Equilibrium	0	2.3e	N/A	14.5
III	Number density	5	0.1 to 1	1 to 10	0.2
IV	Number of bins	5-18	2.3	1.60 – 5.75 (See Figure 3a-d)	0.2
V	Size spectrum	7	2.3	Varying, see Figure 3e	0.2

4 Results

4.1 The base run

4.1.1 Particle sizes

Figures 4a-c show the average diameter per grid box on the 96 hPa pressure level after a 10-day model run using the 'FixedDens' approach for 20th January, 3rd February and 26th February, respectively. We have chosen this format for comparison reasons, since similar figures are shown by Carslaw et al. [2002] for the same periods. Here, the average diameter ($\bar{d}$) is obtained by weighting the diameter of particles that reside in each respective size bin with the mass fraction of total NAT (hereafter referred to as $[NAT]_{tot}$) present in each size bin according to equation (3):

$$\bar{d} = \sum_{n=1}^{n=n_{tot}} \bar{d}_n \cdot \frac{[NAT]_n}{[NAT]_{tot}} \qquad (3)$$

Where n = the size bin number and n_{tot} = the maximum size number
The largest particles form during the first period, where the minimum vortex temperature is continuously below 191 K at θ = 475 K (see Figure 2). The maximum $\bar{d}$ values obtained for the first period in the 'FixedDens' run range from 22-24 μm, which is comparable to, but slightly higher than, the maximum particle diameter measured by the MASP instrument (~20 μm) on the same day at approximately the same altitude [Fahey et al., 2001]. The model results of Carslaw et al. [2002], which were obtained by applying the same growth/sedimentation algorithm in a Lagrangian model, also show somewhat smaller particle sizes, with a maximum diameter of 16-18 μm at between θ = 420-440K (*c.f.* Figure 2 in Carslaw et al. [2002]). It should be noted that the particle number concentrations at this θ level are lower than those obtained by Carslaw et al. [2002] by ≥50% across the entire size spectrum as a consequence of fixing the particle number density for each size bin in the 'FixedDens'

approach (*c.f.* Figure 3 in Carslaw et al. [2002]). This has consequences regarding the growth rate of the NAT particles (see Section 4.2.2.). For the other simulation periods, which experienced higher temperatures and less NAT formation, the maximum $\overline{d}$ values are smaller than those obtained in the first period by ≥ 3μm. This results in a similar absolute difference with Carslaw et al. [2002] when comparing particle diameter sizes for the respective end dates, 3rd and 26th February. These differences in maximum $\overline{d}$ using the 'FixedDens' approach and those obtained by Carslaw et al. [2002] we feel are acceptable, considering the difference in the treatment of particle transport and the large uncertainties associated with both the particle number density and size distribution.

Figures 4d-f show the corresponding plots of the $\overline{d}$ values when using the 'FixedRad' approach for identical dates. Here, $\overline{d}$ is somewhat smaller than that for the 'FixedDens' run, with the maximum $\overline{d}$ being ~20 μm for the first interval, with the differences in maximum $\overline{d}$ decreasing between the two methods for the second simulation period (*c.f.* Figures 4b with 4e). Remarkably, in the third period $\overline{d}$ is larger for the 'FixedRad' approach. The differences between both approaches are more clearly illustrated in Figure 5, which shows the vertical distribution of $\overline{d}$ at 80°N for each end date.

The integrated area over which large NAT particles are present is larger for the 'FixedRad' runs compared to the 'FixedDens' runs. However, even though larger particles exist over a wider area for 'FixedRad', the actual number of such particles can be rather small (*e.g.* the mass of tracer NAT#4 is between 0-100 pptv at pressures < 30hPa). In fact during the analysis of the data a filter was applied to equation (3) to avoid including extremely small [NAT] concentrations. When the NAT total number density was less than 5×10^{-9} cm^{-3} the data were effectively ignored.

A major cause for these differences between the two approaches is the way in which atmospheric mixing processes affect $\overline{d}$. In the 'FixedRad' approach, mixing will decrease n_{bin}, while the particle size remains the same. In the 'FixedDens' approach, mixing will decrease the particle radius. In fact, at the end of the winter mixing processes become so apparent that the 'FixedRad' radii are slightly larger. An additional effect originates from the particle size discretization in the 'FixedRad' approach. In cold periods, during strong particle growth, the radius is artificially reduced towards the average bin radius, and vice versa during slow particle growth (warmer periods). In the 'FixedDens' approach the radius increase is not limited.

It is interesting to note that in Figure 5 the base level at which NAT occurs drops with respect to the simulation date due to descent of air within the vortex. These figures clearly show that the largest particles reside at the bottom of the vortex for both approaches as a consequence of the sedimentation.

Figure 4. Gridbox average NAT particle diameters after 10 day simulations with the end dates 20th January (upper), 3rd February (middle) and 26th February (lower). The plates on the left side show the results for the 'FixedDens' method and the 'FixedRad' results are shown on the right side. A comparable figure is shown by Carslaw et al. [2002, Figure 2], who applied a Lagrangian model of NAT growth and transport for identical periods.

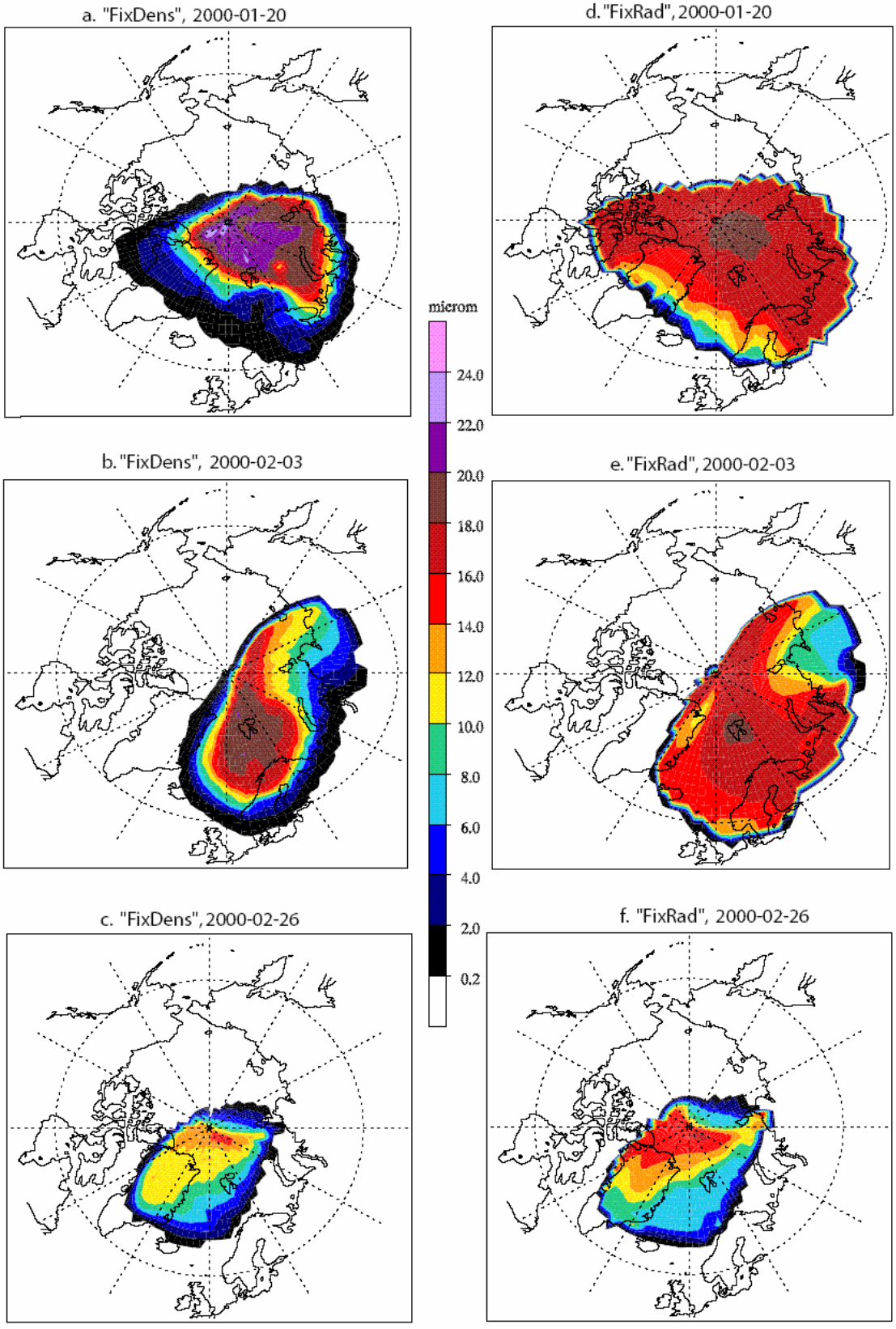

Figure 5. Vertical cross section at 80º N of the gridbox average NAT particle diameter [µm] after 10-day simulations with the end dates 20th January (a+d), 3rd February (b+e) and 26th February (c+f), using both the 'FixedDens' (a-c) and the 'FixedRad' (d-f) approaches.

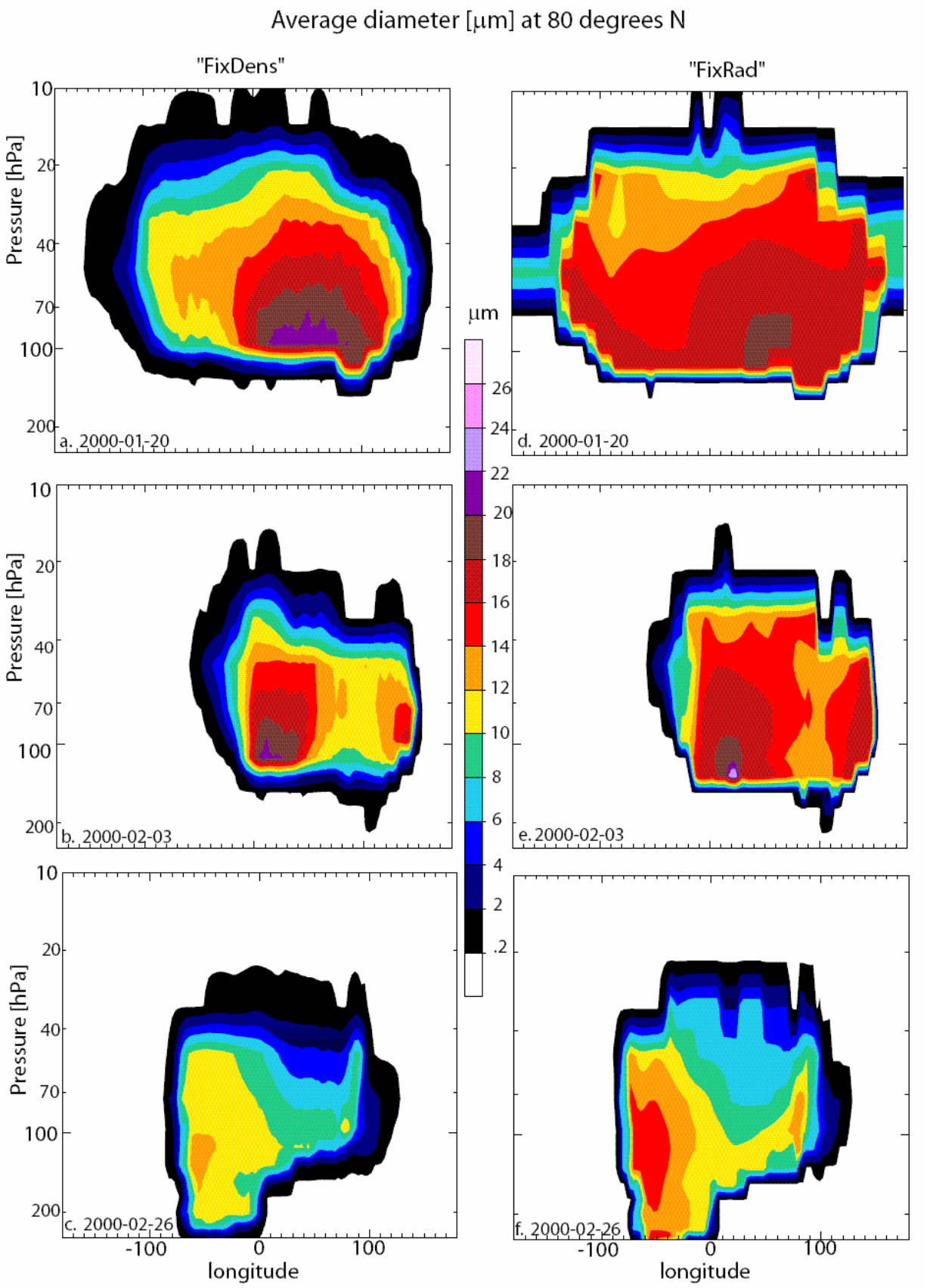

4.1.2 Denitrification

Figure 6 shows a direct comparison of the percentage change in HNO_3 calculated by each of our methods against equivalent latitude for the three chosen simulation periods. Here, two potential temperature levels are shown which correspond to the altitude domains where the maximum amount of nitrification (θ = 380 K) and denitrification (θ = 475 K) occur in the first simulation period.
The 10^{th}-20^{th} January model run gives the greatest ΔHNO_3 of all three chosen simulation periods due to the persistence of unusually cold temperatures. At 20^{th} January there is more nitrification in 'FixedDens' (~25%) than in 'FixedRad' (~10%). This is because 'FixedRad' has a smaller number density per size bin, which is related to the differences in mass transport across the edges of the size bins between both approaches. In the 'FixedDens' approach, the full size bin mass is transported to the next size bin when the radius limit is reached. In the 'FixedRad' approach, only the fraction above the size bin number density threshold is transported to the next size bin.
For the second period, between 24^{th} January-3^{rd} February, ~5 and ~12% denitrification is calculated for the 'FixedRad' and 'FixedDens' approaches, respectively. For the final period, on 26^{th} February 2000, practically no (de)nitrification is predicted by the 'FixedDens' approach, despite the maximum $\bar{d}$ of ~17 μm that was calculated (c.f Figure 4c). The 'FixedRad' approach on 26^{th} February still yields a small amount of denitrification (~5%) at the θ = 475 K. Note that the higher temperatures in periods 2 and 3 reduce the sedimentation velocity and the maximum amount of denitrification occurs at a higher altitude.
Due to the smaller amount of denitrification calculated for this period, the maximum (de)nitrification occurs at different altitudes (not shown). This is a consequence of the smaller maximum $\bar{d}$ and the shorter lifetime of the NAT particles.

4.2 Sensitivity studies

As discussed in Section 3.2, a number of prescribed model parameters were used for the base run simulation, where the choice of such parameters could influence performance of the algorithms to describe NAT growth and transport. For this reason we have tested the model sensitivity towards such parameters to quantify the robustness of our approaches. The simulation period of 10^{th} – 20^{th} January was used exclusively for this purpose due to the occurrence of large NAT particles as described earlier. The prolonged period of cold temperatures also ensures that NAT was present throughout the entire period, making differences between the sensitivity runs more easily discernible. For brevity we limit our discussion to the main categories defined in Section 3.3. In addition, we have also tested several other model parameters which resulted in negligible differences in NOy re-distribution for both methods, these being: the number of vertical layers used in the model; the type of advection scheme employed (first order or 2^{nd} moments); doubling the radius of the initial size bin, i.e. the nucleation rate; and increasing the supersaturation of HNO_3 needed for NAT formation to 10. It should be noted that these results pertain to a chemically passive version of TM5 and the sensitivity should be re-tested when adding chemical tracers.

Figure 6.The percentage denitrification (θ= 475 K level) and nitrification (θ=380 K level) against equivalent latitude for (a) 20th January, 2000, (b) 3rd February, 2000 and (c) 26th February, 2000. The results of the 'FixedDens' approach are shown as dotted lines, and the solid lines show the results of the 'FixedRad' approach. The results for the "FixedDens" and "FixedRad" approach are shown as dotted and solid lines, respectively.

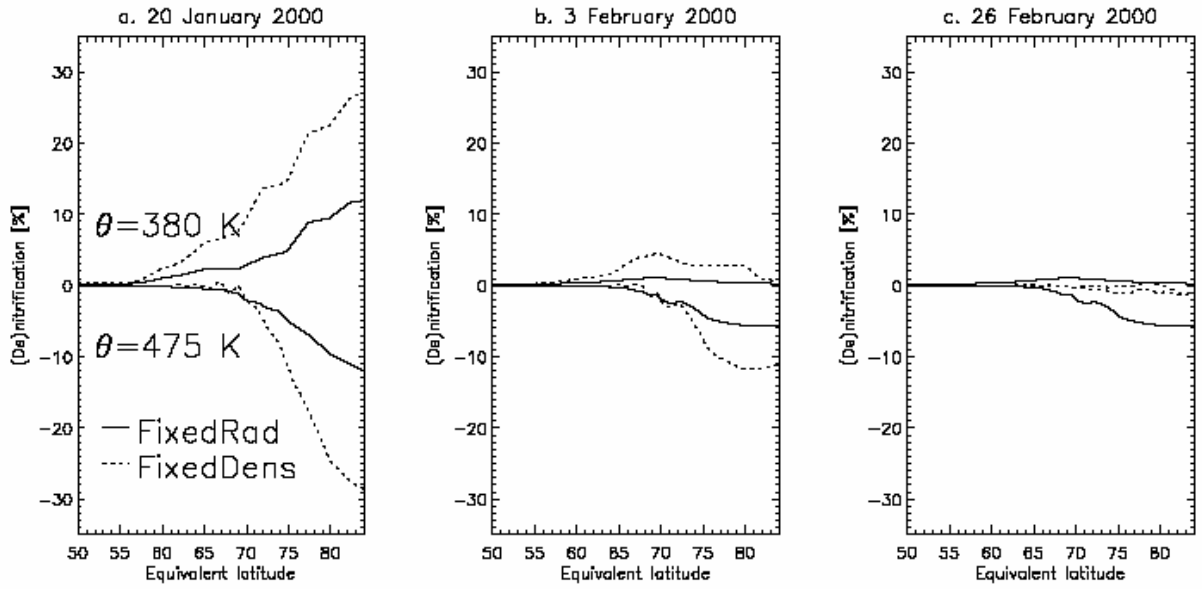

4.2.1 Comparison with the equilibrium approach

To allow a direct comparison of the equilibrium method with the base runs, the total particle number densities and radii for all NAT particles were set constant in two different runs. For the first sensitivity run, the number density and radius were 2.3×10^{-4} cm^{-3} and 7.25 μm, respectively, which equals the average values found by Fahey et al. [2001]. These sizes were observed on 20th January after a persistent cold period. Since the equilibrium approach assumes a constant radius, using the observed radius throughout the integration period may overestimate denitrification. Therefore, smaller radii were assumed in the second sensitivity run, i.e. 4 μm. Again, NAT formation was calculated using T_{NAT} based on the Hanson and Mauersberger criterium [1988] at each model time step (900 s). Figures 7a-d show the vertical redistribution of HNO_3 at 80˚N latitude across all longitudes for the 'FixedDens', 'FixedRad' and both equilibrium runs, respectively. From Figure 7c it becomes apparent that after a 10-day simulation nearly 100% denitrification is simulated using the equilibrium approach with large particles. This is an exaggerated repartitioning, given that an estimated 20-60% is thought to occur in the Arctic over the entire winter [Santee et al., 2000; Popp et al, 2001; Kleinböhl et al., 2003]. However, the magnitude of the calculated denitrification is critically dependent on the values assumed for the prescribed radius and particle number density. By comparing Figures 7c and 7d it can be seen that a smaller radius dramatically reduces denitrification. Tuning these parameters may thus lead to fortuitous agreement between modelled NOy profiles and observations [Kleinböhl et al., 2003; Sinnhuber et al., 2000]. However, the recent observations of large NAT particles constrain the assumptions that can be made regarding these constant parameters.

Another difference between the equilibrium and nonequilibrium approaches concerns the vertical distribution of HNO_3. A maximum of denitrification is found at a higher level (~25 hPa instead of ~50 hPa) in the equilibrium model runs, even with a short

integration time of 10 days. Similar changes in the vertical distribution of denitrification between an equilibrium and nonequilibrium approach were also found by Mann et al. [2002] for the same winter.

Figure 7. HNO_3 volume mixing ratio [ppbv] at 80ºN latitude at 20th January after a 10-day simulation. (a) "FixDens", (b) "FixRad" and (c-d) the Equilibrium Method.

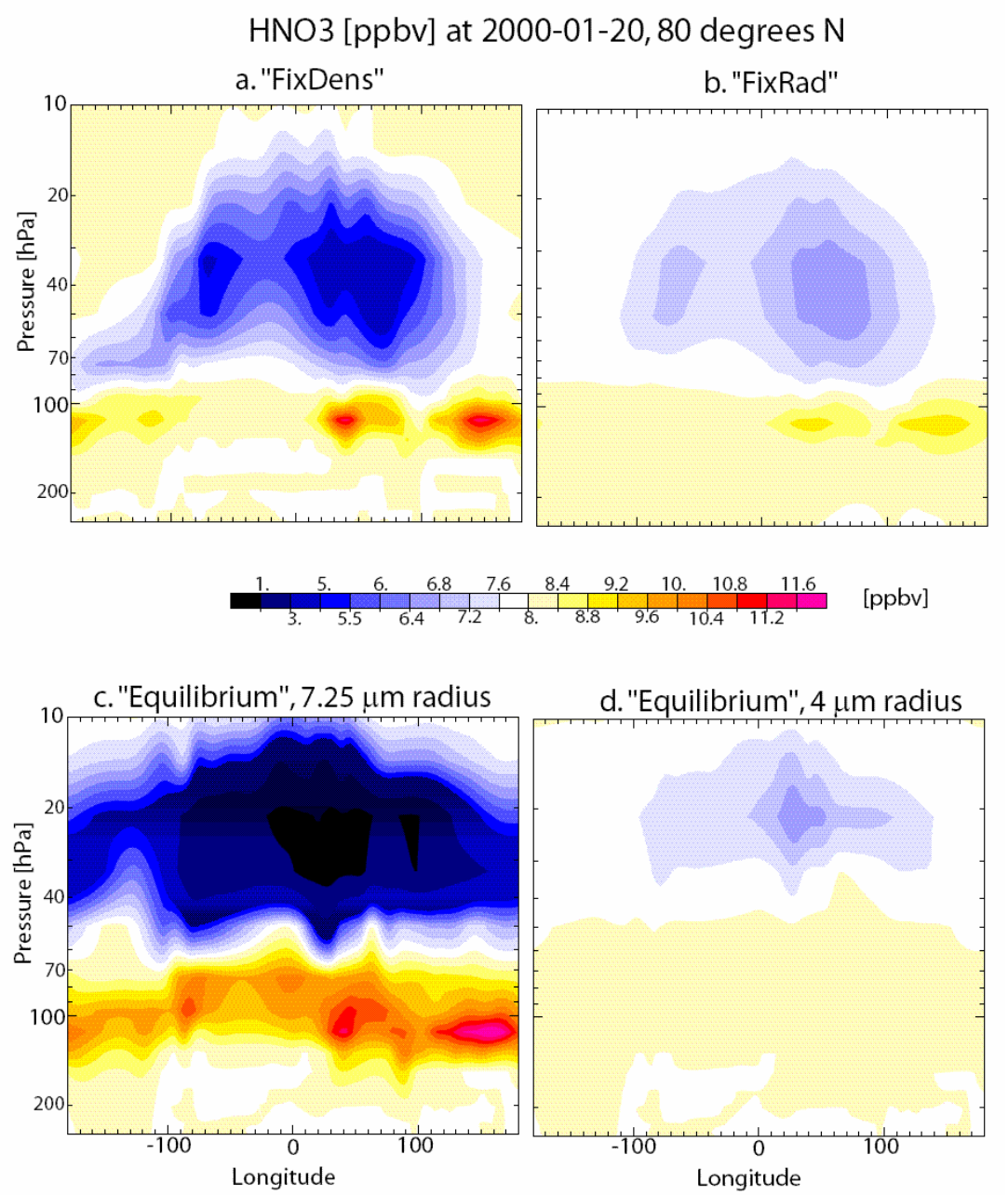

4.2.2 Total number density

The total number density of large particles (> 5 µm diameter) as observed by Fahey et al. [2001] was ~2.3x10^{-4} cm^{-3} on January 20th. The estimated uncertainty of this measurement is ±30% and may vary with the location inside the vortex. To test the model's sensitivity to this parameter, the maximum allowable total number density was varied from 0.5 to 5x10^{-4} cm^{-3}, resulting in an n_{bin} between 0.1 and 1x10^{-4} cm^{-3}, respectively. The resulting size distributions in terms of number concentration are

depicted in Figure 3a, with the blue, black and red line denoting the high, standard and low total number density, respectively.
Figure 8 shows the (de)nitrification at 80ºN equivalent latitude against the total number density for these model runs on θ levels 380 K and 475 K, respectively. Even though the number density is variable within the 'FixedRad' approach (i.e. n_{bin} is merely used to define a threshold instead of a fixed number of particles) the algorithm is still sensitive to this parameter, although less so than the 'FixedDens' approach. (De)nitrification increases with increasing n_{bin} due to an associated increase in the fraction of HNO_3 partitioned into NAT. However, the maximum $\bar{d}$ value becomes lower (decreasing from 24.9μm for $1x10^{-5}$ cm^{-3} to 21.8 μm for $1x10^{-4}$ cm^{-3} at 96hPa using the 'FixedDens' approach (not shown)) indicating that the growth of NAT particles is somewhat moderated by the choice of n_{bin}. This is due to a related increase in particle mass (Δm_p) in equation (2). This change is non-linear with respect to n_{bin} due to the increase in $[NAT]_{tot}$. In all cases, the $[NAT]_{tot}$ for the 'FixedDens' method exceeded that of the 'FixedRad' approach by 30-40%. This increase in (de)nitrification with n_{bin} would eventually reach a maximal value due to the associated reduction in the available $[HNO_{3(g)}]$ within the vortex. The latter would result in a limitation to particle growth, especially when a non-uniform $HNO_{3(g)}$ profile is considered. However, this situation would only be reached when prescribing high number densities or during longer model runs. Moreover, temperature fluctuations would also limit the magnitude of the (de)nitrification by introducing periods where the evaporation of particles would hinder the sedimentation. Varying n_{bin} from 0.25 to $1x10^{-4}$ cm^{-3}, which is equivalent to halving or doubling the total number density, leads to an increase in denitrification from 12 to 34% at an equivalent latitude of 80ºN and θ = 475 K for the 'FixedDens' run, and from 5 to 15% for the 'FixedRad' run (see Figure 8).

4.2.3 The number of size bins

To make the algorithm as efficient as possible, it is important to know how many size bins are required to model denitrification. Figure 9 shows the (de)nitrification at 80ºN equivalent latitude calculated using an increasing number of size bins on identical θ levels as those shown in Figure 8 for both model approaches. Due to the substantial increase in the redistribution of HNO_3 with increasing particle number density (see Section 4.2.2.), the total number density was kept constant throughout at $2.3x10^{-4}$ cm^{-3}, as prescribed in the base run. Since the size bin limits were not identical for each sensitivity run, the shape of the resulting size distributions varies depending on the number of bins used (c.f. Figure 3a-d). However, it can be seen that the size spectrum essentially becomes flat once 7 or more bins are prescribed.
A pronounced result is that the methods are quite robust in calculated denitrification, since only small differences occur when the amount of size bins is doubled. The 'FixedDens' approach results in more (de)nitrification than the 'FixedRad' approach regardless of the number of size bins used. But, remarkably, the differences in the vortex averaged values between both approaches fall below 10% when the number of size bins exceeds 7. 'FixedRad' is less sensitive and only varies between 8 and 12% across the range of the chosen number of size bin numbers, while the 'FixedDens' denitrification clearly decreases with an increasing number of size bins, from 25% in the 5 bin simulation to 15% in the 18 bin run. This is due to the fact that the 'FixedDens' particle growth is more sensitive to the resolution of the size spectrum (i.e. number of bins). The full content of the size bin is moved up or down at growth

Figure 8. De- and nitrification [%] on 20th January at 80ºN equivalent latitude, at 475 K and 380 K, respectively, using different total number densities (see Table 2) and both approaches; 'FixedDens' (dotted line) and 'FixedRad' (solid line).

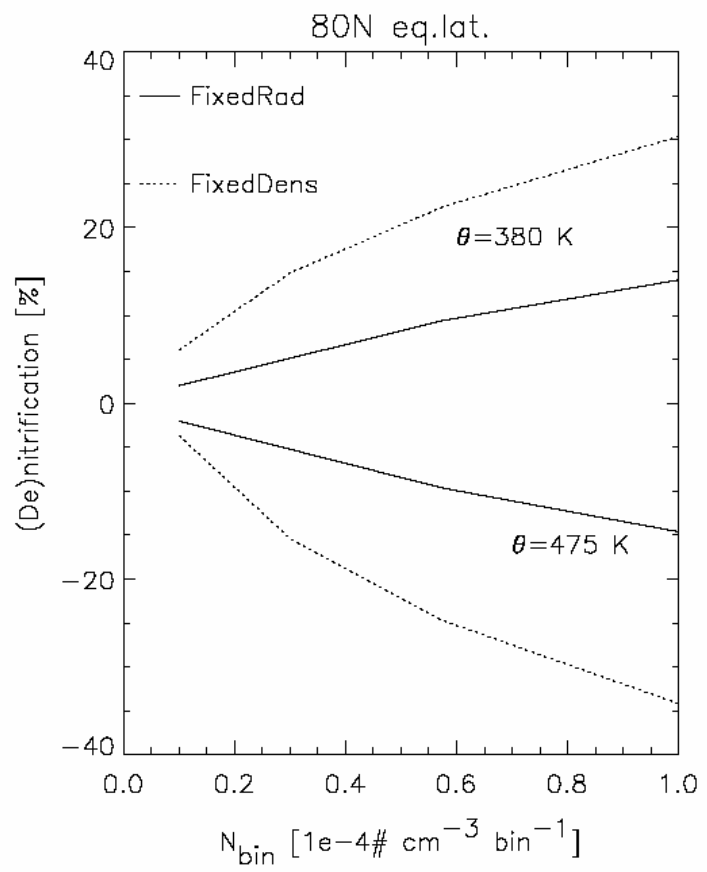

Figure 9. De- and nitrification [%] on 20th January at 80ºN equivalent latitude, at 475 K and 380 K, respectively, using a different number of size bins (see Table 2) and both approaches. The crosses mark the number of size bins in the integrations that were done.

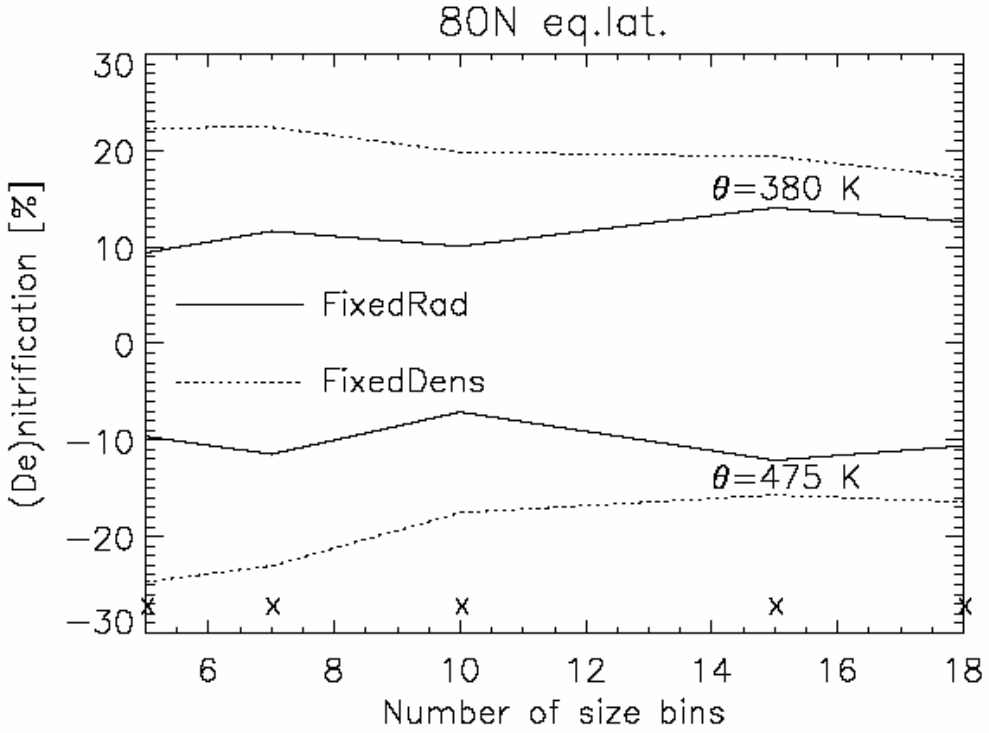

or evaporation, while in the 'FixedRad' approach the mass transport occurs only once the threshold n_{bin} is exceeded. The use of more size bins, with each of them a lower number density than the size bins in the standard run, results in a more concise and variable distribution of the mass over the size bins.

4.2.4 The shape of the size distribution

The particle size distributions measured by Fahey et al. [2001] suggest that constraining the model with a flat size distribution across the entire size spectrum maybe an oversimplification (as performed for the 7, 10, 15 and 18 bin sensitivity runs, *c.f.* Figures 3b-d). To provide further insight into the extent to which the prescribed size spectrum has on the calculation of denitrification, we chose to alter the shape of the permitted size spectrum in a number of ways. For this purpose, we have performed runs with 7 bins using three distinctively different size distributions: one with decreasing and one with increasing n_{bin} values from bin 2 to bin 7 (creating a negative and a positive 'slope', respectively) and one based on the distribution observed by Fahey et al. [2001]. The shapes of these size distributions are shown in Figures 3e-f and defined as the standard flat (black line), negative (blue), in Figure e, and positive (green) and observed (red) distribution, in Figure f, respectively.
Figures 10a and b show comparisons of the resulting (de)nitrification at θ levels 380 and 475K versus equivalent latitude for the 'FixedDens' and 'FixedRad' approaches, respectively. In summary it can be seen that the (de)nitrification changes by < 5% for both approaches indicating that they are relatively robust with respect to the prescribed shape. For the run with the observed size spectrum the model became unstable using the 'FixedRad' approach due to the last bin 'overflowing' on the ninth day of the integration.
However, the amount of NAT formed became rather excessive (> 2ppbv) in small regions of the vortex (not shown) meaning that no further discussion of this run is warranted. Prescribing an observed size distribution has the inherent weakness that the size distribution must remain similar during the entire winter period. Unfortunately the size distributions shown in Northway et al. [2002b] indicate that the both the total number density and size distribution change between January 20th and February 3rd in the Arctic vortex for this winter. Therefore constraining the model with an observed size distribution would only be possible if many more measurements were available, during the whole winter, which is not feasible.

5 Discussion and conclusions

In this study we present an efficient and concise algorithm for the formation and sedimentation of NAT particles, which has been implemented in a global Eulerian 3D chemistry transport model using a non-equilibrium approach. For this purpose the transport of such particles is achieved by segregating the particles into distinct size bins, each of which is treated as an advected tracer. Two separate approaches were tested, one which prescribes a fixed particle number density ('FixedDens') and the other a fixed particle radius for each respective size bin ('FixedRad'). This algorithm has been applied in simulations over three selected 10-day periods during the Arctic winter 1999/2000, and the resulting particle sizes and number concentrations were found to agree favourably with those observed 'in-situ' [Fahey et al., 2001; Brooks et al., 2003]. Comparisons made with the results of a Lagrangian model study [Carslaw et al., 2002], from which the microphysical component of our algorithm was taken,

Figure 10. De- and nitrification [%] along equivalent latitudes, at 475 K and 380 K, respectively, depending on the shape of the size distribution (see Figure 3e-f). For (a) the 'FixedDens' approach and (b) the 'FixedRad' approach the number of size bins and total number density are fixed to seven and $2.3x10^4$ cm^{-3} respectively.

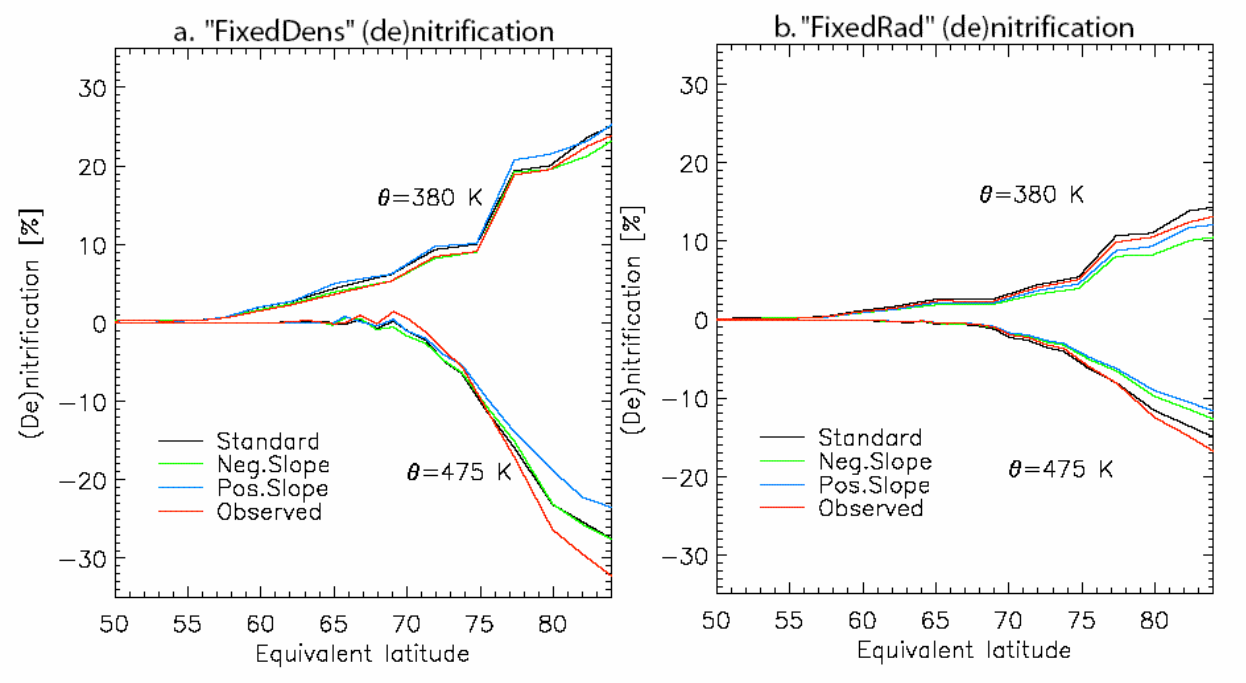

reveals differences of between 0-4 µm for the diameters of the largest NAT particle formed, depending on the adopted approach (with the Eulerian model producing the larger sizes). Considering the differences in the performance and underlying concepts of both models we feel that agreement within ±20% is a satisfactory result. Moreover, the resulting denitrification simulated by our routine also lies within the range of measured values (20-60%) for the Arctic winter 1999/2000 [Popp et al., 2001; Kleinböhl et al., 2003; Santee et al., 2000], although for a more realistic comparison model runs need to be extended over the entire winter using realistic HNO_3 profiles, with a full stratospheric chemistry scheme.

Substantial differences were found in both the extent of denitrification and vertical redistribution of HNO_3, when compared against the results obtained using a simple equilibrium approach. Applying the equilibrium approach resulted in an unrealistically high removal of HNO3 when using an observed particle radius. Decreasing the particle radius to 4 µm significantly reduced the HNO_3 removal, indicating the potential danger of using such an approach. This large effect justifies the use of the computationally more expensive, but more realistic, treatment of NAT particle growth and sedimentation. The results of the 'FixedDens' and the 'FixedRad' method differ somewhat, but these differences are small compared to other uncertainties introduced in the model.

The results from the sensitivity studies suggest that the model is rather robust and relatively insensitive to the number of size bins used, as long as the total particle number density remains constant. The 'FixedRad' approach shows the smallest variation in denitrification when changing the number of size bins. The differences between both approaches become ≤ 10% for 10 size bins or more. This has advantages in that just a limited number of extra tracers are needed to account for nonequilibrium treatment of NAT and denitrification in a full chemistry run. Another

important finding is that both approaches are also quite insensitive to the shape of the size distribution. However, they are sensitive to the total particle number density (~17% difference in 10-day denitrification upon changing the total number density in the 'FixDens' approach from 0.4×10^{-4} to 1×10^{-4} cm^{-3}, see Figure 8), although the 'FixedRad' approach proved to be more robust also in this parameter. Considering the observed variability during 1999/2000, similar observations of the NAT total number density would be beneficial for future Arctic winters, as well as a continued effort in clarifying the details of the formation mechanisms of NAT. Our approaches do not require detailed knowledge on the shape of the size distribution, at least for the 1999/2000 winter.

For a more rigorous validation of our algorithms we are currently performing simulations over the entire Arctic winter period of 1999/2000 with comprehensive chemistry active, as well as for more moderate Arctic winters. It was already shown with a Lagrangian model that the nonequilibrium treatment of NAT calculates significant denitrification in other, more moderate winters [Mann et al., 2003]. Using the Eulerian approaches, we are now able to test the effect of denitrification during such a more moderate winter period to try and assess whether these differences lead to additional ozone depletion that warrants the increase in computational costs.

Acknowledgements

We would like to thank Ken Carslaw, Stewart Davies, Graham Mann from the School of the Environment at the University of Leeds for their introduction to their nonequilibrium NAT algorithm and fruitful discussions. Joachim Buchholz, Stefanie Meilinger and Jos Lelieveld are also thanked kindly for their help and advice.

6 References

Bregman, A., J. Lelieveld, M. van den Broek, H. Fischer, P. Siegmund and O. Bujok, The N_2O and O_2 relationship for mixing processes as represented by a three-dimensional chemistry-transport model, *J. Geophys. Res., 105*, 17,279-17,290, 2000.

Bregman, A., M.C. Krol, H. Teyssedre, W.A. Norton, A. Iwi, M. Chipperfield, G. Pitari, J.K. Sundet and J. Lelieveld, Chemistry-Transport model comparison with ozone observations in the midlatitude lowermost stratosphere, *J. Geophys. Res., 106*, 17,479-17,496, 2001.

Bregman, A., A. Segers, M. Krol, E. Meijer, and P. van Velthoven, On the use of mass-conserving wind fields in chemistry-transport models, *Atm. Chem. Phys., 3*, 447-457, 2003.

Brooks, S.D., D. Baumgardner, B. Gandrud, J.E. Dye, M.J. Northway, D.W. Fahey, T. Paul Bui, O.B. Toon, and M.A. Tolbert, Measurements of large stratospheric particles in the Arctic polar vortex, *J. Geophys. Res., 108*, D20, 4652, doi: 10.1029/ 2002JD003278, 2003

Carslaw, K.S., J.A. Kettleborough, M.J. Northway, S. Davies, R.S. Gao, D.W. Fahey, D.G. Baumgardner, M.P. Chipperfield, and A. Kleinböhl, A vortex-scale simulation of the growth and sedimentation of large nitric acid hydrate particles, *J. Geophys. Res., 107*, D20, 8300, doi:10.1029/2001JD000467, 2002

Chipperfield, M.P., Multiannual simulations with a three-dimensional chemical transport model, *J. Geophys. Res., 104*, 1781-1805, 1999

Crutzen, P., and Arnold, F., Nitric acid cloud formation in the cold Arctic stratosphere, a major cause for the springtime "ozone hole", *Nature, 324*, 651-655, 1986

Davies, S., M.P. Chipperfield, K.S. Carslaw, B.-M. Sinnhuber, J.G. Anderson, R.M. Stimpfle, D.M. Wilmouth, D.W. Fahey, P.J. Popp, E.C. Richard, P. von der Gathen, H. Jost and C.R. Webster, Modeling the effect of denitrification on Arctic ozone depletion during winter 1999/2000, *J. Geophys. Res., 108*, D5, 8322, doi :10.1029/2001JD000445, 2003

Drdla, K., M.R. Schoeberl, and E.V. Browell, Microphysical modelling of the 1999-2000 Arctic winter: 1. Polar stratospheric clouds, denitrification, and dehydration, *J. Geophys. Res., 108*, D5, 8312, doi:10.1029/2001JD000782, 2003

Drdla, K., R. P. Turco, and S. Elliott, Heterogeneous chemistry on Antarctic polar stratospheric clouds - a microphysical estimate of the extent of chemical processing, *J. Geophys. Res.*, 98, D5, 8965-8981, 1993

Fahey, D.W., R.S. Gao, K.S. Carslaw, J. Kettleborough, P.J. Popp, M.J. Northway, J.C. Holecek, S.C. Ciciora, R.J. McLaughlin, T.L. Thompson, R.H. Winkler, D.G. Baumgardner, B. Gandrud, P.O. Wennberg, S. Dhaniyala, K. McKinney, Th. Peter, R.J. Salawitch, T.P. Bui, J.W. Elkins, C.R. Webster, E.L. Atlas, H. Jost, J.C. Wilson, R.L. Herman, A. Kleinböhl, and M. von König, The detection of large HNO3-containing particles in the winter Arctic Stratosphere, *Science*, 1026-1031, 2001

Fahey, D.W., K.K. Kelly, S.R. Kawa, A.F. Tuck, M. Loewenstein, K.R. Chan and L.E. Heidt, Observations of denitrification and dehydration in the winter polar stratospheres, *Nature, 344*, 321-324, 1990

Fahey, D.W., K.K. Kelly, G.V. Ferry, L.R. Poole, J.C. Wilson, D.M. Murphy, M. Loewenstein, and K.R. Chan, In situ measurements of total reactive nitrogen, total water and aerosol in a polar stratospheric cloud in the Antarctic, *J. Geophys. Res., 94*, 11,299-11,315, 1989

Hanson, D. and K. Mauersberger, Laboratory studies of the nitric acid trihydrate: Implications for the South polar stratosphere, *Geophys. Res. Lett., 15*, 855-858, 1988

Jensen, E.J., O.B. Toon, A. Tabazadeh and K. Drdla, Impact of polar stratospheric cloud particle composition, number density, and lifetime on denitrification, *J. Geophys. Res., 107*, D20, 8284, doi:10.1029/2001JD000440, 2002

Kleinböhl, A., H. Bremer, M. von König, H. Küllmann, K.F. Künzi, A.P.H. Goede, E.V. Browell, W.B. Grant, G.C. Toon, T. Blumenstock, B. Galle, B.-M. Sinnhuber, and S. Davies, Vortexwide denitrification of the Arctic polar stratosphere in winter 1999/2000 determined by remote observations, *J. Geophys. Res., 108*, D5, 8305, doi :10.1029/2001JD001042, 2003

Knopf, D.A., T. Koop, B.P. Luo, U.G. Weers and T. Peter, Homogeneous nucleation of NAD and NAT in liquid stratospheric aerosols: insufficient to explain denitrification, *Atmos. Chem. Phys., 2*, 207-214, 2002

Koike, M., Y. Kondo, N. Takegawa, F. Lefevre, H. Ikeda, H. Irie, H.D.E. Hunton, A.A. Viggiano, T.M. Miller, J.O. Ballenthin, G.W. Sachse, B.E. Anderson, M. Avery, and Y. Masui, Redistribution of reactive nitrogen in the Arctic lower stratosphere in the 1999/2000 winter, *J. Geophys. Res., 107*, D20, 8275, doi :10.1029/2001JD001089, 2002

Krol, M.C., S. Houweling, B. Bregman, M. van den Broek, A. Segers, P. van Velthoven, W. Peters, F. Dentener, and P. Bergamaschi, The two-way nested global chemistry-transport zoom model TM5 : Algorithm and applications, *Atm. Chem. Phys. Disc.*, 3975-4018, 2004

Krol, M.C., J. Lelieveld, D.E. Oram, G.A. Sturrock, S.A. Penkett, C.A.M. Brenninkmeier, V. Gros, J. Williams and H.A. Scheeren, Continuing emissions of methyl chloroform from Europe, *Nature, 421*, 131-135, 2003

Mann, G.W., S. Davies, K.S. Carslaw, and M.P. Chipperfield, Factors controlling Arctic denitrification in cold winters of the 1990s, *Atmos. Chem. Phys., 3*, 403-416, 2003

Mann, G.W., S. Davies, K.S. Carslaw and M.P. Chipperfield, Polar vortex concentricity as a controlling factor in Arctic denitrification, *J. Geophys. Res. 107*, D22, 4663, doi:10.1029/20002JD002102, 2002

Manney, G.L. and J.L. Sabutis, Development of the polar vortex in the 1999-2000 Arctic winter stratosphere, *Geophys. Res. Lett., 27*, 2,589-2,592, 2000

Northway, M.J., R.S. Gao, P.J. Popp, J.C. Holecek, D.W. Fahey, K.S. Carslaw, M.A. Tolbert, L.R. Lait, S. Dhaniyala, R.C. Flagan, P.O. Wennberg, M.J. Mahoney, R.L. Herman, G.C. Toon and T.P. Bui, An analysis of large HNO_3-containing particles sampled in the Arctic stratosphere during the winter of 1999/2000, *J. Geophys. Res., 107*, D20, 8298, doi:10.1029/2001JD001079, 2002a.

Northway, M.J., P.J. Popp, R.S. Gao, D.W. Fahey, G.C. Toon and T.P. Bui, Relating inferred HNO_3 flux values to the dinitrification of the 1999-2000 Arctic Vortex, *Geophys. Res. Lett.*, *29*, D16, 1816, doi: 10.1029/2002GL015000, 2002b.

Poole, L.R., C.R. Trepte, V.L. Harvey, G.C. Toon, and R.L. VanValkenburg, SAGE III observations of Arctic polar stratospheric clouds – December 2002, *Geophys. Res. Lett., 30*, no. 23, 2216, doi :10.1029/2003GL018496, 2003

Popp, P.J., M.J. Northway, J.C. Holecek, R.S. Gao, D.W. Fahey, J.W. Elkins, D.F. Hurst, P.A. Romashkin, G.C. Toon, B. Sen, S.M. Schauffler, R.J. Salawitch, C.R. Webster, R.L. Herman, H. Jost, T.P. Bui, P.A. Newman, and L.R. Lait, Severe and extensive denitrification in the 1999/2000 Arctic winter stratosphere, *Geophys. Res. Lett., 28*, 2875-2878, 2001

Prather, M.J., Numerical advection by conservation of second-order moments, *J. Geophys. Res., 91*, 6671-6681, 1986

Rex, M., R.J. Salawitch, P. von der Gathen, N.R.P. Harris, M.P. Chipperfield, and B. Naujokat, Arctic ozone loss and climate change, *Geophys. Res. Lett., 31*, L04116, doi:10.1029/ 2003GL018844, 2004

Rex, M., N.R.P. Harris, P. von der Gathen, R. Lehmann, G.O. Braathen, E. Reimer, A. Beck, M.P. Chipperfield, R. Alfier, M. Allaart, F. O'Connor, H. Dier, V. Dorokhov, H. Fast, M. Gil, E. Kyrö, Z. Litynska, I.S. Mikkelsen, M.G. Molyneux, H. Nakane, J. Notholt, M. Rummukainen, P. Viatte, and J. Wenger, Prolonged stratospheric ozone loss in the 1995-1996 winter, *Nature, 389*, 835-838, 1997

Richard, E.C., K.C. Aikin, A.E. Andrews, B.C. Daube, Jr. C. Gerbig, S.C. Wofsy, P.A. Romashkin, D.F. Hurst, E.A. Ray, F.L. Moore, J.W. Elkins, T. Deshler and G.C. Toon, Severe chemical ozone loss inside the Arctic polar vortex during winter 1999/2000 inferred from in situ airborne measurements, *Geophys. Res. Lett., 28*, 2197-2200, 2001

Russell, G.L., and J.A. Lerner, A new finite-differencing scheme for the tracer transport equation, *J. Appl. Meteorol., 20*, 1,483-1,498, 1981

Santee, M.L., G.L. Manney, N.J. Livesey, and J.W. Waters, UARS Microwave Limb Sounder observations of denitrification and ozone loss in the 2000 Arctic late winter, *Geophys. Res. Lett., 27*, no. 19, 3213-3216, 2000

Shindell, D.T., D. Rind, and P. Lonergan, Increased polar stratospheric ozone loss and delayed eventual recovery due to increasing greenhouse gas concentrations, *Nature, 392*, 582-592, 1998

Sinnhuber, B.-M., M.P. Chipperfield, S. Davies, J.P. Burrows, K.-U. Eichmann, M. Weber, P. von der Gathen, M. Guirlet, G.A. Cahill, A.M. Lee, and J.A. Pyle, Large loss of total ozone during the Arctic winter of 1999/2000, *Geophys. Res. Lett., 27*, no. 21, 3473-3476, 2000

Sugita, T., Y. Kondo, H. Nakajima, U. Schmidt, A. Engel, H. Oelhaf, G. Wetzel, M. Koike, and P.A. Newman, Denitrification observed inside the Arctic vortex in February 1995, *J. Geophys. Res., 103*, 16,221-16,233, 1998

Tabazadeh, A., Commentary on 'Homogeneous nucleation of NAD and NAT in liquid stratospheric aerosols : insufficient to explain denitrification' by Knopf et al., *Atmos. Chem. Phys., 3*, 863-865, 2003

Van den Broek, M.M.P., M. v. Aalst, A. Bregman, M. Krol, J. Lelieveld, G.C. Toon, S. Garcelon, G.M. Hansford, R.L. Jones and T.D. Gardiner, The impact of model grid zooming on tracer transport in the 1999/2000 Arctic polar vortex, *Atmos. Phys. Chem., 3*, 1833-1847, 2003

Van den Broek, M.M.P., A. Bregman and J. Lelieveld, Model study of stratospheric chlorine activation and ozone loss during the 1996/1997 winter, *J. Geophys. Res., 105*, p. 28,961-28,977, 2000

Waibel, A.E., Th. Peter, K.S. Carslaw, H. Oelhaf, G. Wetzel, P.J. Crutzen, U. Pöschl, A. Tsias, E. Reimer and H. Fischer, Arctic ozone loss due to denitrification, *Science, 283*, 2064-2069,1999

CHAPTER V

Conclusions

In this thesis, various key processes that affect ozone concentrations in the Arctic winter stratosphere have been examined by using a 3D CTM. A full stratospheric chemistry scheme, including the heterogeneous conversion of chlorine that leads to ozone depletion, has been implemented in the TM3 transport model and was tested for the 1996/1997 winter. Next, the processes causing the largest model uncertainties in this study, the transport of atmospheric trace gases and the representation of NAT particles, were tested separately for the 1999/2000 winter, using the TM5 model. The sensitivity of these processes to key model parameters and input values covers an important part of this thesis.

In Chapter II, the stratospheric version of the TM3 model, including full chemistry, was introduced. The chemistry routine used Euler Backward Iterative as a numerical solver, which was successfully tested against the stable but computationally expensive Facsimile solver. Chlorine activation and ozone depletion were then calculated for the 1996/1997 and compared to observations. An ozone depletion rate of 14 ppbv/day was calculated at the 50 hPa level during February and March of this winter. This was an underestimate compared to the average ozone loss rate of 20 ppbv/day that was calculated from observations. ClO concentrations, a measure for chlorine activation, were underestimated as well. Three model parameters were found to be of importance in explaining this underestimate: (i) The temperature uncertainty in the ECMWF model. Recently, comparisons of the ECMWF re-analysis data (ERA-40) with temperature soundings showed much that the model off-set has decreased for this winter, which would reduce this uncertainty [Knudsen, 2003]; (ii) The assumptions made regarding the temperature of NAT formation. The way NAT particles are treated in CTMs was the subject of chapter IV of this thesis; (iii) The chlorine abundance. Since the inorganic chlorine concentration has a large vertical gradient in the lower stratosphere, its abundance is highly affected by meridional and vertical transport. Model transport in the Arctic vortex region is addressed and discussed in chapter III of this thesis.

Using the TM5 model, simulations of the long-lived atmospheric trace gases HF and CH_4 have been carried out during the Arctic winter of 1999-2000 to study stratospheric transport in the polar vortex in detail. A good agreement with observations was found outside the polar vortex, for horizontal resolutions form 3ºx2º upward. South of 30ºN, a resolution of 9ºx6º was even sufficient, which shows the applicability of the TM5 zooming algorithm. Applying a 9ºx6º resolution globally produced large errors and should be advised against for CTM and climate studies addressing the Arctic stratosphere. Independent of horizontal resolution, the comparison of model results with observations showed discrepancies inside the vortex, such that the net downward transport was underestimated.

The suggestion was made that the on-set of vortex formation is not well represented within the ECMWF model, which provided the input meteorology data for TM5. Recently, it was found that the type of advection scheme, i.e. only advecting the mass and the 1st order tracer gradients, and the use of a reduced grid around the poles, inhibit the net downward flux. The use of a 2nd moments advection scheme and increasing the advection time step around the poles can largely explain the differences between model and observations [Bregman et al., manuscript in preparation].

These findings on inner vortex transport are relevant for the ozone depletion discussed in Chapter II. An increased downward flux would lead to higher O_3 and Cly concentrations in the lower stratosphere, improving the agreement between modelled and observed ClO.

The subject of Chapter IV was the treatment of NAT particles within the TM5 model. These particles form the surface for heterogeneous chlorine conversion and lead to denitrification. For the first time, an algorithm has been developed that describes the growth and transport of NAT particles within a Eulerian model. In previous model studies, both with the TM3/TM5 model and other 3D CTMs, NAT was not transported and an equilibrium size was calculated. Two different approaches were introduced for NAT growth, making assumptions regarding either the number density or the particle radius. These approaches have been tested for three 10-day periods during the 1999-2000 winter. The calculated particle sizes coincided well with those calculated by a more detailed Lagrangian model [Carslaw et al., 2002]. The differences between the previously used equilibrium calculation of NAT and the new methods were substantial, both in extent and in vertical distribution. Within the equilibrium method, the choice of the radius and the number density largely determine the amount of denitrification calculated, introducing the danger of non-physical 'tuning'. The new method is sensitive to the total number density of NAT, but is quite robust to the number of size bins. It remains to be investigated how the new algorithm affects the calculation of chemical ozone loss in the Arctic winter. Given the large differences in denitrification compared to the classical equilibrium approach we expect that the differences will be significant.
Overall, this thesis has led to a more realistic model representation of the processes leading to ozone depletion in the Arctic stratosphere. The task of integrating these findings on model transport, chemistry and particle growth is now the first one to be accomplished. In the future, climate models may profit from these findings. Moreover, further analysis of the past cold winters in the Arctic winter stratosphere will help us increase our understanding of Arctic stratospheric ozone and its future behaviour.

References

Carslaw, K.S., J.A. Kettleborough, M.J. Northway, S. Davies, R.S. Gao, D.W. Fahey, D.G. Baumgardner, M.P. Chipperfield, and A. Kleinböhl, A vortex-scale simulation of the growth and sedimentation of large nitric acid hydrate particles, *J. Geophys. Res., 107*, D20, 8300, doi:10.1029/2001JD000467, 2002

Knudsen, B.M., On the accuracy of analysed low temperatures in the stratosphere, *Atm. Chem. Phys., 3*, 1759-1768, 2003

Kondo, Y., H. Irie, M. Koike, and G.E. Bodeker, Denitrification and nitrification in the Arctic stratosphere during the winter of 1996-1997, *Geophys. Res. Lett., 27*, 337-340

Author biography

The author, Miranda van den Broek, was born on January 26, 1970 in Heeswijk-Dinther and raised in that same village as the eldest of four children. After graduating at the local Gymnasium Bernrode, she moved to Wageningen in 1988 to start her studies in Environmental Sciences at Wageningen University. She got her MSc degree in 1995, with master theses in Meteorology and Air Quality. A research stage in atmospheric chemistry was carried out at the Max Planck Institut for chemistry in Mainz, where she first got acquainted with the world of atmosphere modeling.
In December 1995 she started to work as an O.I.O. at the Space Research Organization of the Netherlands (SRON) in Utrecht, in the Earth Observation Science (EOS) group, then led by Albert Goede and later by Avri Selig. She was working under supervision of Bram Bregman and professor Jos Lelieveld. From 2000 until 2003 she continued to work for SRON as a junior researcher. From 1996 to 2002, her office was situated at the Institute of Marine and Atmospheric research in Utrecht (IMAU). The past year, the KS-AS group of Henny Kelder, at the Royal Dutch Meteorological Institute (KNMI) has been the last stop on the way to this thesis.

Publications

Peer review journals:

van den Broek, M.M.P., J.E. Williams and A. Bregman, Implementing Growth and Sedimentation of NAT particles in a global Eulerian Model, *Atmos. Chem. Phys. Disc.*, 3089-3126, 2004

van den Broek, M.M.P., M.K. van Aalst, A. Bregman, M. Krol, J. Lelieveld, G.C. Toon, S. Garcelon, G.M. Hansford, R.L. Jones and T.D. Gardiner, The impact of model grid zooming on tracer transport in the 1999/2000 Arctic polar vortex, *Atmos. Chem. Phys., 3*, 1833-1847, 2003

van den Broek, M.M.P., A. Bregman and J. Lelieveld, Model study of stratospheric chlorine activation and ozone loss during the 1996/97 winter, *J. Geophys. Res., 105*, 28,961-28,977, 2000

Krol, M., S. Houweling, B. Bregman, M. van den Broek, A. Segers, P. van Velthoven, W. Peters, F. Dentener, P. Bergamaschi, The two-way nested global chemistry-transport zoom model TM5: algorithm and applications, *Atm. Chem. Phys. Disc.*, 3975-4018, 2004

Van Aalst, M.K., M.M.P. van den Broek, A. Bregman, C. Brühl, B. Steil, G.J. Roelofs and J. Lelieveld, Trace gas transport in the 1999/2000 Arctic vortex: comparison of nudged GCM runs with observations, *Atm. Chem. Phys.*, 3, 2465-2497, 2004.

Bregman, A., J. Lelieveld, M.M.P. van den Broek, H. Fischer, P. Siegmund and O. Bujok, The N_2O and O_2 relationship in the lowermost stratosphere: A diagnostic for mixing processes as represented by a three-dimensional chemistry-transport model, *J. Geophys. Res., 105*, 17,279-17,290, 2000

Bregman, A., M.M.P. van den Broek, K.S. Carslaw, R. Müller, T. Peter, M.P. Scheele, and J. Lelieveld, Ozone depletion in the late winter lower Arctic stratosphere: Observations and model results, *J. Geophys. Res., 102*, 10815-10828, 1997.

Conference proceedings:

Broek van den, M.M.P., Aalst van, M.K., Bregman, B., Krol, M., Lelieveld, J., eds. N.R.P. Harris, G.T. Amanatidis, J.G. Levine, 3D model validation of the northern hemisphere during SOLVE/THESEO winter 1999-2000 (I): results from TM5, Stratospheric ozone 2002, Proc. of the Sixth European Symposium, pp. 71-74, 2003

Broek, M.M.P. van den, Bregman, A., Lelieveld, J., Chlorine conversion during the arctic winter of 1996-97, some model studies, EC - Air Pollution Res. Rep. 73: Proc. 5th Eur. Symp. Stratospheric Ozone 1999, St. Jean de Luz, France,ed. N.R.P. Harris, M. Guirlet and G.T. Amanatidis, EUR 19340, p. 216, 2000.

Kleipool, Q.L., Helmich, F.P., Goede, A.P.H., Schrijver, H., Broek, M. van den, Künzi, K., Küllmann, H., Bremer, H.K., König, M. von, Hetzheim, H., Measurements

of ClO and HCl profiles during the arctic winter of 1999 with consequences for ozone depletion, EC - Air pollution Res. Rep. 73: Stratospheric ozone 1999, Proc. 5th Eur. Symp. Stratospheric Ozone 1999, St. Jean de Luz, France, ed. N.R.P. Harris, M. Guirlet and G.T. Amanatidis, EUR 19340, p. 276, 2000.

Tanzi, C.P., Goede, A.P.H., Broek, M.M.P. van den, Aben, I., Burrows, J.P., Weber, M., Wittrock, F., Platt, U., Wagner, T., Pfeilsticker, K., Monks, P., Llewellyn-Jones, D., Corlett, G.K., Arlander, D.W., Hansen, G., Perner, D., Harder, H., Taalas, P., Kelder, H., Piters, A., Eskes, H., GODIVA, an EC Climate and Environment project for the improvement of GOME data, ESAMS '99 - European Symposium on Atmospheric Measurements from Space, ESTEC, Noordwijk, the Netherlands, 18-22 January 1999, ESA WPP-161, Vol. 2, pp. 687-691, 1999.

Urban, J., Birk, J.M., Bremer, H., Broek, M. van den, Crewell, S., Ellison, B., Eyring, V., Franke, B., Claude, S., Goede, A., Golstein, H., Graauw, T. de, et al., Recent airborne heterodyne receivers for the submillimeter-wave range, Proc. Int. Workshop Submm-wave Observation of Earth's Atmosphere from Space, Earth Observation Research Center, National Space Development Agency of Japan, Tokyo, Jan 27-29 1999, pp. 151-163, 1999.